Max-Planck-Institut für Metallforschung
Stuttgart

Processing of Carbon Fiber reinforced Composites with Particulate-filled Precursor-derived Si-C-N Matrix Phases

Sea-Hoon Lee

Dissertation
an der
Universität Stuttgart

Bericht Nr. 163
Juni 2004

Processing of Carbon Fiber reinforced Composites with Particulate-filled Precursor-derived Si-C-N Matrix Phases

Von der Fakultät Chemie der Universität Stuttgart
zur Erlangung der Würde eines Doktors der
Naturwissenschaften (Dr. rer. nat.) genehmigte Abhandlung

Vorgelegt von

Sea-Hoon Lee

aus Seoul, Republik Korea

Hauptberichter:	Prof. Dr. rer. nat. F. Aldinger
Mitberichter:	Prof. Dr. rer. nat. Dr. h. c. mult. G. Petzow
Mitprüfer:	Prof. Dr. Ir. E. J. Mittemeijer
Prüfungsvorsitzender:	Prof. Dr. Ir. E. J. Mittemeijer
Tag der mündlichen Prüfung:	18. 06. 2004

Institut für Nichtmetallische Anorganische Materialien der Universität Stuttgart
Max-Planck-Institut für Metallforschung
Pulvermetallurgisches Laboratorium / Abteilung Aldinger

Stuttgart 2004

Acknowledgement

This Ph. D. work has been carried out from July 2000 to April 2004 in the Max-Planck-Institute for Metals Research, Stuttgart and University of Stuttgart. Financial support of Max-Planck-Institute is gratefully acknowledged.

I would like to thank my advisor Prof. Dr. F. Aldinger for encouraging me to investigate the topic of this work which I found very interesting. I particularly appreciate his teaching on the way of life as well as many aspects of scientific research. Without the encouragement and continual support from Prof. Dr. F. Aldinger in my time of difficulties, this work would have been not possible.

I want to thank Prof. Dr. G. Petzow, who friendly helped me and agreed to become the “Mitberichter” (co-examiner) for my examination.

I also thank to Prof. Dr. E. J. Mittemeijer who kindly agreed to become the “Mitprüfer” for my examination.

My special thanks to my former group leader Dr. A. Zimmermann, who kindly arranged the experimental schedules and discussed about the mechanical properties. Many thanks to Dr. M. Weinmann who intensively polished my thesis and discussed with a view of chemistry.

There were many people in MPI-PML who taught me and helped me. Thank you Mr. P. Gerstel for the kind help and intensive discussion during whole my Ph. D. works. Dr. D. Matsch kindly helped the experiment and gave many fruitful discussions. With Dr. J. Bill and Dr. A. Müller I had many intensive discussions. Ms. M. Thomas helped to do XRD analysis. Mr. H. Kummer helped to do TGA and dilatometry investigations. Mr. L. Mager helped to

measure creep behavior. Mr. H. Eckstein always helped me with kind smile. I would like to take this opportunity to express my sincere thanks to them.

There were many other people in PML who made my life full of fun. Ms. S. Paulsen and Ms. D. Klink always helped me with a smile. I thanks to Ms. C. Garsia for the kind smile and help. Dr. T. Ludwig, Dr. A. Rosinus, Dr. G. Stieger, Dr. G. Peng, Dr. S.-J.Jia, Mr. R. Kuma and Mr. S. Wang are nice officemates. I also thanks to my Korean colleagues working at MPI. Dr. K. Ahn, Dr. S. Kim, Dr. J. Lee, Dr. K. Kim, Dr. J. Lee, Dr. J. Yu, Dr. S. Lee, Dr. B. Choi, Dr. S. Oh, Dr. Y. Woo, Mr. N. Ku, Mr. S. Lee, Mr. T. Lee, Ms. H. Kim, all are good colleagues and friends. I also have many nice memories with my korean colleagues came from Han Yang university to serve the OJRL project. Dr. J. Yeo, Mr. J. Park, Mr. H. Jung and Mr. K. Ahn, thank you all for the kind help.

My aunt Ms. K. Lee in Berlin and her friend Ms. I. Kim always takes care of me like my mother. Thank you aunts.

My family has always been behind me and always been a source of support in my life.
I dedicate this thesis to my parents.

Sea-Hoon Lee

Processing of Carbon Fiber reinforced Composites with Particulate-filled Precursor-derived Si-C-N Matrix Phases

(Ph.D. Thesis)

by

Sea-Hoon Lee

Abstract

The present thesis reports on investigations and optimisation of factors, which govern the processing and thermal/mechanical properties of fiber-reinforced composites (FRC) composed of carbon fibers and precursor-derived Si-C-N matrix containing filler materials. For this objectives, five topics were sequentially examined.

In the first topic, the processing condition of particulate-reinforced composites (PRC), which is a matrix of particulate-filled FRC, was optimized and the influence of the pyrolysis atmosphere was studied. Compared to conventional process, the total pyrolysis time decreased into ~1/3 without the loss of properties by the control of pyrolysis schedule. A surface oxidation, which was not observed in particulate-free Si-C-N ceramics, occurred during pyrolysis of the PRC made with SiC filler and Si-C-N matrix. The pronounced oxidation of the PRC is most probably due to the larger surface area (8.5 m^2/g) compared to that of pure Si-C-N ceramics (0.27 m^2/g). Preventing the contamination of the pyrolysis atmosphere is an important prerequisite for the fabrication of PRC or particulate-filled FRC using PIP technique, because the surface oxidation during pyrolysis affected mechanical properties and high temperature stability of the composites.

Second, the use of filler materials for the matrix phase which decrease processing time and inhibit excessive shrinkage of fiber-reinforced green bodies during pyrolysis were investigated. For that purpose, four different filler materials (Al_2O_3, Y_2O_3, SiC and Si_3N_4) were tested for PRC having Si-C-N matrix. Oxide fillers reacted with Si-C-N matrix during pyrolysis, and volume shrinkage together with secondary phase formation (Si_5AlON_7, $Y_8Si_4N_4O_{14}$) occurred during pyrolysis. Oxide PRC exhibited six to eight times lower cutting rate after the 1st pyrolysis than non-oxide PRC, but deterioration by flaw formation was observed after repeated pyrolysis cycles. The different CTE between filler material and matrix material (~5×10^{-6}/K) and reactions between them are believed to induce flaws in oxide PRC

during thermolysis. SiC-PRC offered the highest relative density (~91%), strength (525 MPa), Young's modulus (240 GPa), hardness (1622 Hv), and fracture toughness (4.0 $MPa \cdot m^{1/2}$) among the PRC after densification. SiC-PRC also had the lowest weight loss and highest creep resistance at high temperature among the PRC investigated.

Third, a modified infiltration technique of SiC slurries into carbon fiber woven fabrics was explored. Compared to conventional pressure casting, the infiltration behavior of SiC slurry was improved by developing a foil at the bottom of the mold, which deforms outward during infiltration in order to compensate the volume expansion of the fabrics. Highly concentrated SiC slurries having up to 43 vol% solid loading were homogeneously infiltrated into stacked 2D woven fabrics by the application of modified casting technique. The suppression of shear thickening of concentrated slurries during the penetration between the woven fabrics is believed to be the main reason for the improved infiltration behavior. Very dense (~72% relative density) C_{fiber}/SiC_{filler} compact could be succesfully obtained by the modified technique.

In the fourth topic, FRC with SiC filler (C_{fiber}/SiC_{filler}/Si-C-N_{matrix}) were fabricated based on the results of the earlier topics. The cross-linking time for the production of FRC was reduced into ~1/3 and flaw formation was suppressed by the application of sealed metal container for cross-linking. Swelling of the FRC occurred during the first pyrolysis due to the softening of the cross-linked precursor and gas formation. The density of the FRC was $2.14 g/cm^3$ after 10 process cycles. Crack formation occurred in the FRC due to the difference of CTE between carbon fiber and SiC_{filler}/Si-C-N matrix. Nevertheless, fairly high bending strength (286MPa) was measured by 4 point bending test. Cracks propagated through pyrocarbon coatings, and well-developed fiber pull out was observed on the fracture surface of FRC.

The high temperature strength of the FRC was investigated in the last topic. 73% of strength was retained even after the heat treatment at 1350°C for 24h in Ar. The XRD and microstructure analysis indicated the formation of SiO_2 coating and SiC whisker, and showed the deterioration of SiC_{filler}/Si-C-N matrix during the heat treatment. To clarify the mechanism of matrix deterioration, SiC-PRC was prepared using SiC pellets heat-treated at different temperatures (350^oC, 1750^oC). Heat treatment of SiC pellet was performed to control the amount of surface SiO_2 of filler, which was the reason for the formation of SiO_2 coating and SiC whisker on the surface of PRC and particulate-filled FRC after heat treatment. Relative density, mechanical properties such as room temperature strength and hardness, high temperature stability and creep resistance of the PRC were clearly worsened by the surface SiO_2 layer of SiC filler. The strength and hardness values of SiO_2-free PRC (> 639 MPa, 1068

Hv) were two times higher than those of SiO_2-containing PRC (329 MPa, 542 Hv) after a heat treatment at 1400^{o}C for 2h. The results explain that the deterioration of C_{fiber}/SiC_{filler}/Si-C-N FRC after heat treatment was partly due to the weakening of the particulate-reinforced matrix by the decomposition of SiO_2. Pre-heat treatment of the filler material to remove the SiO_2 surface layer is thus a very important prerequisite for producing high temperature FRC using the PIP method.

Contents

List of symbols and abbreviations

Al_2O_3-PRC	PRC made with Al_2O_3 filler and Si-C-N precursor-derived ceramics
BET	Brunauer, Emmett & Teller
350-PRC	PRC which was made with dried SiC pellets at 350^{o}C for 6 h in vacuum
CMC	ceramic matrix composites
CTE	coefficient of thermal expansion
CVI	chemical vapor infiltration
Deform-casting	modified vacuum/pressure casting
EPMA	electron probe micro analyser
FRC	fiber-reinforced composite(s)
F-PRC	SiC-PRC which was pyrolyzed using fast heating rate (5^{o}C/min)
1750-PRC	PRC which was made with heat treated SiC pellets at 1750^{o}C for 2 h in Ar
LSI	liquid silicon infiltration
LPI	liquid-phase infiltration
MEMs	micro-electro-mechanical systems
MSA	minimum solid area
PEI	polyethylenimine
PIP	precursor impregnation and pyrolysis
PRC	particulate-reinforced ceramic(s)
Press-casting	conventional vacuum/pressure casting
RTM	resin-transfer-molding
S-PRC	SiC-PRC which was pyrolyzed using slow heating rate (1^{o}C/min)
Si/SiC	siliconized silicon carbide
SiC-PRC	PRC made with SiC filler and Si-C-N precursor-derived ceramics
Si_3N_4-PRC	PRC made with Si_3N_4 filler and Si-C-N precursor-derived ceramics
TGA	Thermo-gravimetric analyzer
UV	ultraviolet
Y_2O_3-PRC	PRC made with Y_2O_3 filler and Si-C-N precursor-derived ceramics

Introduction

Fiber-reinforced ceramic matrix composites (CMC) have been intensively investigated for application in automotive brakes [01Gad], high-efficiency engine systems [01Lut] or re-entry space vehicles which are exposed to high temperature and/or long life time conditions [01Fle].

Chemical vapor infiltration (CVI) [97Ohz], liquid silicon infiltration (LSI) [00Bha] and precursor impregnation and pyrolysis (PIP) [00Wei] techniques have been most frequently reported as the fabrication methods of fiber-reinforced composites (FRC). Different from CVI technique, ceramic matrix composites (CMC) prepared by liquid-phase infiltration (LPI) (such as LSI or PIP) benefit from low production costs. For example, a low price ceramic brake disk system made by LSI technique was reported [01Elh]. However, several problems may occur if using LSI technique for the fabrication of FRC: first, local silicon melting may act as a source of failure [01Lut]. Second, SiC fibers appear to exhibit grain growth when in contact with molten Si, leading to a significant loss of strength [99Bal]. The PIP technique does not suffer from such problems, and it is more cost-efficient than the CVI technique. However, repeated impregnation and pyrolysis cycles are required to increase the density of FRC high enough, which increases the production costs. Tanaka *et al.* reported that FRC had 5% open porosity even after 10 times of impregnation and pyrolysis [95Tan]. Moreover, such materials often contain large closed pores between fiber yarns, which caused their low relative density (~83%) [95Tan].

Filler materials applied to fill up the spaces between the fiber yarns inhibit excessive shrinkage and pore formation of FRC matrix during pyrolysis and by that reduce the necessary number of impregnation and pyrolysis cycles and decrease the processing time. Rak [01Rak] reported that a high slurry packing was achieved within the fiber preform by using SiC powder as filler. FRC with high densities (2.32g/cm^3) and moderate bending strengths (105 MPa) were obtained already after the first impregnation/pyrolysis cycle using commercially available liquid Si-C-N precursor CERASET^{TM} [01Rak].

Filler materials are generally added by infiltrating slurry into woven fabrics using pressure and drying it to remove the suspension media. However, homogeneous infiltration of highly concentrated slurry into stacked woven fabrics is one of the challenging research topics, and some techniques have been proposed to get over this problem. Singh *et al.* [88Sin] proposed to dip each woven fabrics into a slurry of such powders and subsequently stack the infiltrated fabrics to guarantee for homogeneous infiltration. Donato *et al.* [96Don] used slurries composed of filler and a liquid precursor to decrease the time of the process proposed by Singh *et. al.*

By introducing filler materials, the matrix phase of the FRC becomes a particulate-reinforced composite (PRC). The processing of such composites is different from those of unfilled precursor-derived matrices. There have been many reports published about the fabrication of FRC using filler material, but the properties of filler-containing matrix have not been investigated so frequently [00Wan, 01Li2]. The improvement of filler-containing matrices is important because such types of matrix materials affect the mechanical and thermal properties of FRC [99Müh].

It is the purpose of this study to investigate on the properties of particulate-reinforced precursor-derived ceramic matrix, and to report on the optimisation of factors which govern the processing of FRC under special consideration of filler materials, and on the mechanical and thermal properties of FRC obtained. For this purpose, five topics were examined sequentially:

1. Processing studies of particulate-filled precursor-derived Si-C-N composites with special emphasis to the pyrolysis schedule and to the influence of the atmosphere on the polymer pyrolysis in order to prevent oxidation of the composites during pyrolysis.
2. Investigation of oxide (Al_2O_3, Y_2O_3) and non-oxide (SiC, Si_3N_4) filler materials in order to select the most effective one.
3. Development of a novel processing technique for the advanced infiltration of the free space in stacked woven fiber fabrics with particulate filler material to overcome the technical limitations of pressure casting
4. Fabrication and characterization of carbon fiber-reinforced composites made with the most effective particulate-reinforced matrix phase and optimized processing conditions developed in the previous topics.
5. Investigation of influences of oxide layers formed on the surface of SiC filler to the material processing and to the mechanical and thermal properties of the composite material at high temperature as well as room temperature.

1. Processing of particulate-reinforced precursor-derived Si-C-N ceramics: optimization of pyrolysis atmosphere and schedules

Precursor-impregnation and pyrolysis (PIP) technique has been intensively investigated during the last few years for the fabrication of structural composites applied to severe environmental conditions [99Sug].

The general procedure of PIP technique is to impregnate woven fiber fabrics with a liquid precursor, cross-linking the polymer precursor by heating or UV lightening, and to pyrolyze the assembly at temperatures in the range of 1000°C - 1400°C in a controlled atmosphere.

Weight loss and density increase (~1.0g/cm^3 → ~2.3g/cm^3) during pyrolysis induce shrinkage of the precursor-derived ceramics [92Rie]. Because of the volume shrinkage (20 - 30%) and pore formation during the thermal polymer-to-ceramic conversion [98Kle], the porosity of composites hardly decreases during pyrolysis. Therefore, the preparation of dense FRC by the PIP technique is difficult, and the impregnation/pyrolysis process has to be repeated several times [99Zie], which is time consuming and expensive [99Che]. Accordingly, filler materials such as SiC have been applied to reduce the number of impregnation/pyrolysis cycles [01Rak].

Precursor-derived Si-C-N ceramics are mainly applied because of their excellent oxidation resistance. Butchereit *et al.* [00But] reported that the oxidation of such ceramics started only at 1100°C, and the weight gain by oxidation was less than 1% until 1500°C. In accordance with these results, oxidation was not observed after pyrolysis of compacted precursor powders without filler materials in the present studies. However, PRC made with Si-C-N ceramics and SiC filler always had surface oxidation during pyrolysis. The surface oxidation should be suppressed in order to obtain reliable and reproducible composites.

In the PIP process, pyrolysis schedules have been commonly slowed down to prevent flaw formation by the gas generated during pyrolysis [99Che]. Since repeated cycles of impregnation and pyrolysis are required for the densification, minimizing the pyrolysis time without sacrificing mechanical properties is important to reduce production costs.

Therefore, in this chapter, processing of particulate-filled precursor-derived Si-C-N composites was investigated with special emphasis to the influence of the pyrolysis atmosphere and schedule on the properties of PRC. The possible reason for the oxidation behavior of such materials was surveyed, and the influence of surface oxidation of PRC during pyrolysis on their microstructure, mechanical and thermal properties was investigated. Subsequently, the pyrolysis behavior of the PRC with different heating rates was studied, and

the mechanical and thermal properties of PRC obtained using different pyrolysis schedules were analyzed.

1.1. Experimental procedure

1.1.1. Processing of PRC

The fabrication of particulate-reinforced composites by PIP technique was studied in order to investigate the processing conditions of particulate-filled fiber-reinforced composites with a simplified system. As a model system, SiC particulate-reinforced Si-C-N matrix composites (SiC_{filler}/Si-C-N_{matrix}) were studied. Fabrication of such PRC was performed by cold compacting powders of SiC (A-10, H. C. Starck, d_{50}: 0.51μm, oxygen content: 0.9wt%) and impregnating the compacts with a commercially available liquid Si-C-N precursor (VL20, polysilazane, KION).

At first, SiC powder was milled intensively in isopropanol by planetary milling for 5h using SiC balls. After milling, the slurry was dried at 70°C for 24h while stirring. The powder received was then compacted at 600 MPa by cold isostatic pressing into pellets (ϕ 1.4 cm, thickness 4 mm). The pellets were intensively dried with a graphite furnace at 1750°C for 2h in Ar (1.5 atm) to completely remove moisture from the surface of the fillers.

The Si-C-N precursor was dissolved in tetrahydrofuran (b_p: 66°C, 1 : 1 by volume) in order to decrease its viscosity. After impregnating the solution into the pellets in a metal mold by vacuum infiltration, the solvent was removed by vacuum distillation at 40°C for 6h. The mold was then capped and put into a sealed metal container for the cross-linking of the polymer precursor at 430°C for 6h.

Subsequently, the samples were pyrolyzed at 1350°C for 2h in Ar (Argon 4.8, >99.998vol%, Messer). For controlling the purity of the atmosphere during pyrolysis, a gas providing system was used consisting of PVC pipes and screwed joints (termed normal pyrolysis, Fig. 1.1 (a)). In order to minimize humidity and oxygen impurities in the atmosphere and avoid oxidation of the PRC samples during pyrolysis as much as possible, the system was improved by using Cu pipes, high vacuum sealing, and a gas purification system (oxisorb®, Messer, guaranteed final purities: Oxygen<5ppb, moisture<20ppb, termed purified Ar pyrolysis, Fig. 1.1 (b)). Since the pyrolysis schedule can also affect the surface oxidation, different heating rates (0.5°C/min, 1°C/min, 5°C/min) were used for the ceramization process. During the fabrication process, the samples were carefully handled to prevent contact with air.

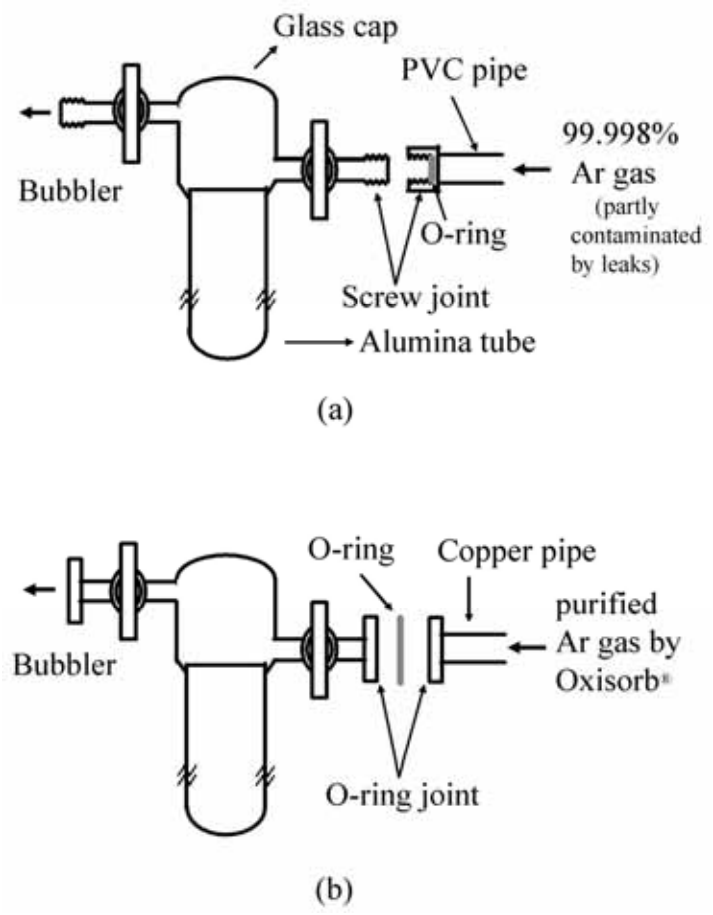

Fig. 1.1: Schematic of equipment used for (a) normal and (b) purified Ar pyrolysis condition

As outlined above, the residual porosity of the as-thermolyzed samples was decreased and by that their density increased by repeating the impregnation and pyrolysis cycles up to six times.

1.1.2. Characterization of precursor-derived Si-C-N ceramics and PRC

True density and chemical compositions of the precursor-derived Si-C-N ceramics used in the present investigation (VL 20) were analyzed in order to understand the properties of resultant PRC. To measure the true density ($\rho_{Si\text{-}C\text{-}N}$) by helium pycnometry (Pycnomatic 200, CE Instruments), cross-linked precursors were crushed into a fine powders in a nitrogen atmosphere using a vibrator mill (Scheibenschwingmühle, Siebtechnik GMBH), and subsequently pyrolyzed in an Ar atmosphere (5^{o}C/min, 1350^{o}C, 2h). Chemical composition was analyzed by using a combination of different equipment (N, C, H: Vario EL, Elementar - combustion in oxygen process, O: TC-436DR, Leco - combustion gas hot extraction process, Si: ICP, Ciros CCD, Spectro - Inductively coupled plasma). For measuring of CTE, bulk material was produced by compacting the cross-linked precursor powder into disk at 180^{o}C

using uniaxial warm pressing (DSP 475, DR. Fritsch GMBH). The disk was machined into a bar ($4\times4\times15mm^3$) and pyrolyzed at 1350°C for 2h, and the resultant Si-C-N ceramic bar was used to measure CTE (25°C-1000°C) by dilatometry (Dil 802, Baehr Thermoanalyse) in an Ar atmosphere.

The ceramic yield of Si-C-N precursor with and without filler was measured by a TGA (Netzsch, STA 409) over a temperature range of 25-1450°C under Ar. In order to understand the pronounced weight loss of PRC compared to pure Si-C-N ceramics above 1350°C during the measurement of TGA, the average pore size of the SiC pellet was measured by mercury porosimetry (Porosimeter 2000, Carlo Erba Inst.). The ceramic yield of the precursor in the pellet was estimated by comparing the weight of pellets before and after precursor impregnation, cross-linking and pyrolysis.

The volume fraction of SiC filler (t_{SiC}) and Si-C-N matrix ($t_{Si\text{-}C\text{-}N}$) was estimated by measuring the weight and true density (ρ_{SiC}, $\rho_{Si\text{-}C\text{-}N}$) of each component, respectively. The true density of PRC (ρ_{PRC}) was calculated after each cycle from the volume fraction (t_{SiC}, $t_{Si\text{-}C\text{-}N}$) and the true density of each component by using equation $\rho_{PRC} = t_{SiC}\cdot\rho_{SiC} + t_{Si\text{-}C\text{-}N}\cdot\rho_{Si\text{-}C\text{-}N}$. The relative density of PRC was estimated by measuring the bulk density and divided the value into true density.

In order to analyze the effect of heating rate on the ceramic yield of pure Si-C-N precursor, TGA (Netzsch, STA 409) was measured with different pyrolysis schedules (1°C/min, 5°C/min). The effect of pyrolysis schedule on the crystallization of PRC was analyzed by X-ray powder diffraction (XRD, D 5000, Siemens) with CuK_α radiation.

After the pyrolysis using different gas providing systems described above, microstructure, element and phase analysis of the oxidized layer were performed by scanning electron microscopy (SEM, DSM 982, Zeiss), electron probe micro analyser (EPMA, SX-100, Cameca), and XRD. The surface area of the samples was measured using BET (Gemini, Micrometrics).

The relative density of PRC was ~70 % after the first impregnation/pyrolysis cycle, and the samples were not strong enough to be machined for the production of specimen for mechanical testing. Therefore, the mechanical properties were evaluated by comparing the cutting behavior of the samples. A low speed cutter (Minicut, Scandia) with a diamond wheel (diameter: 100 mm, Buehler) was used for precise cutting. In order to analyze the cutting rate under defined conditions, the wheel speed was set to 150 r.p.m. (revolutions per minute), which corresponds to 785 mm/sec at the cutting point, and the wheel was dressed two times after each measurement. The cutting rate was expressed as the cutting area per second

(mm^2/sec). The thickness of the wheel (0.5mm) and that of the sample at the cutting area was constant in all cases.

A Netzsch STA 501 was used for the high-temperature TGA of the as-pyrolyzed PRC in Ar over a temperature range of 25-2100°C (heating rate: 20°C/min at T<1000°C, 3°C/min at T>1000°C) to measure the effect of surface oxidation on the high temperature mass stability of PRC.

After six cycles of impregnation and pyrolysis, the samples were strong enough for machining into disks (diameter: 10mm, thickness: ~300μm). One side of the disks was polished up to 1μm finish. The strength of the samples was measured by the "ball on three balls" test [02Bor]. The Poisson's ratio of the samples, which is required to calculate the strength, was determined by a resonance frequency and damping analyzer (RFDA system 23, IMCE). Hardness and fracture toughness of the PRC were measured by the Vickers indentation method (Micromet, Buehler) [81Ans]. The morphology of the fracture surface was observed with SEM, and Netzsch STA 501 was used for the high-temperature TGA of the samples (Ar, 25-2100°C, 3°C/min).

1.2. Results and discussion

1.2.1 Processing of PRC

The density of Si-C-N ceramics used in the present investigation was measured as 2.56g/cm^3 after the pyrolysis at 1350°C for 2h, which value is higher than that of typical Si-C-N ceramics (~2.30 g/cm^3) pyrolyzed at 1000°C [92Rie, 00Hal]. With increasing the pyrolysis temperature, the densification of precursor-derived ceramics may be enhanced during pyrolysis. Traßl *et al.* reported a density increase of 19.4% (2.30 g/cm^3 → 2.75 g/cm^3) by increasing the pyrolysis temperature of Si-C-N precursor from 800°C to 1500°C [00Tra].

The chemical composition and CTE of the filler-free precursor-derived ceramics was $SiC_{0.68}N_{0.91}$ and 3.2×10^{-6}/K (25°C-1000°C), respectively after the pyrolysis in Ar at 1350°C for 2h.

After the first impregnation/pyrolysis cycle, the increase of relative density of the as-thermolyzed PRC was 9.4% (60.6% → 70.0%). XRD peaks of Si_3N_4 due to the crystallization within the amorphous Si-C-N matrix during pyrolysis at 1350°C were detected neither in the pure Si-C-N nor in the SiC-filled PRC.

Fig. 1.2 shows TGA curves of samples of cross-linked Si-C-N precursor and SiC pellet impregnated with precursor before pyrolysis. The particulate-free sample revealed a higher ceramic yield (81.7%) than the thermolyzed precursor impregnated in the SiC pellet (~74%).

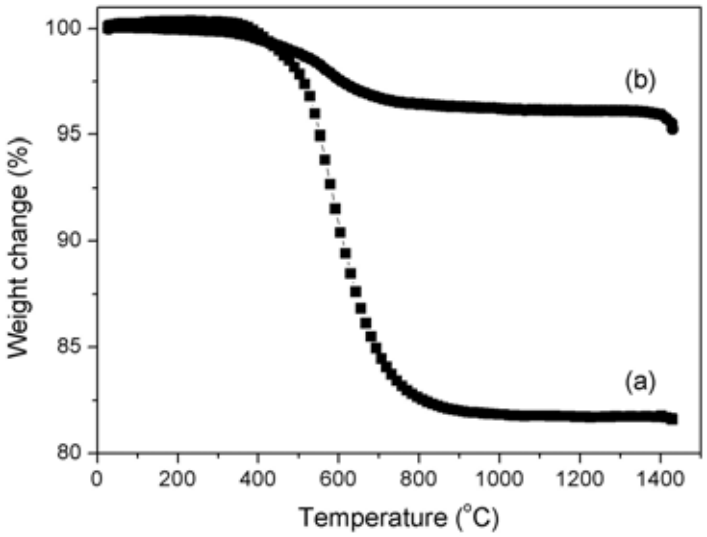

Fig. 1.2: TGA of precursor and particulate-reinforced green bodies. 100ml/min Ar flow, heating rate: 5°C/min (a) pure precursor (b) precursor-impregnated SiC pellet

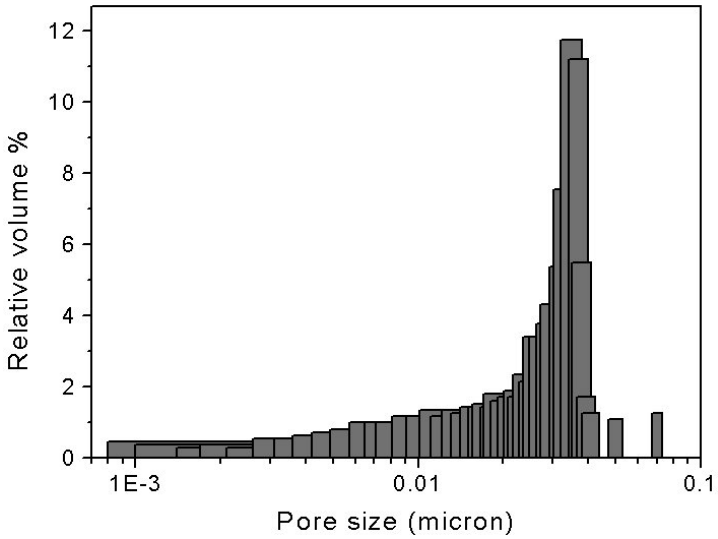

Fig. 1.3: Pore distribution of the SiC compact (average pore size: 38nm)

Different from pure Si-C-N ceramics, an additional step of weight loss occurs in PRC at around 1350°C. The different weight loss behavior of the two systems at high temperature can be partly explained by the different surface area and thickness of the porous Si-C-N matrix. First, the surface area of porous as-thermolyzed Si-C-N was 0.27m^2/g, where as those of PRC was thirty times higher (8.5 m^2/g). The decomposition of precursor-ceramics was reported to be enhanced when their surface area increases [98Kle]. Second, the average pore size of SiC pellet is 38 nm, and most of the pores are in the range of 20 – 40 nm (Fig. 1.3). The Si-C-N matrix of the PRC is formed in those pores of the powder compact. Consequently, the average cross-sectional size of Si-C-N matrix has to be smaller than 40nm. Kleebe *et al.*

[98Kle] reported that very thin samples of Si-C-N matrix (300 – 500 nm) showed enhanced SiC nucleation and crystallization after annealing at 1250^{o}C for 6h, while thick one did not crystallize at the same condition. The crystallization of Si-C-N is often accompanied by decomposition [96Rie] which induces weight loss. The weight loss above 1350^{o}C may be one of the reasons for the enhanced crystallization and decomposition of the thin Si-C-N matrix.

1.2.2 Analysis of the oxidized surface layer

Fig. 1.4 shows the cross-sectional morphology and microstructure of samples pyrolyzed under normal conditions. By optical microscopy many pores and cracks are observed inside of pure Si-C-N ceramics, and no severe oxidation was observed at the surface of them (Fig. 1.4 (a)). However, SEM studies revealed a thin oxide layer (thickness: 0.5 μm) formed during pyrolysis (Fig. 1.4 (c)).

On the other side, an oxidized layer with 500μm thickness was formed on the surface of the PRC (Fig. 1.4 (b)). An area (thickness: ~30μm) was observed between the oxidized surface layer and the sample inside (Fig. 1.4 (d)). Filler particles were pulled out during polishing in this area termed boundary area (Fig. 1.4 (e)). In contrast, such a particle pull out did not occur in the oxidized surface layer nor in the sample inside. The observation suggests that the bonding strength between the filler and matrix within the boundary area is weaker than in the other areas. The possible reason for this behavior is discussed in detail in the next paragraph.

Fig. 1.5 shows the XRD data of the samples pyrolyzed with normal pyrolysis condition. The peak intensity of SiC in the as-pyrolyzed PRC (Fig. 1.5 (b)) was lower than that in unimpregnated SiC pellets (Fig. 1.5 (a)). Because of the oxidation of PRC during pyrolysis, peaks of cristobalite (SiO_2) are also present in the pattern of the PRC. The main peak of which can be seen clearly, while less intensive peaks are mostly overlapped by those of SiC. The intensity of the main peak increased with the number of impregnation/pyrolysis cycles (Fig. 1.5 (c)).

After pyrolysis of PRC with rather slow heating rate (0.5^{o}C/min) using normal pyrolysis condition, the oxidized layer is rather thick (500μm, Fig. 1.4 (b)). The surface oxidation decreased with increasing heating rate (Fig. 1.6 (a), (b)). By the application of purified Ar, surface oxidation of PRC was suppressed further (Fig. 1.6 (c), (d)). The surface oxidation of PRC was completely suppressed by the application of purified Ar condition and fast heating schedule (5^{o}C/min) during pyrolysis (Fig. 1.6 (d)).

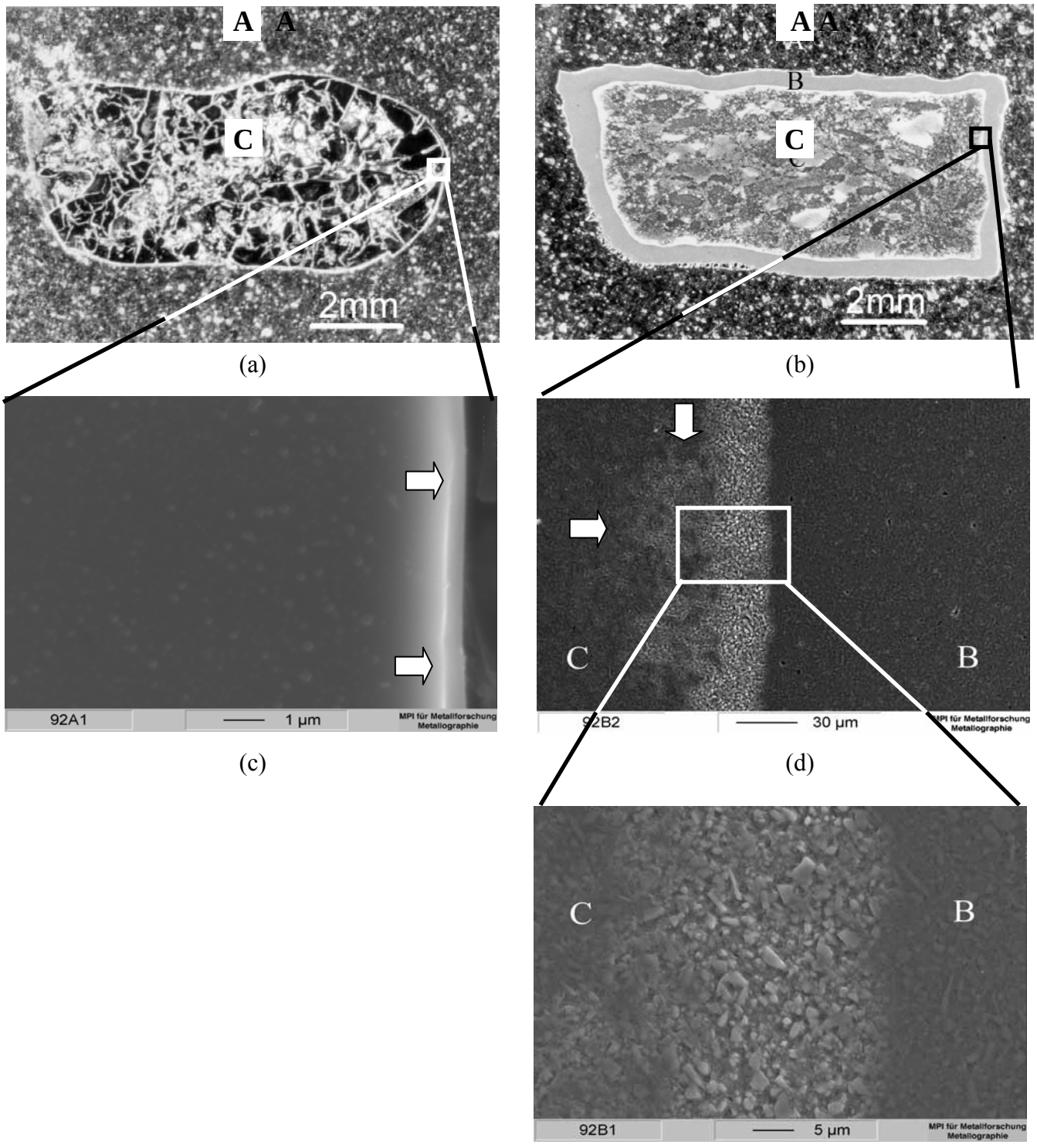

Fig. 1.4: Cross-sectional morphology of samples after pyrolysis with normal pyrolysis condition (0.5°C/min, 1350°C, 2h), (a) Si-C-N precursor-derived ceramics (A: mounting resin, C: sample inside), (b) SiC_{filler}/Si-C-N_{matrix} PRC (B: oxidized layer), (c) high magnification of the surface area of Si-C-N precursor-derived ceramics (⇨: oxide layer), (d) high magnification of the area between oxidized layer and inner part of SiC_{filler}/Si-C-N_{matrix} PRC (⇨: boundary area that expands into sample inside) and (e) higher magnification of (d)

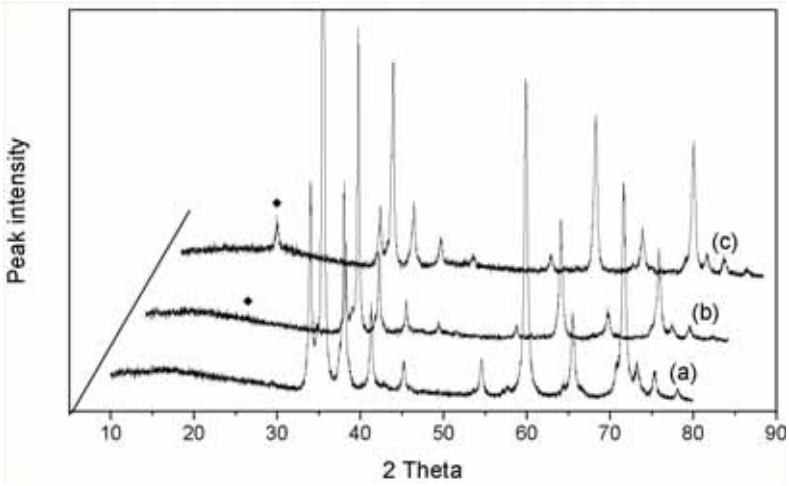

Fig. 1.5: XRD patterns of (a) SiC (pellet), (b) SiC_{filler}/Si-C-N PRC after pyrolysis with normal pyrolysis condition, and (c) after 3 times of impregnation and pyrolysis of sample (b) (♦: cristobalite, other peaks: α-SiC)

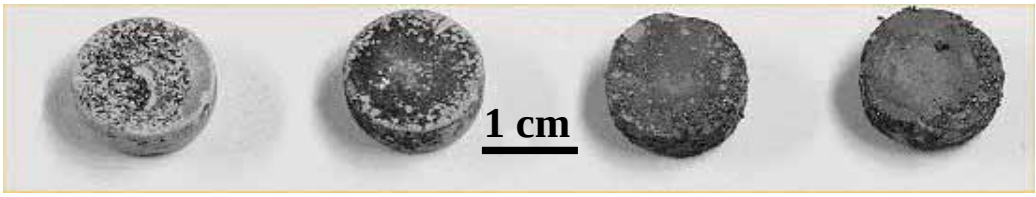

(a) (b) (c) (d)

Fig. 1.6: Morphology of PRC pyrolyzed at different conditions: (a) normal pyrolysis, 1°C/min; (b) normal pyrolysis, 5°C/min; (c) purified Ar, 1°C/min, and (d) purified Ar, 5°C/min

The reason why SiC-filled PRC is more susceptible to oxidation during pyrolysis than precursor-derived pure Si-C-N ceramics can not be explained by the difference of high temperature oxidation resistance between SiC and Si-C-N. Both materials possess excellent oxidation resistance. Presumably, the different oxidation behavior is connected to the thirty times larger internal surface area of PRC (8.5 m^2/g) than that of pure Si-C-N ceramics (0.27 m^2/g).

Fig. 1.7 shows results of EPMA (electron probe micro analyser) investigations which visualize the distribution of Si, O, C, and N in and near the boundary area seen in Fig. 1.4 (e). The oxygen content in the oxidized layer is higher compared to that within the boundary area and the sample inside. Carbon content is lowest in the oxidized layer, and its amount increases from the boundary area to the inner regions of the sample. Similarly, the nitrogen content in the oxidized layer is significantly lower than in other parts of the sample. The distribution of Si is rather homogeneous all over the sample.

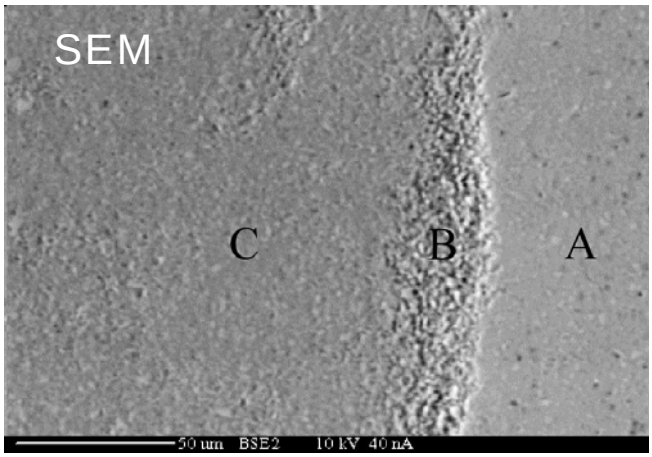

(a)

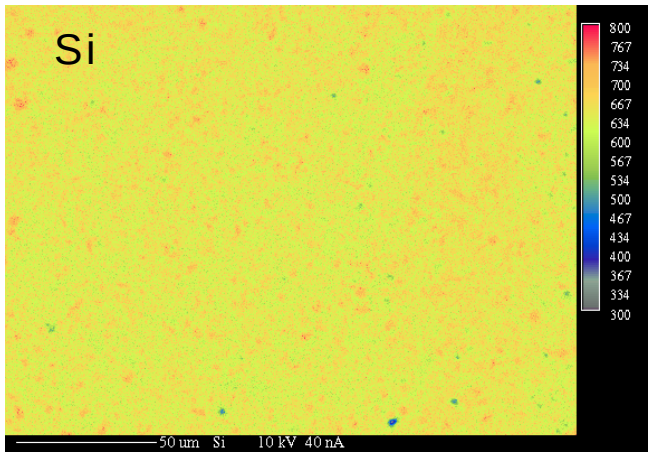

(b)

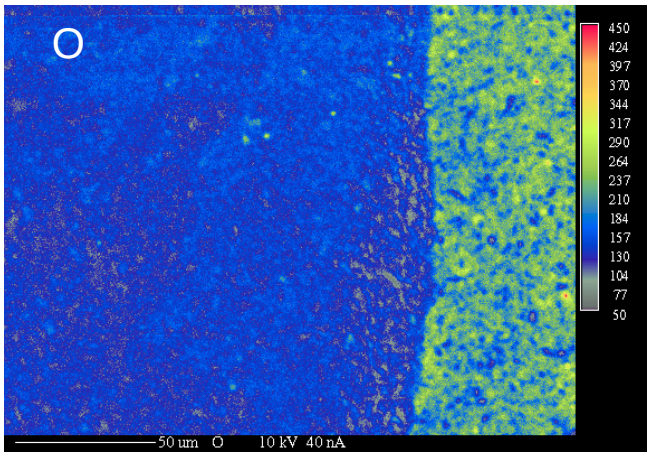

(c)

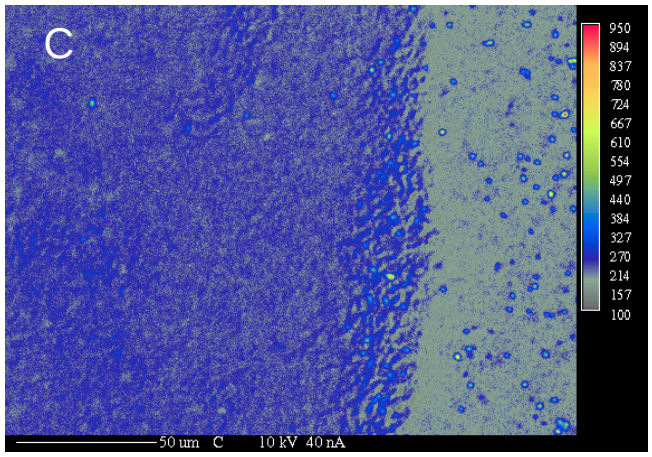

(d)

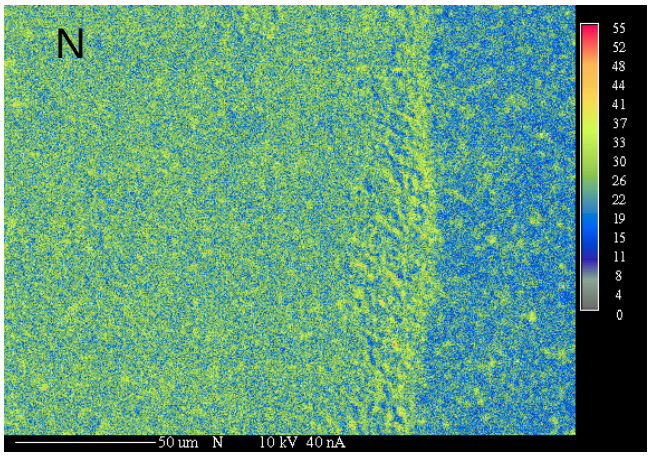

(e)

Fig. 1.7: Chemical composition of the oxidized layer, boundary area and inside measured with EPMA (electron probe micro analyser). Different c/s (count/sec) values are used in each compositions for clear comparison: (a) SEM (A: oxidized layer, B: boundary area, C: sample inside), (b) Si (c/s: 300-800), (c) O (c/s: 50-450), (d) C (c/s: 100-950) and (e) N (c/s: 0-55)

1.2.3 Effect of the oxidation on the mechanical and thermal properties of PRC

The results outlined above suggest that the reason for the weak bonding of the filler particles within the boundary area in Fig. 1.4 (e) is due to the burn out of free carbon in the Si-C-N matrix. During pyrolysis, oxygen impurity in the Ar atmosphere diffused through the porous oxidized layer, and oxidizes free carbon in the boundary area (Fig. 1.7 (d)). Once the Si-C-N matrix becomes more porous by this process, the strength of the interface between the matrix and filler particles decreases. This behavior is somewhat in agreement with Bahloul *et al.* who reported that the weight loss of Si-C-N ceramics at 600°C – 800°C during oxidation was a consequence of the burn out of free carbon [92Bah].

The higher adherence of filler particles in the oxidized layer as compared to the boundary area is presumably due to the volume expansion of both Si-C-N (36% in $SiC_{0.6}N_{0.9}$ [01Raj]) and SiC during oxidation. Riedel *et al.* reported that sealing of the pore mouth of porous Si-C-N ceramics by oxide formation occurred during oxidation at 1400°C [95Rie]. SiO_2 formation, however, is not observed in the boundary area yet (Fig. 1.7 (c)).

As surface oxidation proceeds, oxygen flow to the boundary area is reduced due to the decrease of pore size by the volume expansion during oxidation, and the increase of the thickness of oxidized layer. Therefore, the supplement of oxygen for the equilibrium partial pressure becomes more difficult with increasing thickness of the oxidized layer. The small amount of oxygen, which passes the oxidized layer, reacts preferentially with free carbon in the boundary area already at low temperatures (~700°C). In contrast, oxidation of the matrix phase in this area by the formation of SiO_2 occurs very slowly under such conditions [93Nat]. Therefore, in the boundary area the adherence of SiC to the Si-C-N matrix is presumably weaker than that in the other areas, thus the filler particles pull out during polishing as a result.

Fig. 1.8 shows the cutting rates of the samples pyrolyzed under different conditions. The results reflect the mechanical properties of the PRC at room temperature. The cutting rate reached a maximum when oxidation was suppressed (Fig. 1.8 (d)), and was lowest in oxidized PRC indicating an increased resistance against cutting. The reason for the increased cutting resistance of the oxidized PRC at room temperature is presumably due to volume expansion during the oxidation of SiC and Si-C-N and resultant closing of the pores in the outside of samples.

The beneficial effect of oxidation onto the mechanical properties at room temperature may, however, diminish at higher temperatures. Above 1300°C, SiO_2 reacts in the oxidized layer [91Bib] in the following ways [99Col]:

$$SiO_{2(s)} + 3C_{(s)} \rightarrow SiC_{(s)} + 2CO_{(g)}, \qquad (1.1)$$

$$2SiO_{2(s)} + SiC_{(s)} \rightarrow 3SiO_{(g)} + CO_{(g)}. \quad (1.2)$$

Since both reactions can occur only in the oxidized PRC which contains SiO_2, a worsening of the mechanical properties at high temperature will be observed only if PRC was oxidized. In fact, removing SiO_2 from the PRC by a heat treatment at 1400°C clearly decreased the mechanical properties of PRC, which will be described in chapter 5.

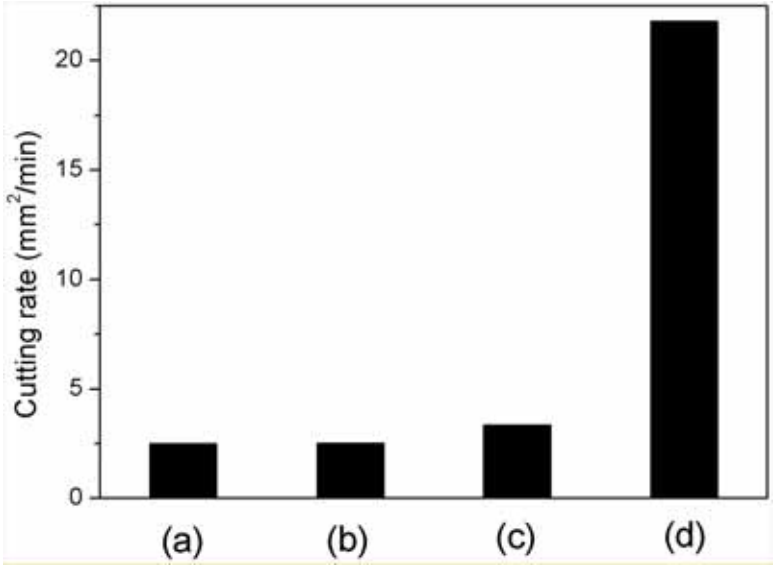

Fig. 1.8: Cutting rate of the samples pyrolyzed with different conditions
(a) normal pyrolysis (1°C/min), (b) normal pyrolysis (5°C/min), (c) purified Ar pyrolysis (1°C/min) and (d) purified Ar pyrolysis (5°C/min)

The thermal stability of the PRC is also affected by the oxidation. Fig. 1.9 shows results of TGA investigations of PRC pyrolyzed under different conditions. Intensive weight losses are observed between 1400°C and 1700°C in both cases. The weight loss of non-oxidized PRC (Fig. 1.9 (a)) is a result of the decomposition of Si-C-N matrix, *e.g.* by reaction (1.3) [96Rie] and/or (1.4) [02Pen]:

$$Si_{1.73}C_{1.0}N_{1.56(s)} \rightarrow 0.24\ Si_3N_{4(s)} + 1\ SiC_{(s)} + 0.3\ N_{2(g)}, \quad (1.3)$$

$$Si_3N_{4(s)} + 3C_{(s)} \rightarrow 3\ SiC_{(s)} + 2\ N_{2(g)}. \quad (1.4)$$

In oxidized PRC, additionally, SiO_2 decomposes at high temperature by reaction (1.1) and/or reaction (1.2). As a consequence, the weight loss of PRC pyrolyzed with normal pyrolysis condition (Fig. 1.9 (b)) is higher than that of PRC obtained in a purified Ar atmosphere (Fig. 1.9 (a)).

1.2.4 Optimization of pyrolysis schedule

After getting over the problem of surface oxidation, the pyrolysis schedule was optimized. Fig. 1.10 shows the TGA plot of the Si-C-N precursor using different heating rates. Increasing heating rate raises the onset of decomposition towards higher temperature. The weight loss begins at 380°C if heating with 5°C/min, whereas it is observed already at 300°C if heating rate was as low as 1°C/min. This behavior is in accordance with earlier results [93Bah]. Importantly, the ceramic yield is not affected; it has been in both cases 82% at 1300°C. The result is different from that of Bahloul *et al.* where the ceramic yield was strongly affected by the heating rate [93Bah].

Fig. 1.11 shows the dependence of the relative density of PRC on the heating rates of pyrolysis with increasing numbers of impregnation/pyrolysis cycles. At slower heating (1°C/min), the relative density is somewhat smaller than at faster heating (5°C/min). Thus the heating rate affects the densification behavior of SiC-PRC, although the ceramic yield of filler-free precursor was not affected by the schedule.

Different crystallization behavior of the two PRC can be considered to explain this observation. Fig. 1.12 shows the XRD reflections of slow heated (S-PRC) and fast heated (F-PRC) PRC after 6 impregnation/pyrolysis cycles. In S-PRC, due to the crystallization of the Si-C-N matrix, Si_3N_4 peaks were detected at 1350°C. This is in accordance with earlier results that crystallization of Si-C-N occurred at 1400-1500°C [01Iwa, 02Sch].

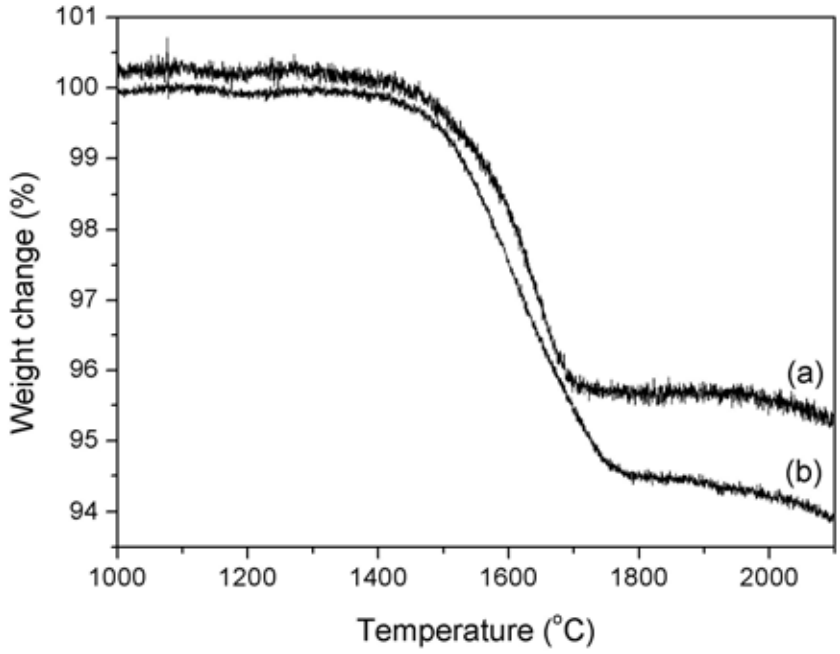

Fig. 1.9: TGA of PRC (heating rate: 3 °C/min) in Ar atmosphere
(a) with, and (b) without gas purification

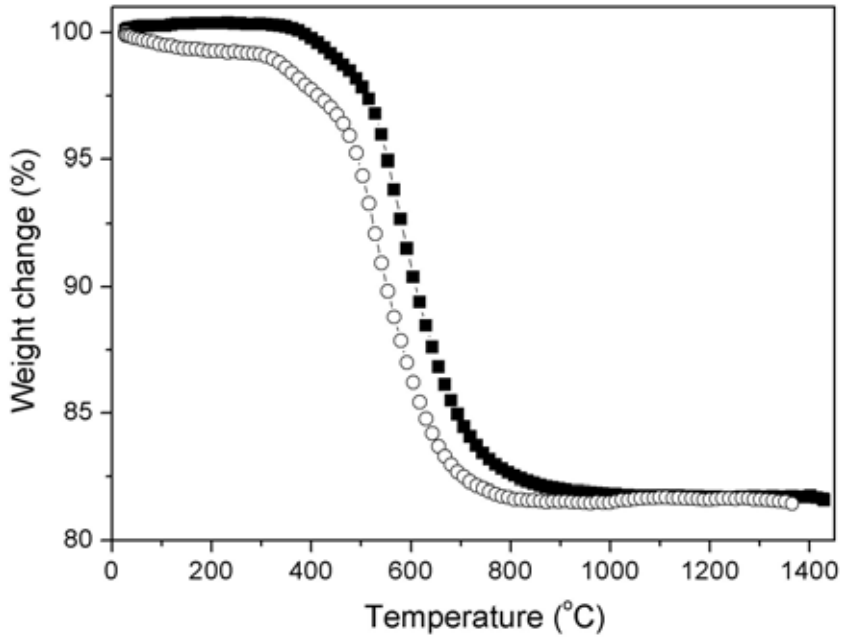

Fig. 1.10: TGA of Si-C-N precursor using heating rates of 1°C/min (○), and 5°C/min (■)

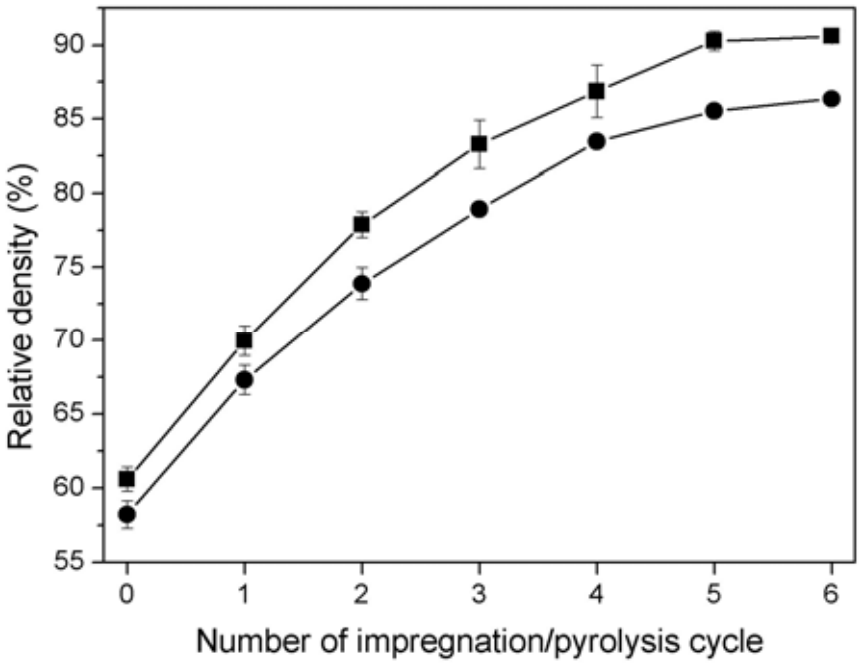

Fig. 1.11: Relative density of SiC-PRC after 1 to 6 impregnation/pyrolysis cycles using different heating rates of pyrolysis (■: F-PRC, 5°C/min, ●: S-PRC, 1°C/min)

In contrast to this, with faster heating no crystallization of Si_3N_4 was detected at 1350°C (Fig. 1. 12 (a)). Since the faster heating rate decreased the duration time at high temperature, the crystallization of Si-C-N matrix was not occurred in F-PRC. Because the crystallization is often accompanied by decomposition, it may cause a decrease in density of PRC according to, *e.g.* reaction (1.3).

The weight loss of PRC was not affected by the heating rate up to 1400°C (Fig. 1.13). However, above 1400°C where both F-PRC and S-PRC exhibited rapid weight loss, there is an influence on the amount of weight loss. The decomposition was finished in both cases at ~1700°C and no additional weight loss was observed up to 1900°C.

The heating rate also affects the mechanical properties of PRC (Table 1.1). F-PRC had higher values of Young's modulus (E) and hardness than S-PRC, most probably, due to the higher relative density. The difference of hardness values between the PRC is bigger than that of E values, which is in agreement with a report of Rice who stated that hardness more strongly depends on porosity than Young's modulus [98Ric]. F-PRC also had higher fracture toughness than S-PRC. Different from the other properties, the strength of S-PRC was somewhat higher than that of F-PRC. However, bending strength more strongly depends on the size and shape of flaws than on the relative density of PRC [00Ric]. F-PRC presumably had more flaws than S-PRC because of the faster generation of gas during pyrolysis. This is also supported by the fact that F-PRC had also a higher standard deviation in strength (Table 1.1).

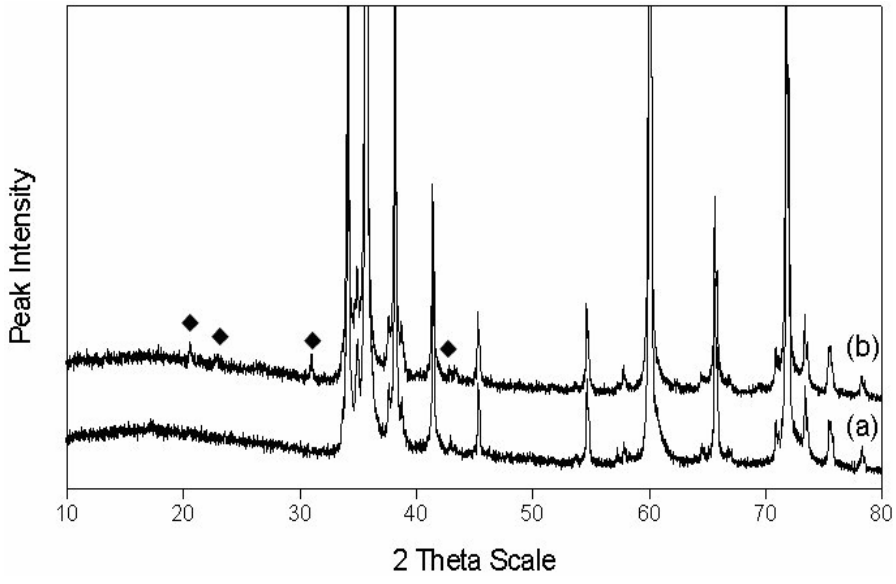

Fig. 1.12: XDR data of SiC-PRC after heating to 1350°C: (a) F-PRC and (b) S-PRC. α-Si_3N_4 reflections are indicated with (♦). Other peaks: SiC

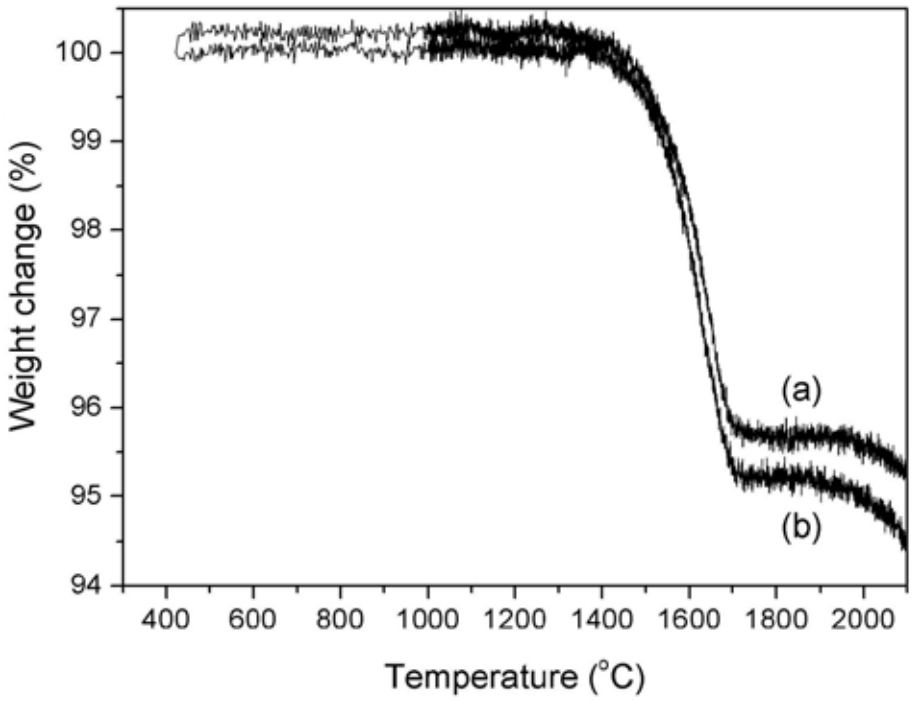

Fig. 1.13: TGA data of (a) F-PRC and (b) S-PRC in an Ar atmosphere (after 6th process cycle, heating rate: 20^{o}C/min (25-1000^{o}C) and 3^{o}C/min (1000^{o}C-2100^{o}C))

Table 1.1. Dependence of the heating rate (1^{o}C/min, 5^{o}C/min) during thermolysis on processing and mechanical properties of SiC-PRC

Processing properties	F-PRC	S-PRC	Mechanical properties after 6 processing cycles	F-PRC	S-PRC
Green density (%)	60.6	58.2	Young's modulus (Gpa)	240	185
Relative density after 6th pyrolysis (%)	90.6	86.3	Hardness (Hv)	1622	776
Detected phases	α-SiC	α-SiC α-Si_3N_4	Toughness (MPa·m$^{1/2}$)	4.0	2.9
Shrinkage after 1st pyrolysis (%)	0.1	0	Strength (MPa)	525	576
Shrinkage after 6th pyrolysis (%)	0	0	Standard deviation	70.0	49.9

Fig. 1.14 shows the SEM image of a fracture surface of PRC. Transgranular fracture is the dominant fracture mode in both cases, but some intergranular fracture is also observed in S-PRC.

The total pyrolysis time of S-PRC is 5 times longer than that of F-PRC which exhibits a higher relative density and better mechanical properties (except a small reduction of strength) than S-PRC. Possibly, the flaws which decreased the strength and increased the standard deviation of strength of F-PRC can be formed during the first pyrolysis due to the weak strength of ceramic powder compact. Chew *et al.* [99Che] reported similar pyrolysis schedules to save processing time without deteriorating the mechanical properties of FRC.

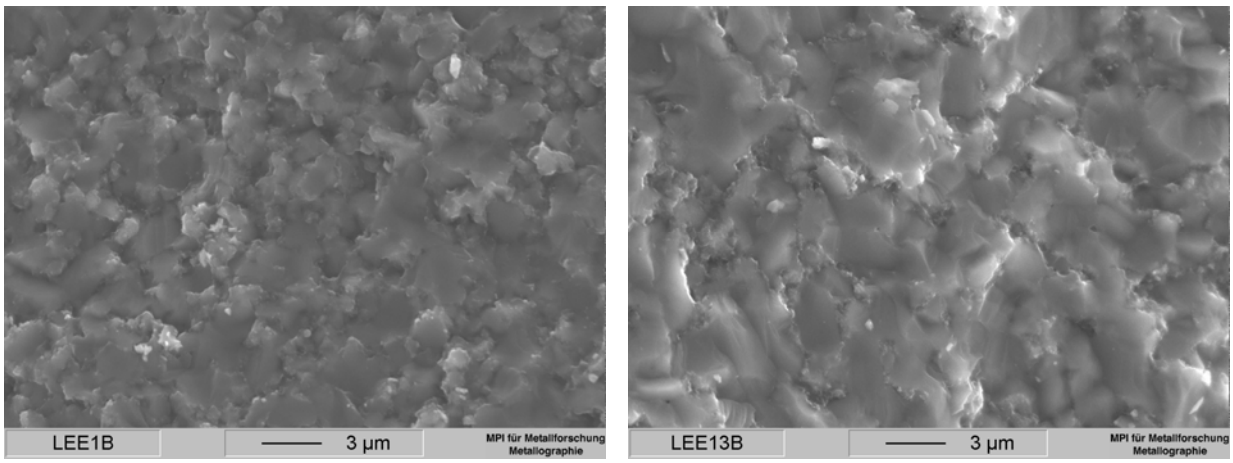

(a) (b)

Fig. 1.14: Fracture surface of PRC after the 6th pyrolysis cycle at different heating rate (a) S-PRC and (b) F-PRC. Transgranular fracture behavior is observed in both PRC.

1.3. Summary and Conclusions

A surface oxidation occurred during pyrolysis of the particulate-reinforced composites (PRC) made with SiC filler and Si-C-N precursor-derived ceramic matrix. In contrast, such oxidation was not observed in pure Si-C-N ceramics. The pronounced oxidation of the PRC is most probably due to the larger surface area (8.5m^2/g) compared to that of pure Si-C-N ceramics (0.27 m^2/g). The surface oxidation during pyrolysis affected mechanical properties and high temperature stability of the PRC. Therefore, it is very important to prevent the contamination of the pyrolysis atmosphere with oxygen for the fabrication of PRC or particulate-reinforced FRC using PIP technique. The surface oxidation was successfully suppressed by the application of purified Ar condition and fast pyrolysis schedule. The pyrolysis schedule affects the relative density, Young's modulus, fracture toughness and strength of SiC-PRC. Fast heating (5^{o}C/min) does not deteriorate the properties of PRC

except a small decrease in strength, whereas total processing time can be reduced to ~1/3 compared to the procedure using a heating rate of 1^{o}C/min. Based on these results, the faster heating rate of 5^{o}C/min seems to be more adequate for the production of FRC (see chapter 3).

2. Investigation of different oxide and non-oxide filler materials for particulate- and fiber-reinforced precursor-derived Si-C-N ceramics

The process to fabricate particulate-reinforced precursor-derived Si-C-N composites by PIP technique was investigated in the first chapter. SiC-filled PRC could be successfully fabricated and pyrolysis schedule was optimized with respect to heating rate. Based on the achievements, in this chapter, the type of filler will be varied in order to find the most appropriate filler system for the fabrication of FRC by PIP technique.

When investigating the near-net shaping of composites, Greil added fillers to the precursor used in order to control the volume change of components during processing [95Gre]. He proposed to use active or passive (inert) fillers. When active filler particles are used, near-net-shape conversion can be achieved because of compensation of the polymer shrinkage by filler expansion. Various kinds of active fillers such as Ti, Cr, V, Mo, Si, B, $CrSi_2$, $MoSi_2$ have been reported. However, the application of active fillers to the fabrication of FRC has not been so frequently investigated [97Sut] presumably due to the following reasons:

1. The diameter of the fibers for the application of FRC is generally ~10μm, and sub-micron filler powder should be used for the homogeneous infiltration of fillers into the woven fabrics made with these fibers [95Lan][98Lau]. However, sub-micron metal powders are very expensive and generally react very intensively with oxygen once exposed to air [64Clo]. Accordingly, the particle size of the active filler have to be within the range of 1 - 10μm [00Gre].

2. The specific weight of such fillers is high except with B and Si (B: 1.73, Si: 2.33, Ti: 4.5, V: 5.98, Cr: 7.19, Mo: 10.23g/cm^3), thus they tend to sediment in a slurry.

Accordingly, inert fillers such as SiC [94Shi] and Si_3N_4 [95Nak] have been widely used for the fabrication of FRC. Substantial decrease of processing time have been achieved for the production of dense FRC.

Filler materials can, however, decrease the strength of resultant FRC [95Nak, 98Tan]. Gonon *et al.* [99Gon] reported that despite the lower porosity achieved by applying Si_3N_4 powder (8.8% instead of 15.7%), such particulate-filled FRC had much lower flexural strength (145 MPa instead 289 MPa) than FRC without filler materials. They observed that the bonding between Si_3N_4 filler and the pyrolyzed polysilazane-derived matrix was very week.

Beside these results, there appeared some publications supporting the beneficial effect of filler materials. Imuta *et al*. [99Imu] reported that a fairly high strength value (520 MPa) was achieved by nine-fold impregnation/pyrolysis cycles of a FRC composed as $SiC_{fiber}/SiC_{filler}/SiC_{matrix}$.

The above reports clearly show the importance of filler materials to improve the properties of particulate-filled FRC. Therefore, in this chapter, different types of filler materials and their effects on the processing as well as mechanical and thermal properties of PRC are investigated. Four different filler materials (Al_2O_3, Y_2O_3, SiC and Si_3N_4) have been studied using the same commercial Si-C-N precursor (VL20) as in chapter 1. Al_2O_3 have been selected because it offers low cost and well developed processing conditions, Y_2O_3 provides high temperature stability, Si_3N_4 has good mechanical properties and a CTE (coefficient of thermal expansion) comparable to that of the Si-C-N matrix, and SiC has good mechanical properties and high temperature stability.

2.1. Experimental procedure

2.1.1 Fabrication of PRC using different filler materials

Table 2.1 shows selected properties of the filler materials chosen and of the Si-C-N ceramics derived from VL20 by pyrolysis at 1350°C for 2h ($SiC_{0.68}N_{0.91}$, density: 2.56g/cm^3). The non-oxide fillers have a smaller average particle size than the oxide fillers. Young's modulus follows the order SiC > Al_2O_3 > Si_3N_4 > Y_2O_3. Galusek *et al.* [01Gal] measured Young's modulus of Si-C-N ceramics ($SiC_{0.67}N_{0.80}$) with the nano indentation technique, and reported the values as 125 Gpa, which value is lower than that of SiC, Al_2O_3 and Si_3N_4. The CTE of VL20-derived $SiC_{0.68}N_{0.91}$ ceramics between 25°C-1000°C measured here (3.2×10^{-6}/K) is similar to the value reported by Ziegler *et al.* for similar material (3.0×10^{-6}/K) [99Zie]. The eutectic temperature between the filler materials and SiO_2 represent the temperatures of liquid phase formation during the oxidation of related PRC, and intimates their maximum application temperature in air.

The fabrication conditions of the SiC-PRC are described in chapter 1. Same conditions were used for the fabrication of PRC with the other filler materials except for the drying conditions of the pressed pellets before the impregnation of liquid precursor. Pellets of SiC

Table 2.1. Properties of filler material and Si-C-N matrix.

	Al_2O_3	Y_2O_3	Si_3N_4	SiC	Si-C-N
Powder designation	Taimei Chem.	H. C. Starck	UBE	H. C. Srarck	Kion
	Ultra pure	Grade C	SN E10	A-10	VL 20
Average particle size (d_{50}, μm)	1.70	4.48	0.55	0.51	-
Young´s modulus (GPa)	366	114	320	440	-
CTE (20-1000°C, 10^{-6}/K)	8.3	8.0	2.9-3.5	4.5-4.9	3.2
Eutectic temp. with SiO_2 (°C)	1587	1660	1726	1726	1726

and Si_3N_4 were dried in a graphite furnace at 1750°C for 2h in Ar (1.5 atm) and 0.5h in N_2 atmosphere (3 atm) respectively to completely remove moisture from the surface of the filler particles. Pellets of both oxide powders were dried at a much lower temperature (400°C) in a vacuum for 3h to prevent any sintering during the heat treatment. Based on the results of chapter 1, high purity argon which passed a gas purification system (oxisorb®, Messer) was used to suppress the oxidation of the samples during pyrolysis (pyrolysis condition: 5°C/min, 1350°C, 2h). The cycle of impregnation and pyrolysis was repeated six times to obtain sufficiently dense PRC. The samples were carefully handled during the whole process in closed systems in order to prevent any contact with air.

The ceramic yield of precursor with and without filler material was measured by TGA (Netzsch, STA 409, see chapter 1)

The relative density of samples received was estimated by measuring the dimensions of the samples and the weight gain after each impregnation/pyrolysis cycle as described in chapter 1. The diameter of pellets was measured after each cycle to determine the linear shrinkage. Phase formation within the PRC with different filler system was investigated by X-ray diffraction (XRD, D 5000, Siemens) using CuK_α radiation. In order to unify the area of X-ray radiation, the PRC were machined into disks with a diameter of 1cm. The surface area of the samples was measured by BET (Gemini, Micrometrics).

2.1.2 Mechanical and thermal properties

The mechanical properties of the PRC after the first and sixth impregnation/pyrolysis cycle were measured in order to understand the effect of different fillers. After the first cycle, the cutting rate of the samples was analyzed as a first mean of the measurement of mechanical properties of PRC. The equipment and conditions used for the measurement are described in chapter 1.

After the six impregnation/pyrolysis cycles, the strength, hardness, fracture toughness and morphology of the fracture surface of PRC were measured with the methods described in chapter 1. Young's modulus of the PRC was determined by a resonance frequency and damping analyzer (RFDA system 23, IMCE).

Netzsch STA 501 was used for the high-temperature TGA of the samples (Ar, 25-2100^{o}C, 3^{o}C/min) to measure the effect of the different filler material on the high temperature mass stability of PRC. Creep tests were performed with PRC samples ($2\times2\times8mm^3$) under a compressive stress of 100 MPa at 1350^{o}C (SiC-PRC: 1350^{o}C, 1400^{o}C) for 60h in air (Amsler DSM 6101).

2.2. Results and discussion

2.2.1 Effects of fillers on processing and phase formation of PRC

Table 2.2 shows selected properties of ceramic pellets obtained by cold isostatic pressing of filler powder and different numbers of subsequent impregnation/pyrolysis cycles.

Importantly, deterioration of the oxide-containing PRC was observed during the repeated impregnation/ pyrolysis cycles. For example, Y_2O_3-PRC could not be pyrolyzed for more than four process cycle because of the intensive cracking at the edge of the pellets. In contrast, such a phenomenon was not observed in PRC of the non-oxides. The possible reasons of cracking and its effect on the mechanical properties of oxide PRC will be described in the next paragraph.

After the first impregnation/pyrolysis cycle, the shrinkage of oxide-containing PRC is higher than those containing non-oxides. This is probably due to the reaction between the oxide filler and the Si-C-N matrix. XRD data indicate second phase formation in the oxide-containing PRC during pyrolysis (Al_2O_3-PRC: Si_5AlON_7, Y_2O_3-PRC: $Y_8Si_4N_4O_{14}$). Wan *et al.* [02Wan] reported that the shrinkage during sintering of Si-C-N compacts began at ~1300^{o}C when using Y_2O_3 as a sintering additive due to the formation of a low viscous phase and rearrangement of particles in the powder compact.

Table 2.2. Properties of powder pellets and pyrolyzed PRC. Properties of Y_2O_3-PRC were not measured after 6th process cycle because of their deterioration.

Filler System / Properties		Al_2O_3	Y_2O_3	α-Si_3N_4	α-SiC
Surface area (m^2/g)	ceramic pellet	12.1	12.9	11.0	11.1
	after 6th pyrolysis	10.2	-	13.2	8.5
Relative density (%)	ceramic pellet	55.0	55.2	51.3	60.6
	after 1st pyrolysis	65.1	68.9	62.4	70.0
	after 6th pyrolysis	88.7	-	78.6	90.6
Shrinkage after 1st pyrolysis (%)		1.4	2.5	0.2	0.1
Detected phases after 6th pyrolysis		α-Al_2O_3 β-Sialon	Y_2O_3 $Y_4Si_2N_2O_7$	α-Si_3N_4 α-SiC	α-SiC

Fig. 2.1 shows the XRD data of Al_2O_3-PRC after the first and sixth process cycle. Aside from Al_2O_3 reflections, peaks which correspond to Si_5AlON_7 (β-Sialon) are visible. Their intensity increases with the number of impregnation/pyrolysis cycles. As the number of process cycles increases, the amount of Si-C-N matrix in the PRC increases, and so does that of second phase formed by the reaction between filler and matrix. The Si-C-N matrix might have reacted with Al_2O_3 and with SiO_2 in the matrix originated from the contamination of oxygen (0.4 wt%) during the fabrication process, and β-Sialon (Si_5AlON_7) was formed as a result. Naik *et al.* [78Nai] reported the formation of β-Sialon after sintering of powder mixtures composed of Si_3N_4, AlN, Al_2O_3 and SiO_2. In the present experiment, formation of β-Sialon occurred presumably by the reaction between amorphous Si-C-N, Al_2O_3 and amorphous SiO_2 contamination.

Y_2O_3-PRC also formed a secondary phase ($Y_4Si_2N_2O_7$) after pyrolysis at 1350°C. Gauckler *et al.* [80Gau] reported the formation of $Y_4Si_2N_2O_7$ at 1500°C by the reaction between Si_3N_4, Y_2O_3, and SiO_2.

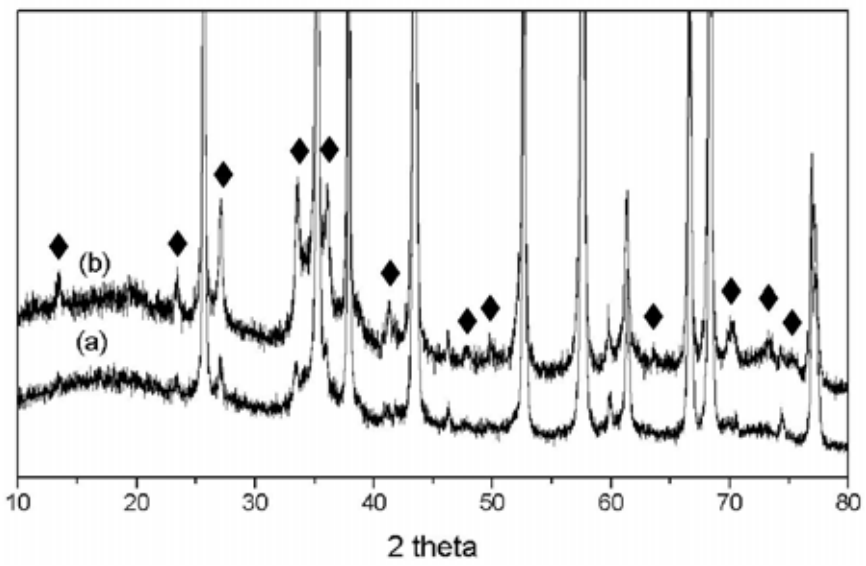

Fig. 2.1: XRD patterns of Al_2O_3-PRC after first (a) and sixth (b) process cycle. Reflections of Si_5AlON_7 (♦) are observed beside Al_2O_3 (the other peaks). The intensity of Si_5AlON_7 reflections increases with increasing number of process cycles.

In Si_3N_4-PRC, crystallization of SiC occurred, either, due to the reaction of Si_3N_4 according to reaction (1.4) and/or the crystallization of the amorphous as-thermolyzed Si-C-N matrix (Table 2.2). In contrast, XRD peaks of SiC or Si_3N_4 due to the crystallization of the Si-C-N matrix are detected neither in the oxide-containing PRC nor in the SiC-PRC.

Fig. 2.2 shows the relative density of PRC as a function of the number of impregnation/pyrolysis cycles. Y_2O_3-PRC showed the highest increase in relative density after the first pyrolysis step due to a large shrinkage (Table 2.2). During the following pyrolysis cycles, however, Y_2O_3-PRC revealed substantial weight loss due to the cracking at the edge of the pellets mentioned above. Among the PRC investigated, SiC-PRC have advantages in terms of both the relative density and low shrinkage during pyrolysis (Table 2.2).

Fig. 2.3 shows TGA curves of samples of cross-linked Si-C-N precursor and pellets of different filler materials impregnated with the same precursor. The pellets show almost similar weight losses except Si_3N_4-PRC. The pronounced weight loss of Si_3N_4-PRC is most probably a consequence of the low relative density of the ceramic pellets (Table 2.2), thus more space available for the precursor which loses weight during pyrolysis. The ceramic yield at 1350°C and the onset temperature of decomposition of the precursor in PRC are lower than those of pure precursor (Si-C-N: 81.7%, Al_2O_3-PRC: ~76%, Y_2O_3-PRC: ~77%, Si_3N_4-PRC: ~74%, SiC-PRC: ~74%).

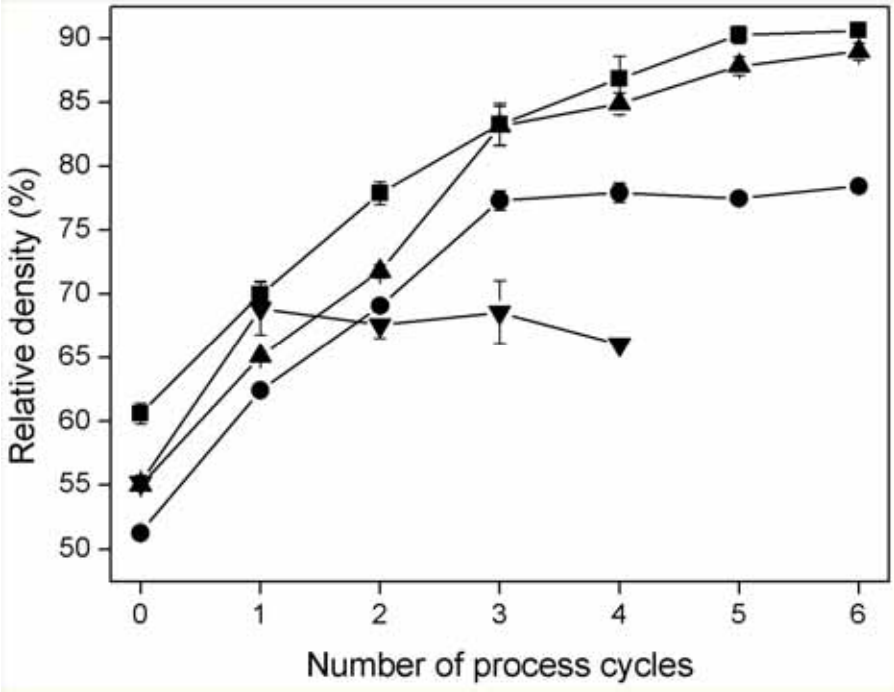

Fig. 2.2: Relative density of PRC as a function of the number of impregnation/pyrolysis cycles (▲ Al_2O_3-PRC, ▼ Y_2O_3-PRC, ● Si_3N_4-PRC, ■ SiC-PRC)

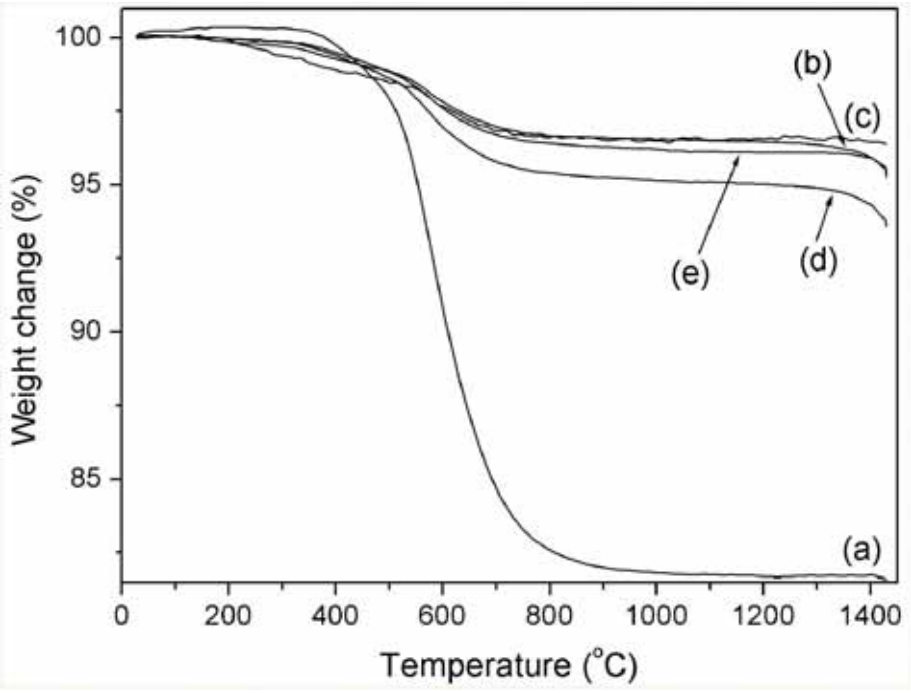

Fig. 2.3: TGA of precursor and particulate-reinforced green bodies: (a) pure Precursor, (b) Al_2O_3-PRC, (c) Y_2O_3-PRC, (d) Si_3N_4-PRC and (e) SiC-PRC (100ml/min Ar flow, heating rate: 5°C/min)

The weight loss of Si-C-N precursor in PRC was calculated based on the assumption that the filler material itself does not decompose during pyrolysis. In fact, except for SiC, reactions of the filler materials with free carbon, which is present in the Si-C-N matrix, have to be considered. Al_2O_3 may cause weight loss above 1350°C in N_2 due to the following reaction [94Che]

$$Al_2O_{3(s)} + 2\ C_{(s)} \rightarrow Al_2O_{(g)} + 2\ CO_{(g)}. \quad (2.1)$$

The decomposition of Y_2O_3 begins in Ar at 1327°C according to [95Bla]

$$Y_2O_{3(s)} + 7\ C_{(s)} \rightarrow 2\ YC_{2(s)} + 3\ CO_{(g)}. \quad (2.2)$$

Si_3N_4 reacts with free carbon in Si-C-N according to reaction (1.4). At 1 atm N_2 the reaction temperature is 1484°C [99Sei]. Lower N_2 partial pressure results in decreased decomposition temperature [02Pen]. However, SiC-PRC, in which no decomposition reaction between filler and matrix is expected, show a similar weight loss as the PRC with other filler materials. Therefore, it is believed that the decomposition reactions between filler and matrix do not intensively occur during pyrolysis up to 1350°C.

PRC have more pronounced weight loss above 1350°C than bulk Si-C-N ceramic. The possible reasons for this behavior were described in detail in chapter 1 (see page 14).

2.2.2 Mechanical properties of PRC

Fig. 2.4 shows the cutting rate of PRC after the first pyrolysis. Non-oxide PRC exhibited a six to eight times higher cutting rate than oxide PRC, whereas the cutting rate was not strongly affected by the relative density of the PRC (Table 2.2). The linear shrinkage of PRC during further impregnation/pyrolysis cycles was measured to understand the higher cutting resistance of PRC with oxides as compared to those with non-oxides (Fig. 2.5). Oxide PRC shrink by 1.5 - 2.5% during the first pyrolysis and reveal a total shrinkage of 2.2 - 7.5% after six cycles. The total shrinkage of non-oxide PRC is less than 0.5%. Presumably, the increased shrinkage and second phase formation during the first pyrolysis is responsible for the enhanced cutting resistance of oxide containing PRC in this stage

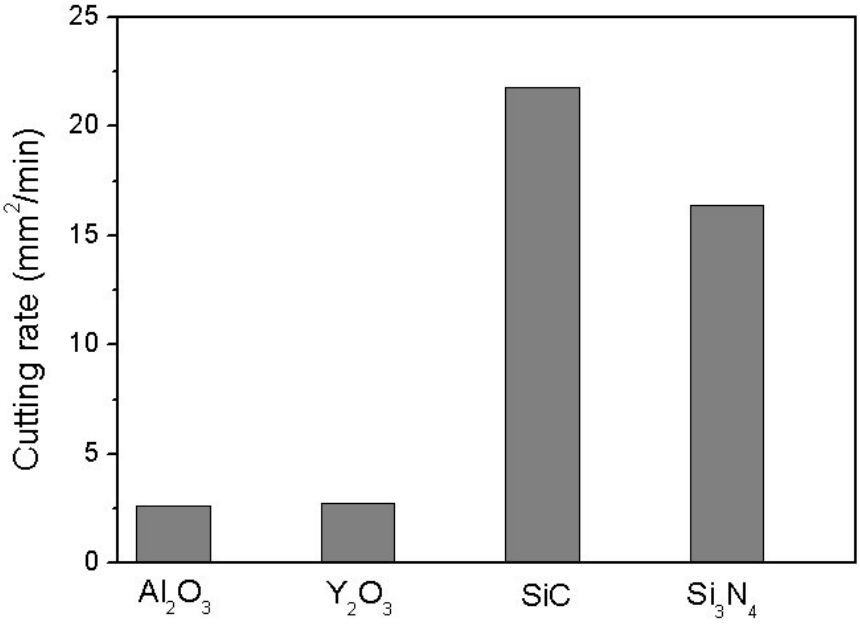

Fig. 2.4: Cutting rate of the PRC after the 1st impregnation/pyrolysis cycle

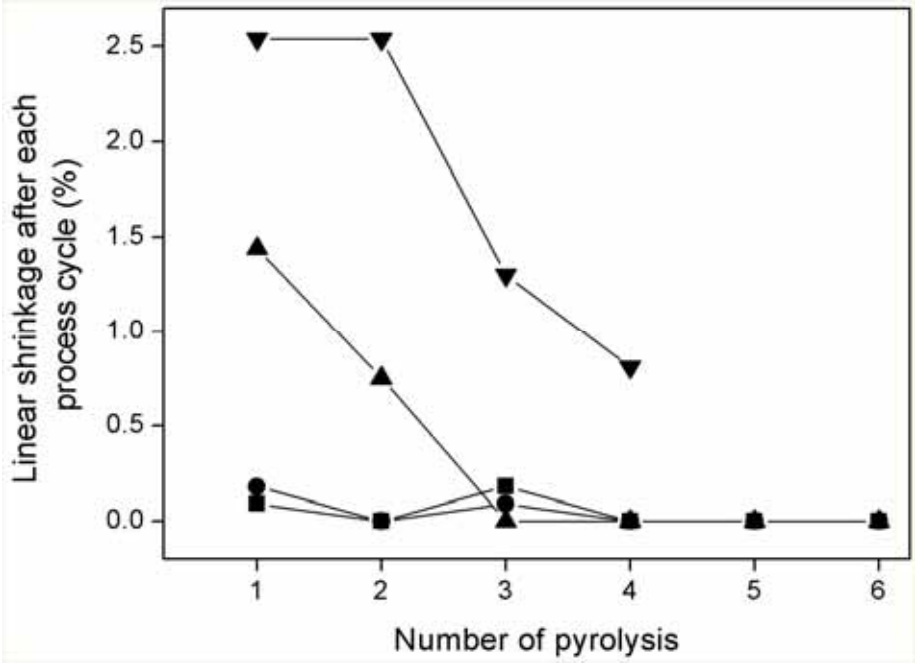

Fig. 2.5: Linear shrinkage of PRC with increasing number of impregnation/pyrolysis cycles (▲: Al_2O_3-PRC, ▼: Y_2O_3-PRC, ●: Si_3N_4-PRC, ■: SiC-PRC)

During the machining of testing samples which were obtained after six PIP cycles, however, all Y_2O_3-PRC and ~30% of Al_2O_3-PRC specimens broke due to flaws which have been formed during pyrolysis. After pyrolysis, mud-cracking appearances were observed on the surface of all PRC. Tu *et al.* [95Tu2] reported that the cracking was possibly initiated during

cross-linking of the precursor layer remained at the surface of the PRC. The cracks proceeded further into the interior during pyrolysis.

Si-C-N ceramics have a similar CTE to non-oxide fillers (Si_3N_4: 2.9-3.5×10^{-6}/K, SiC: 4.5-4.9×10^{-6}/K). In contrast, oxide fillers have much larger CTE values (~8×10^{-6}/K) than Si-C-N matrix. The difference of CTE between Si-C-N matrix and oxide fillers (~5×10^{-6}/K) induces stresses during cooling [94Kag]. The large difference between the CTE of filler and that of the matrix, together with the shrinkage and second phase formation during thermolysis presumably enhanced the crack propagation of oxide containing PRC. In contrast, non-oxide PRC have similar CTE as precursor-derived Si-C-N, and show much lower shrinkage than oxide PRC during pyrolysis.

The mechanical properties of dense PRC are affected by the total porosity. Several models have been proposed to explain the relationship between porosity and mechanical properties. This can be explained in many cases by the minimum solid area (MSA) model [98RiC]. The model proposes a relationship between mechanical properties and porosity with proportionality higher than one:

$$\frac{H}{H_0} \sim \frac{E}{E_0} \sim e^{-bP}. \qquad (2.3)$$

H: hardness of porous sample, H_o: hardness of dense material,
E: Young's modulus of porous sample, E_o: Young's modulus of dense material, P: porosity,
b: semilog slope of the property dependence over the initial range of porosity [98Ric].

Typically, Young's modulus decreases substantially with increasing porosity. In this study, Young's modulus of PRC was affected also by the type of filler: the higher the Young's modulus of filler and the relative density is, the higher is the E value of the PRC (SiC > Al_2O_3 > Si_3N_4, Table 2.3). Rice pointed out that hardness is more dependent on porosity, *i.e.*, b values of 6 ± 3 versus 4 ± 2 than on the elastic modulus [77Ric]. This strong dependence of porosity may explain the higher hardness of dense Al_2O_3-PRC compared to Si_3N_4-PRC, even though the hardness of Si_3N_4 is higher than that of Al_2O_3. Fracture toughness of all PRC investigated was 3.2-4.0 MPa·$m^{1/2}$. Bauer *et al.* [01Bau] measured the fracture toughness of Si-C-N ceramics obtained from polysilazane CERASET^{TM} using an indentation technique and reported K_{IC} to be 2.5 MPa·$m^{1/2}$. Obviously, fracture toughness is improved by the presence of

Table 2.3. Mechanical properties of PRC after the 6th PIP cycle

	Al_2O_3-PRC	Si_3N_4-PRC	SiC-PRC
Young's modulus (GPa)	181	163	240
Hardness (Hv)	1439	989	1622
Fracture toughness ($MPa \cdot m^{1/2}$)	3.2	3.2	4.0
Strength (MPa)	405	420	525
Standard deviation	147	62	70

second phase particles as it is generally true for brittle materials. Nair *et al.* [92Nai] reported the critical requirements for particulate toughening as:

(1) the particle must be well bonded to the matrix, and (2) the particle material should have a larger coefficient of thermal expansion than matrix.

At least the latter criterion is fulfilled by all the fillers which have a higher or a similar CTE compared to the Si-C-N matrix.

SiC-PRC had the highest strength. The strength of Al_2O_3-PRC was lower than that of Si_3N_4-PRC in spite of its higher relative density. Different from the other mechanical properties such as young's modulus and hardness, the level of tensile (and bending) strength of porous ceramics has been reported to be decided mainly not by the porosity but by the flaw size and flaw character [00Ric]. The results intimate that the flaws formed during pyrolysis of oxide PRC, which was mentioned above, decreased the strength of Al_2O_3-PRC. Al_2O_3-PRC also had a higher standard deviation of strength (Table 2.3), most probably due to the high flaw density and broader flaw size distribution.

Fig. 2.6 shows the morphology of the fracture surfaces. Al_2O_3-PRC revealed both inter- and transgranular fracture behavior, while transgranular fracture was dominant in Y_2O_3-, Si_3N_4- and SiC-PRC. In Al_2O_3-PRC, the fracture mode is mainly intergranular for finer grains, and in accordance with the report of Rice [00Ric], it is shifted to the transgranular mode as grain size increases. Transgranular fracture facet, which has been reported in coarse grained alumina [02Dan], was observed in Al_2O_3-PRC. SiC filler could not be differentiated from Si-C-N matrix in the fracture surface of SiC-PRC.

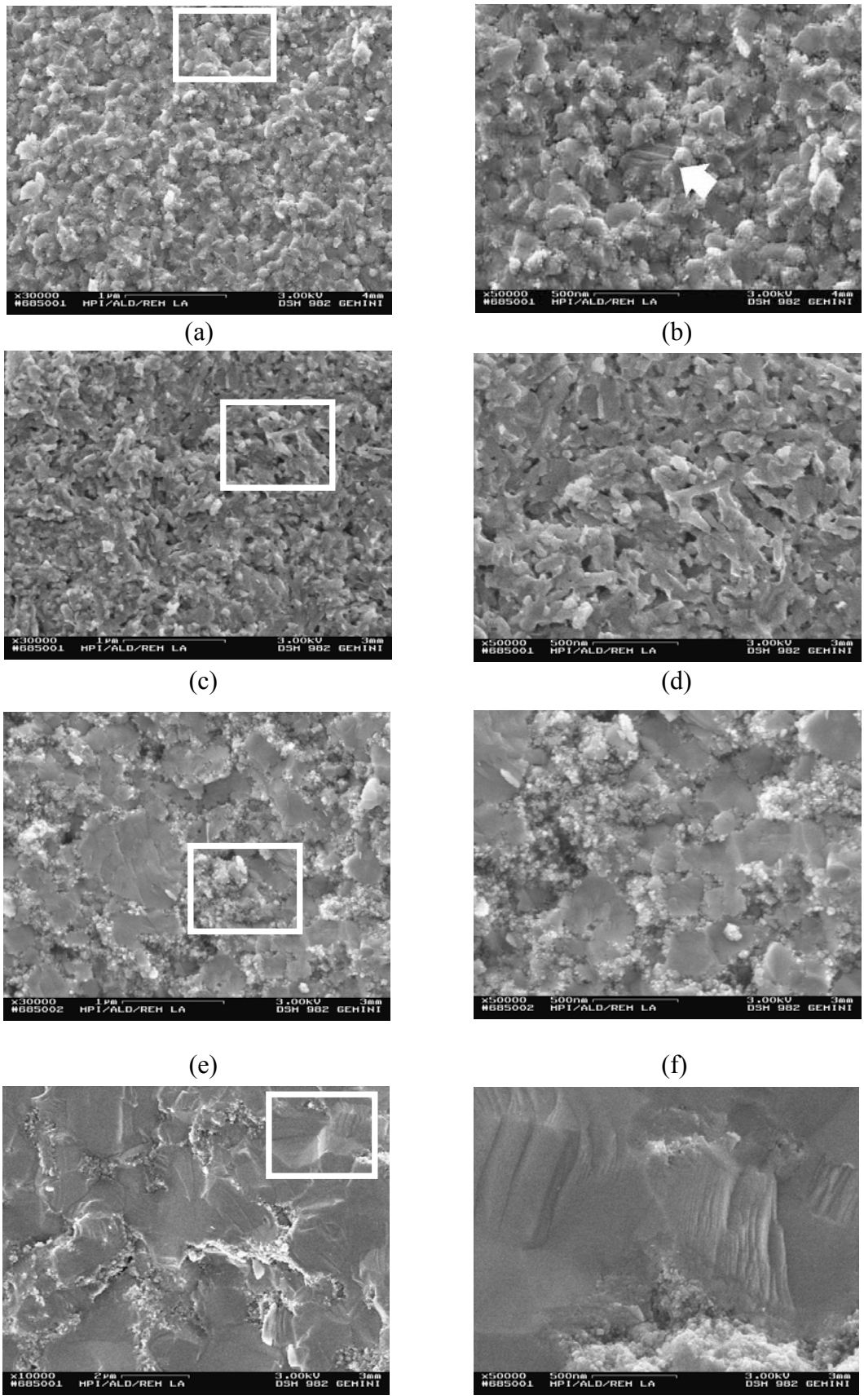

Fig. 2.6: Morphology of the fracture surfaces of PRC after 6 process cycles: (a) and (b) Al_2O_3, (c) and (d) Y_2O_3, (e) and (f) Si_3N_4 and (g) and (h) SiC (⇨: Transgranlar fracture facet)

The results show that among the PRC investigated, SiC-PRC have the highest Young's modulus, hardness, fracture toughness and strength after the six PIP cycles (Table 2.3).

2.2.3 High temperature properties of PRC

Fig. 2.7 shows the high temperature TGA of Si-C-N and different PRC after six PIP cycles. The weight loss of particulate-free Si-C-N ceramics started at 1400°C, which became less intensive above 1700°C. The total weight loss at 2000°C was 26.0%. Al_2O_3-, Y_2O_3- and Si_3N_4-PRC exhibited rapid weight losses above 1400°C due to the decomposition of the Si-C-N matrix and by reaction (2.1), (2.2) and (1.4). In addition, the temperature of the decomposition of Si_3N_4 in Si_3N_4-PRC according to

$$Si_3N_{4(s)} \rightarrow 3Si_{(s)} + 2N_{2(g)} \qquad (2.4)$$

is depending on the N_2 partial pressure.

Considering the partial pressure of N_2 in Ar as $\sim 10^{-4}$ bar (purity of Ar: 99.998%), reaction (2.4) is expected at around 1300°C [01Sei].

SiC-PRC showed up to 2100°C by far the best high temperature stability among the PRC investigated. Different from the other PRC, the weight loss of SiC-PRC originated only from the decomposition of Si-C-N matrix. Consequently, the weight loss behavior is in principle similar to that of pure Si-C-N except for the amplitude (Fig. 2.7 (a) and (e)).

Fig. 2.8 shows the creep behavior of the PRC with different filler materials. In each case the strain rate decreases with time even after 60h of testing, and total strain was as low as 0.21% in the case of SiC-PRC. This behavior is somewhat in agreement with results gained with particulate-free Si-C-N reported by Thurn *et al*. [99Thu]. They measured the compressive creep strain of annealed (1400°C, 20h) Si-C-N ceramics at 1400°C with 100 MPa and reported that the strain was only about 0.25% after 2×10^5 seconds. The compressive creep resistance of PRC was mainly controlled by the deformation of filler compacts. The creep rate of Al_2O_3, Si_3N_4 and SiC densified without sintering additives were reported as 8×10^{-5} [95Wie], 8×10^{-6} [78Gra], and 9×10^{-7}/s [92Hoc], respectively, at 1300°C with 100 MPa loading. This is in agreement with Wiederhorn *et al.* [88Wie]. They measured the compressive creep behavior of siliconized silicon carbide (Si/SiC) near the melting temperature of silicon and reported that the compressive creep was mainly controlled by the deformation of the hard SiC particles. In addition, the creep rate of Al_2O_3-PRC may be affected by the shrinkage of the PRC at high temperatures (Fig. 2.5).

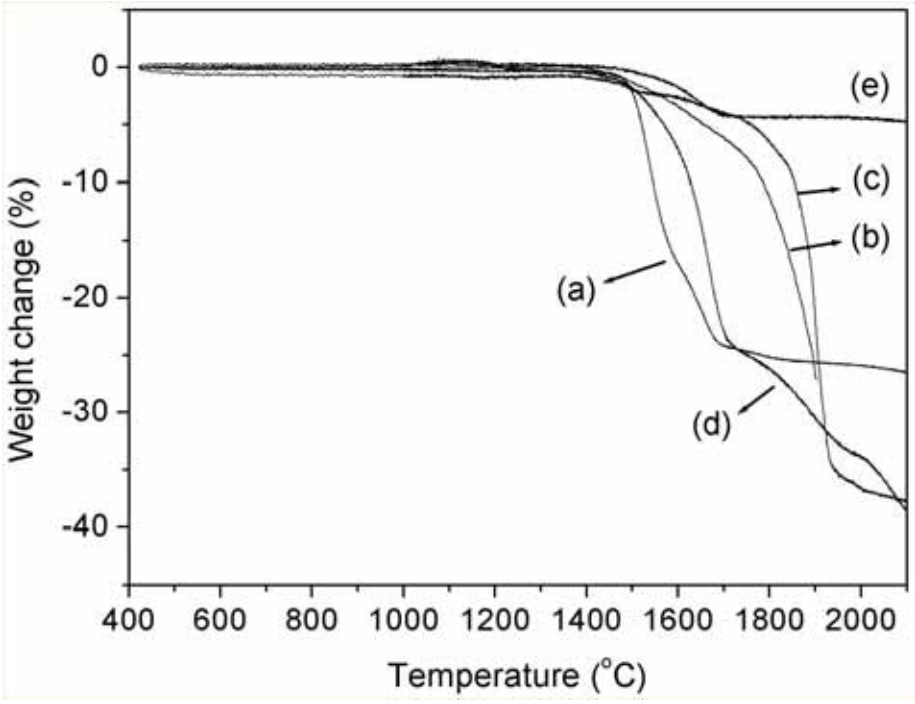

Fig. 2.7: High temperature TGA of (a) pure Si-C-N, (b) Al_2O_3-PRC, (c) Y_2O_3-PRC, (d) Si_3N_4-PRC and (e) SiC-PRC (100ml/min Ar flow, heating rate: 3°C/min)

Based on the above-reported results on processing (relative density), mechanical (Young's modulus, hardness, fracture toughness, and strength) and thermal properties (thermal stability, creep resistance) of the PRC, SiC is the most promising one for the fabrication of FRC among the four filler material investigated.

2.3. Summary and Conclusions

From the investigations about the effects of types of filler materials on the processing, mechanical and thermal properties of particulate-reinforced ceramic composites (PRC), the following conclusions can be drawn:

Oxide fillers reacted with Si-C-N during pyrolysis, and volume shrinkage together with secondary phase formation (Si_5AlON_7, $Y_8Si_4N_4O_{14}$) occurred during pyrolysis. The amount of secondary phases increased with the number of impregnation/pyrolysis cycles. Oxide-containing PRC displayed a better cutting resistance after the first pyrolysis than those containing non-oxides, but deterioration by flaw formation was observed after repeated pyrolysis cycles in oxide-containing PRC. Presumably, the different CTE between filler material and matrix material (Al_2O_3: 8.3×10^{-6}/K, Y_2O_3: 8.0×10^{-6}/K, Si-C-N: 3.2×10^{-6}/K) and reactions between them induce flaws in oxide PRC during thermolysis. SiC-PRC showed the

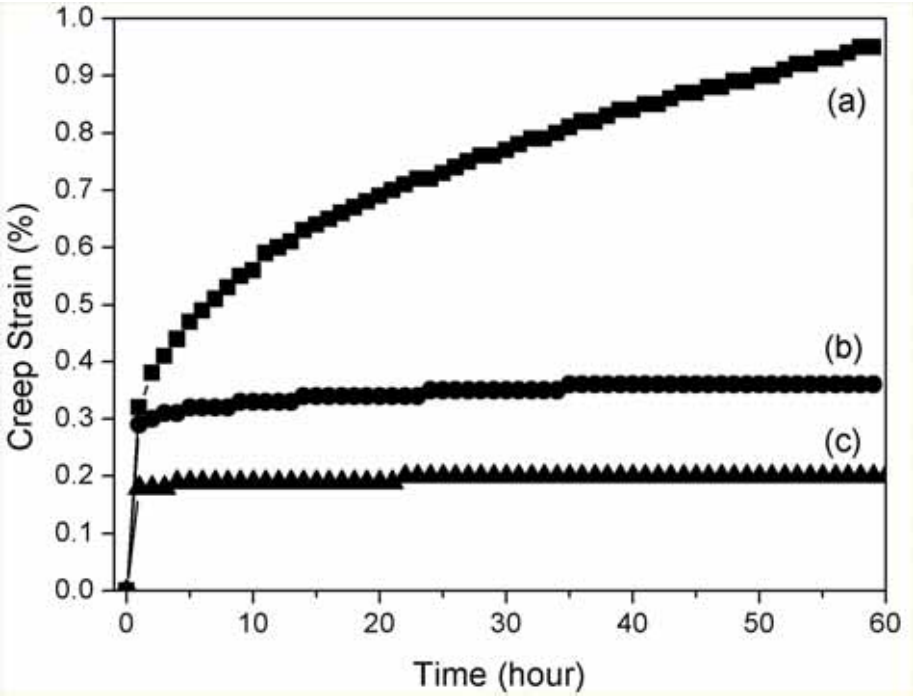

Fig. 2.8: Creep behavior of PRC under compression with different filler systems (a) Al_2O_3-PRC, (b) Si_3N_4-PRC and (C) SiC-PRC (1350^oC, 100MPa)

highest values of relative density, strength, Young's modulus, hardness, and fracture toughness among the four types of PRC after densification. SiC-PRC also offered the lowest weight loss and highest creep resistance at high temperature. The results clearly shows that SiC is the most appropriate filler material for high temperature FRC among the systems investigated.

3. Novel processing technique for improved infiltration of stacked woven fabrics with particle filler materials

The process to fabricate composites by PIP technique was optimized in chapter 1, and an adequate filler material was selected in chapter 2. Based on that, in this chapter, a novel technique for the homogeneous impregnation of the filler material into fiber-woven fabrics will be developed.

PIP method has been investigated as a low temperature fabrication technique for FRC [95Lan]. The general procedure of this technique is to impregnate woven fabrics with a liquid precursor using vacuum and/or pressure casting, to cross-link the impregnated precursor by heat or UV light, and to pyrolyze the composite at temperatures in the range of 1000^{o}C - 1400^{o}C.

Because of degassing and shrinkage of the precursor during pyrolysis, impregnation and pyrolysis cycles must be repeated several times to obtain sufficiently dense composites [99Zie]. This repetition is time-intensive and increases processing costs. It has been shown that the number of impregnation/pyrolysis cycles can be decreased by increasing the relative density of stacked woven fabrics with filler materials such as SiC [95Gre]. However, homogeneous infiltration of highly concentrated slurry into stacked woven fabrics is still a challenging research topic. Singh *et al.* [88Sin] proposed to dip individual woven fabrics into a slurry of such powders and subsequently to stack the infiltrated fabrics to guarantee for homogeneous distribution. Donato *et al.* [96Don] improved this technique by using slurries mainly composed of filler and a liquid precursor. However, these techniques have a limitation such that the large free space between the individual woven fabrics can not be completely filled by the filler material, because the fabric is infiltrated separately.

Accordingly, in this chapter, a novel technique to get over this problem was developed. The effect of a deformable foil, which is attached to the mold during pressure infiltration, on the infiltration behavior of concentrated SiC slurry into stacked woven fabrics was investigated.

3.1. Experimental procedure

Fig. 3.1 shows schematic views of the conventional and of the novel process. The difference between the mold used in conventional vacuum/pressure casting (termed press-casting) [92Kre] and the modified technique (termed deform-casting) applies a deformable foil at the bottom of the casting mold. PVC foils can be used for the deformable mold if no further heat treatment is required after the infiltration of concentrated slurries into 2D-woven fabrics.

However, thermally stable materials, such as teflon or aluminium, must be used if thermal cross-linking of the liquid precursor is needed.

In highly loaded slurries, the movement of particles around each other requires time. Above a particular shear rate, the hindered rotation and particle interference may cause shear-thickening [95Lee]. Also the interspaces between the woven fabrics are very narrow. Therefore, the penetration of concentrated slurries into the fabrics is hindered by to shear-thickening if the fabrics are closely tight (Fig. 3.1 (a)). In contrast, in the modified process, outward deformation of the foil may allow a volume increase between the stacked fabrics during infiltration (Fig. 3.1 (c)) which may suppress the shear thickening of concentrated slurries and thereby the infiltration behavior can be improved.

For infiltration, 12 layers of 2D-woven carbon fabrics (T300J 3K, Toray) [Toray] coated with pyrocarbon (size of the stacked fabrics: 35×35×6 mm) were stacked in the mold. After the mold was closed, a slurry composed of SiC powder dispersed in water was introduced. A rotary pump was used to evacuate the mold, and subsequent infiltration of the slurry into the woven fabrics was enhanced by applying an Ar gas pressure of 1.25 bar.

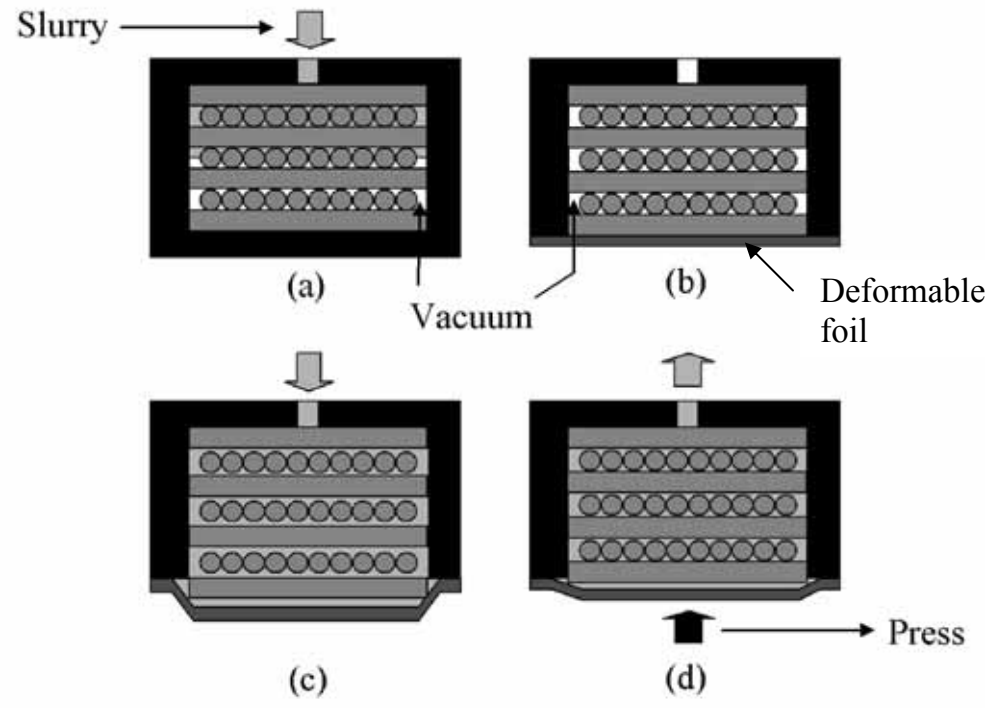

Fig. 3.1: Schematic of conventional resin-transfer-molding (RTM) and modified process. (a) conventional fixture of a firm mold. Woven fabrics suppress the infiltration of slurry. (b) mold with a deformable foil at the bottom, before infiltration. (c) volume increase of stacked fabrics during infiltration by outward deformation of the foil. (d) removal of excess slurry by pressing the foil.

For further enhancement of the infiltration, the rheology of highly filled aqueous SiC slurries was adjusted. At first, polyethylenimine (PEI, M_W ~25,000) as a dispersant was investigated. The zeta potential of suspensions with 1.3 wt% PEI was monitored using a zeta potential probe (Zetamaster, Malvern), and the influence of pH (6.5 - 9.3) on the viscosity of concentrated slurries (30 vol% SiC, 1.5 wt% PEI) was measured using a viscometer (SR-500, Rheometrics).

Using the optimized pH conditions, slurries with 30, 33, 35, 37, 40, 43 or 45 vol% SiC were prepared and the infiltration behavior of the slurries using conventional (press-casting) and modified technique (deform-casting) was compared. The true density and relative density of the C_{fiber}/SiC_{filler} compact were estimated using the method described in chapter 1. After infiltration, the molds were evacuated to remove the entrapped gas, and dried at 80^oC in an oven for 24h to remove the water. Then the weight of the infiltrated filler was estimated by comparing the weight of the dried mold before and after the infiltration. Before the impregnation of the oxygen-sensitive liquid precursor (VL20), the molds were intensively dried at 350^oC in vacuum to minimize residual moisture in the filler-incorporated woven fabrics.

Liquid Si-C-N precursor was diluted with tetrahydrofuran (1 : 1 by volume) in order to decrease its viscosity. The solution was subsequently transferred into the mold containing the stacked and SiC filler impregnated fiber fabrics termed C_{fiber}/SiC_{filler} compact. After the impregnation, the mold was evacuated and the solvent was removed by distillation at 40^oC for 6h. The mold was then capped and put into a sealed metal can for the cross-linking of the precursor at 430^oC for 6h.

The cross-linked samples were demolded within a glove box, and pyrolyzed at 1350^oC for 2h in purified Ar using an alumina tube furnace. During all impregnation/pyrolysis cycles, the samples were handled in an inert gas atmosphere to avoid contact with air. Finally, the microstructure of FRC after ten impregnation/pyrolysis cycles was analysed with scanning electron microscopy (SEM, Jeol, JSM-6400).

3.2. Results and discussion

3.2.1 Fabrication of SiC slurries

In order to obtain highly filled woven carbon fiber fabrics, the solid loading of the slurry used for infiltration should be high whereas its viscosity should be low. Both issues are usually contradictory.

The optimum pH of aqueous SiC slurry without dispersant has been reported to be 11 [97Ken]. However, controlling the pH into high values is not desirable, because residuals of

the base, *e.g.* KOH, which is added to increase the pH of the slurry, can react with the precursor in use [Kion]. Additionally, the surface of SiC powder is covered with SiO_2 formed by oxidation and/or hydrolysis. SiO_2 is reported to dissolve under alkaline conditions above pH 9, which may affect the colloidal stability of the suspension [01Pai].

Therefore, a dispersant was applied to decrease the optimum pH of the slurry to ~7. Before the application, however, possible reactions between the precursor and different dispersants have been taken into account. PEI (Fig. 3.2) was selected because it does not contain oxygen which may react with the precursor to form SiO_2 after pyrolysis [01Li1].

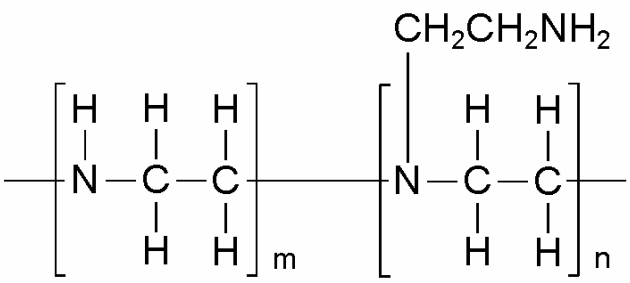

Fig. 3.2: Molecular structure (idealized) of polyethylenimine (PEI)

Fig. 3.3 shows the zeta potential values of the SiC slurries dispersed with PEI versus pH. The iso-electric point (IEP) is at pH 9.7, and the maximum zeta potential value (36mV) was obtained at pH 6.5.

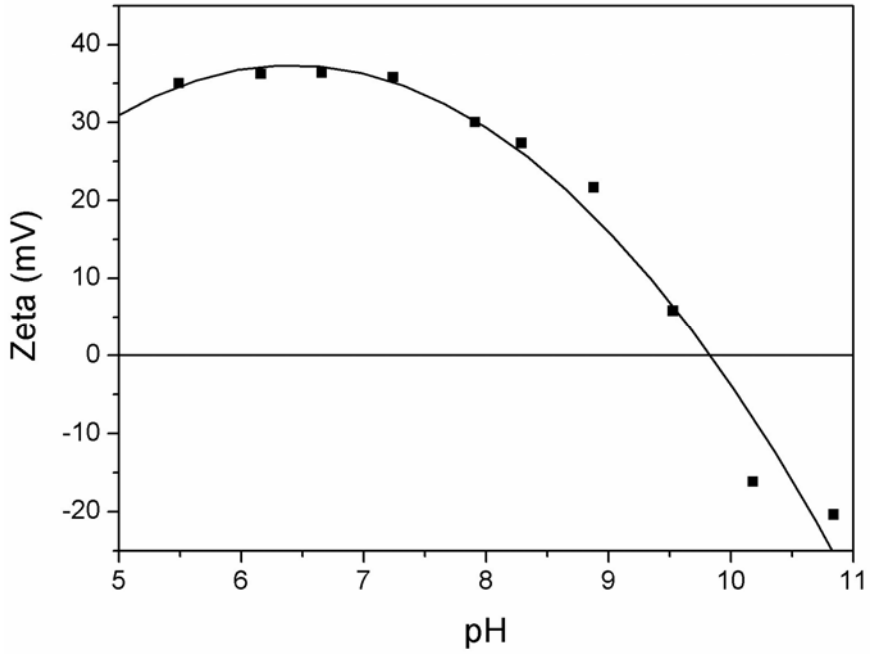

Fig. 3.3: Zeta potential values of aqueous SiC slurries with 1.3 wt% PEI vs. pH

The results on the viscosity studies are summarized in Table 3.1. The viscosity of a concentrated (30 vol%) SiC slurry at pH 6.5 with 1.5 wt% of PEI was lower than that at higher pH by the application of optimal dispersant. Based on these results, the pH of SiC slurries with PEI dispersant were controlled to 6.5 before infiltration.

3.2.2 Infiltration behavior

Fig. 3.4 shows the relative density of C_{fiber}/SiC_{filler} compacts after the infiltration of slurries as a function of solid loading. With conventional press-casting, the relative density of the compacts decreased with increasing solid loading. This might be due to the increase of viscosity with solid loading which strongly suppressed the infiltration of slurries during conventional press-casting. The slurries even did not fully penetrate into the woven fabrics if solid loading exceeded 30 vol% (Fig. 3.5). It turned out that the slurry could not penetrate to the third layer (out of 12) when the solid loading of the slurry was higher than 37 vol%.

In contrast, concentrated slurries with solid loading of up to 43 vol% were homogeneously penetrated into the fabrics using the deform-casting method (Fig. 3.5 (e)). The relative density of the C_{fiber}/SiC_{filler} compacts increased with increasing solid loading (Fig. 3.4 (b)). After drying, the compact was separated from the mold, and was split into 12 layers to check the inside of the samples. A homogeneous distribution of filler was observed throughout the entire sample. A maximum relative density of 72% was obtained by using the 43 vol% slurry. This substantial improvement against press-casting can be understood into a way that during deform-casting, the foil deformed outward by the applied infiltration pressure, and so the spacing between the fabrics increased, thus decreasing shear-thickening of the slurry. After the infiltration, excess slurry was removed by applying pressure to the deformable foil, thus narrowing the fabrics again (Fig. 3.1 (d)). However, the slurry between the woven fabrics was not removed completely, thus the distance between the fabrics is slightly increased but

Table. 3.1 Viscosity (Pa·s) of 30 vol% SiC slurries (+1.5 wt% PEI) with pH

Shear rate(s^{-1})	1	10	100
pH 6.5	0.155	3.4×10^{-2}	1.1×10^{-2}
pH 7.5	0.186	3.9×10^{-2}	1.2×10^{-2}
pH 8.3	0.248	5.1×10^{-2}	1.5×10^{-2}
pH 9.3	0.301	5.9×10^{-2}	1.9×10^{-2}

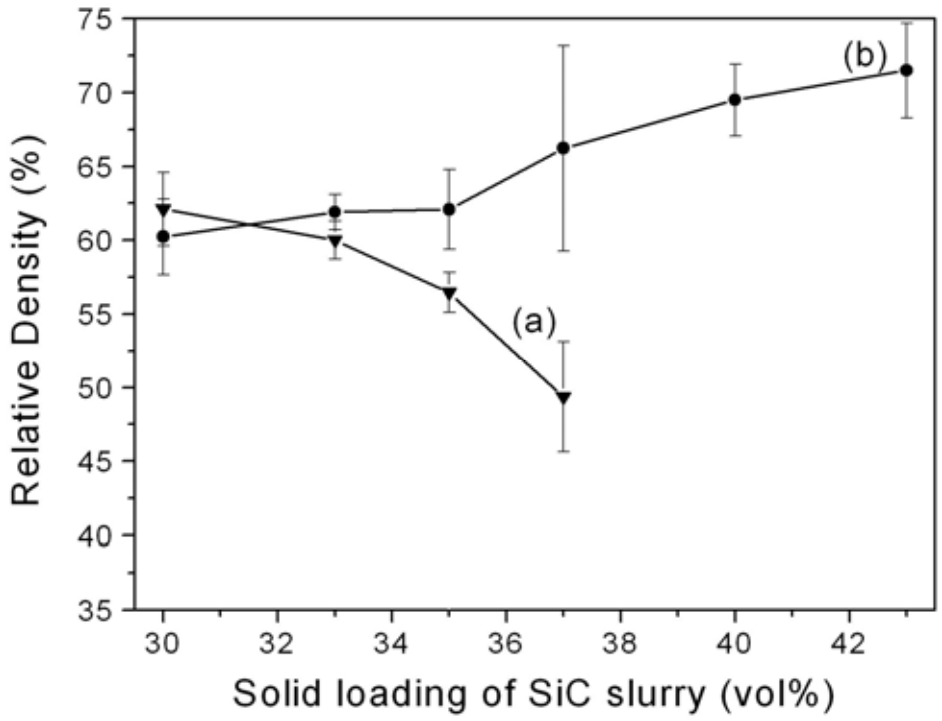

Fig. 3.4: Relative density of C_{fiber}/SiC_{filler} compacts after the infiltration of SiC slurries with different solid loading into 12 layers of carbon fiber fabrics. (a) press-casting and (b) deform-casting

with the benefit that the space between them was completely filled and the filler particles are more densely packed. Therefore, the samples obtained by the deform-casting method were somewhat thicker than the samples obtained by press-casting.

3.2.3 Fabrication of FRC

Fig. 3.6 shows a rather uniform microstructure of the FRC after ten impregnation/pyrolysis cycles. As for the microstructure of ceramic matrix composites made by PIP technique without filler, it has been reported that small spaces between fibers were easily filled by the precursor-derived ceramic matrix, whereas large voids between the woven fabrics were often not completely filled even after several impregnation/pyrolysis cycles [98Tak]. In the present investigation, the cavities between the woven fabrics were completely filled by the fillers and precursor-derived ceramic matrix as a result of the homogeneous infiltration of the slurry into the woven fabrics by the procedure explained in Fig. 3.1. However, some flaws remained even after ten process cycles. A locally insufficient infiltration is believed to be the main reason for the flaw formation.

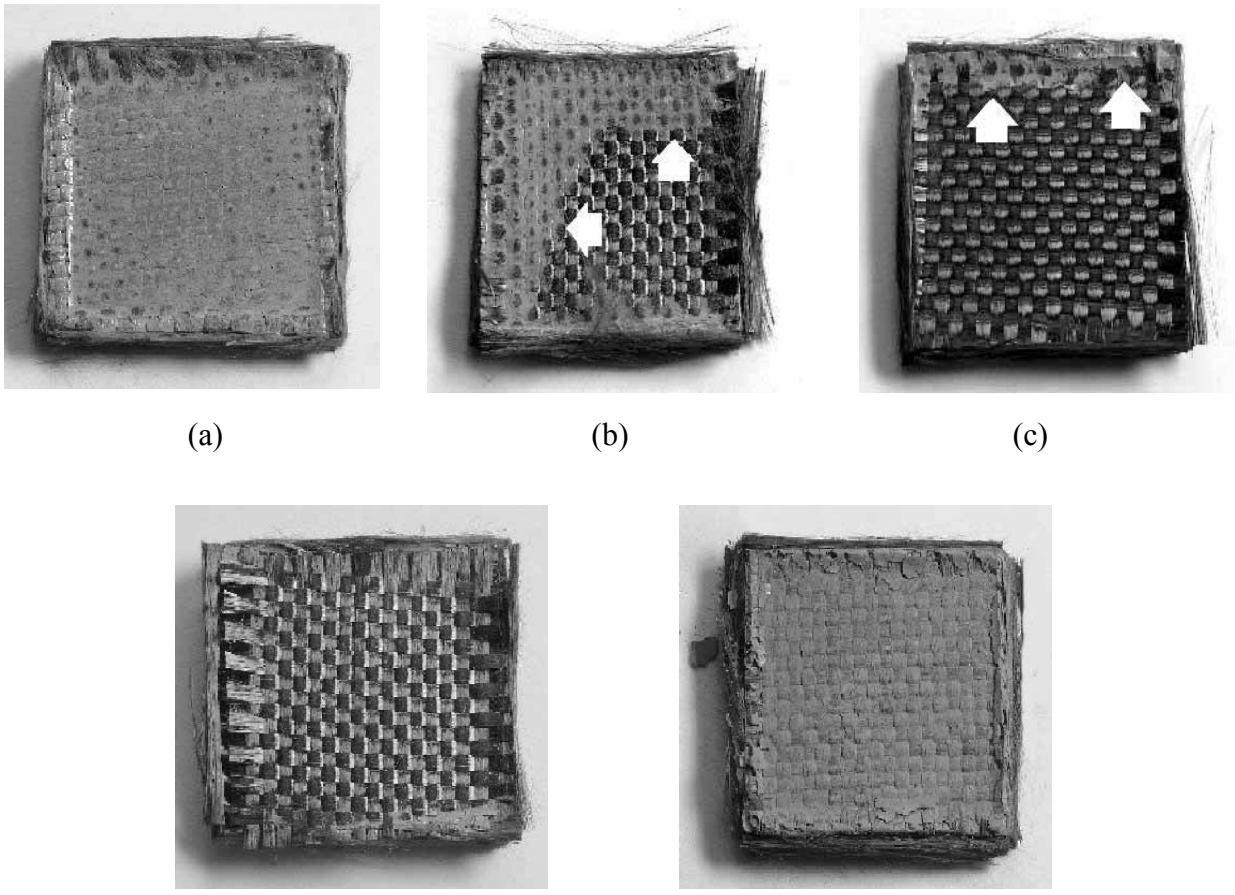

Fig. 3.5: C_{fiber}/SiC_{filler} compacts after infiltration of SiC slurry with different solid loading using press-casting (a) 30 vol% SiC, (b) 33 vol% SiC, (c) 35 vol% SiC, and (d) 37 vol% SiC, and (e) deform-casting, 43 vol% SiC. The image shows the bottom of the specimens. Infiltration was performed from the opposite side. Infiltration using press-casting occurred sufficiently only with low viscous 30 vol% SiC slurry. In contrast, homogeneous impregnation could be achieved using deform-casting method even if 43vol% slurry was used. (⇨: infiltrated area)

3.3. Summary and Conclusions

A new technique for the homogeneous infiltration of concentrated slurries of filler into 2D-woven fabrics of carbon fiber has been developed. Compared to conventional pressure casting, the infiltration behavior was improved by applying a flexible mold. Highly solid-loaded slurries having even 43 vol% SiC were homogeneously infiltrated into stacked 2D woven fabrics by a modified pressure casting technique using a deformable mold. The suppression of shear thickening of concentrated slurries is believed to be the main reason for the improved

infiltration behavior. The relative density of the C_{fiber}/SiC_{filler} compact fabricated by this modified technique was ~72%. Following precursor impregnation and pyrolysis (PIP) process resulted in fiber-reinforced composite with ~92% relative density after 10 impregnation/ pyrolysis cycles. Because of the homogeneous infiltration of the slurry into the woven fabrics, the free-space between the woven fabrics was completely filled by the SiC-reinforced precursor-derived Si-C-N ceramics.

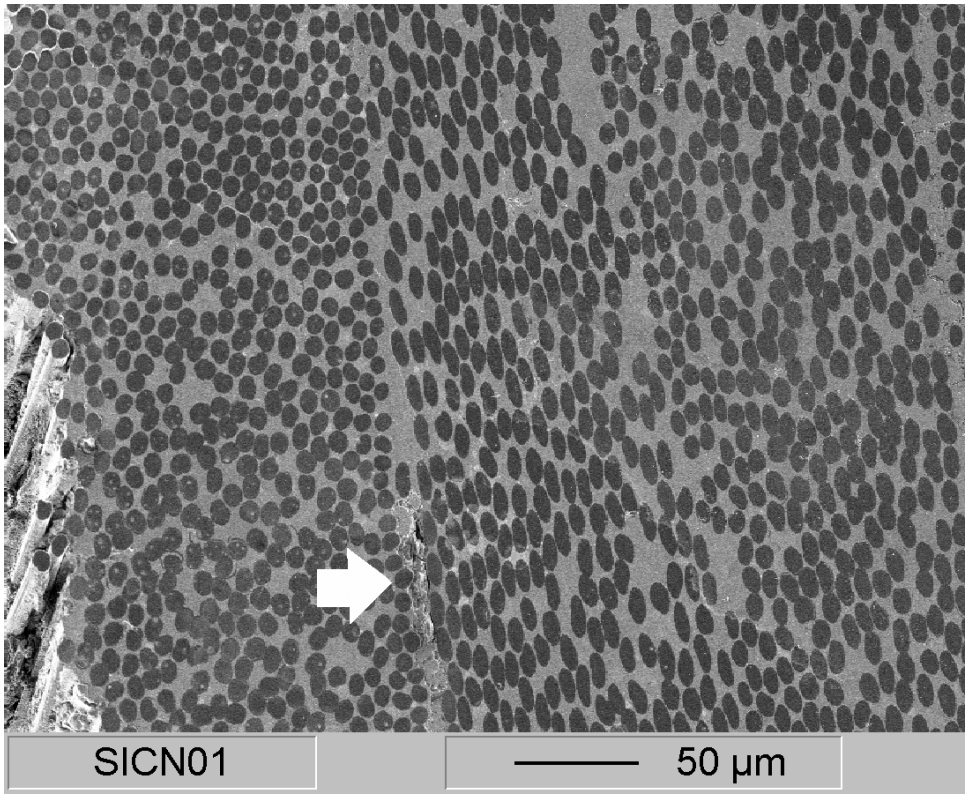

Fig. 3.6: Microstructure of the FRC after 10 impregnation/pyrolysis cycles (⇨ : flaw)
Large voids between the woven fabrics as well as small spaces between the fibers are filled homogeneously.

4. Processing condition and microstructure of particulate-filled and fiber-reinforced precursor-derived Si-C-N composites

Based on the technique mentioned in chapter 3, in this chapter, the processing of particulate-filled and fiber-reinforced precursor-derived Si-C-N composites was optimized, and their microstructure, mechanical property and fracture behavior were investigated.

Important physical-chemical and chemical properties of polymers, such as viscosity, vapor pressure and ceramic yield, depend to a great extent on the degree of cross-linking. Furthermore, during the heat-treatment of a low molecular weight liquid precursor, evaporation of low-weight oligomers takes place, which frequently results in a significant weight loss [96Rie] and flaw formation. Accordingly, cross-linking is an important process step of PIP process, but improvement of cross-linking process has not been so frequently investigated [92Cho] [01Li2].

SiC [99Gon] and carbon fiber [01Rak] have been most frequently used for FRC mainly because of their excellent as-fabricated and high temperature properties. The selection of fiber system depends on the application temperature of the FRC. SiC fiber offers a better room temperature mechanical properties and high temperature properties up to ~1350^{o}C than carbon fiber because of the similarity of CTE with precursor-derived ceramic matrix (SiC: 4.5-4.9×10^{-6}/K, Si-C-N: 3.2×10^{-6}/K, carbon: ~ 0/K [99Zie]). Ziegler *et al.* [99Zie] compared the bending strength of C_{fiber}/Si-C-N_{matrix} FRC and SiC_{fiber}/Si-C-N_{matrix} FRC made by PIP technique, and reported that the former one had a much lower strength due to regular crack formation induced by the mismatch of CTE between fiber and matrix. Carbon fiber retains its strength above 2000^{o}C [96Kow], but the as-fabricated mechanical properties and oxidation resistance of the resultant FRC are lower than that of SiC_{fiber}-FRC. However, commercial SiC fiber lose their strength above 1350^{o}C-1400^{o}C mainly due to the crystallization and coarsening of SiC [00Shi], and accordingly the FRC made with this fiber are prone to deteriorate at high temperature [00Koh]. Therefore, in this study, carbon fibers have been used for the fabrication of FRC.

This chapter reported on the improvement of cross-linking process, and described the microstructure, mechanical property and fracture behavior of the C_{fiber}/SiC_{filler}/Si-C-N_{matrix} FRC for high temperature application.

4.1. Experimental procedure

4.1.1. Fabrication and characterization of FRC

FRC samples were produced on the basis of the results outlined in chapter 1 to 3 and in accordance with the flow sheet shown in Fig. 4.1. SiC was applied as filler material. The carbon fiber (T300J 3K, Toray) used were coated with pyrocarbon in order to induce week bonding between fiber and matrix [94Eva].

12 layers of 2D-woven carbon fiber fabrics (total thickness ~4mm) were stacked in a mold, and an aqueous slurry with 43 vol% SiC and 1.5wt% of PEI (polyethylenimine) was prepared for the infiltration. Detailed conditions of the slurry dispersion and infiltration are described in chapter 3. After the infiltration, the molds were dried at 80°C in an oven for 24h and then at 350°C in a vacuum to minimize the residual moisture in the C_{fiber}/SiC_{filler} compact.

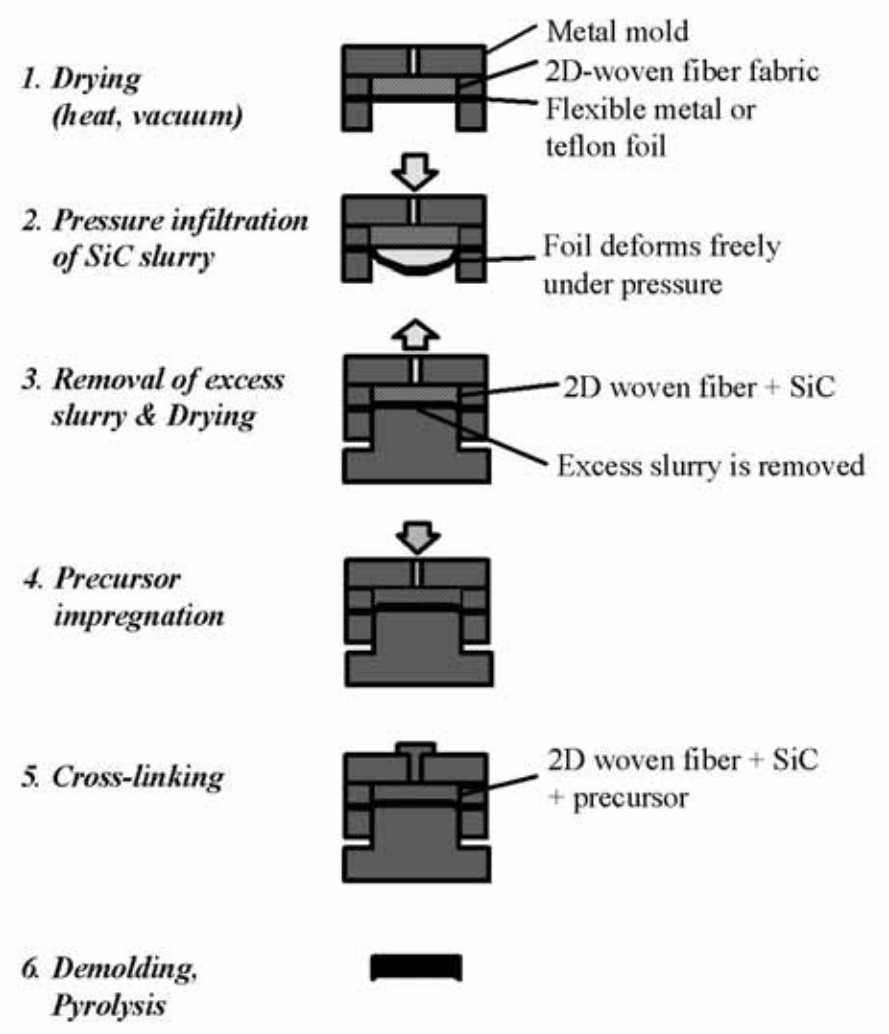

Fig. 4.1: Flow sheet of the FRC fabrication process. The individual steps were performed in the same mold without removing the samples from the mold between the single processing steps.

Subsequently, the liquid Si-C-N precursor (VL 20) was dissolved in tetrahydrofuran (1 : 1 by volume) in order to decrease its viscosity. After impregnating the compact with this solution, the solvent was removed by evacuation of the mold at 40°C for 6h and the mold was then capped and heated for cross-linking. Cross-linking conditions are described in the next paragraph.

After cross-linking, the green bodies were demolded, and pyrolyzed subsequently using the conditions described in detail in chapter 1 (1350°C, 2h, purified Ar atmosphere, heating rates for the first and following cycles: 1°C/min and 5°C/min, respectively). After the first process cycle, formation of a white layer was observed on the surface of FRC samples. Possible reasons for the formation of this layer will be described in chapter 5. The layer was removed prior to the next process cycle by gently grinding the surface. Impregnation and pyrolysis were repeated up to ten times.

The thickness of the FRC increased during the first pyrolysis. To understand this swelling, the deformation of the cross-linked precursor was measured by thermo-mechanical analysis (TMA 2000, Baehr). Analysis was done in the temperature range of 25°C-300°C in an Ar atmosphere with a heating rate of 5°C/min.

After finishing the densification, as-pyrolyzed FRC were machined into bars (30×1.5×2mm) and polished up to 1μm finish for measuring the 4 point bending strength (Hydropuls® PSA, Schenck, upper span: 7mm, lower span: 20mm, 3 samples per measurement). The microstructure of the as-fabricated or fractured samples was investigated by scanning electron microscopy (SEM, Stereoscan 200, Oxford) and optical microscopy (DM RM, Leica).

4.2.2. Optimization of cross-linking process

After the impregnation of liquid precursor into the mold as described above, different conditions were applied for the improvement of cross-linking process (Fig. 4.2).

The equipment shown in Fig. 4.2 (a) is a conventionally used glass tube equipped with a gas bubbler for an easy release of gaseous species developed during cross-linking. In order to reduce vaporization of the precursor during cross-linking, a sealed stainless steel container shown in Fig. 4.2 (b) was developed. It has a very small inner volume and the metal container can sustain increased pressure caused by evaporation. Additionally, a small amount of excess polymer was given into the container so that the equilibrium vapor pressure of oligomer could be achieved in a short time. The precursor was cross-linked by heating both equipments in a furnace for 6h at 370°C or 430°C, respectively. Using lower temperatures in both cases, *e.g.* 340°C or 400°C, respectively, resulted in precursors which were too soft in order to retain shape integrity of the samples.

4.2. Results and discussion

4.2.1 Improvement of cross-linking process

After the first cross-linking, it turned out that the precursor has to be heated slowly in the glass tube to cross-link efficiently. Due to bubble formation and foaming, the precursor became opaque when heating fast (total spent time to reach to the cross-linking temperature: 2h 40min, up to 370^{o}C), whereas a dense and transparent polymer was obtained when heating was slow (total time: 15h 40 min). Bahloul *et al.* pointed out that there is a competition between cross-linking and evaporation. When heating is too fast, evaporation of low molecular weight oligomers is higher before cross-linking can take place [93Bah].

However, since impregnation and pyrolysis must be repeated several times, slow cross-linking significantly increases the total processing time. Fast heating (2h 40min) as mentioned above was therefore applied, and considerable weight loss of samples was suppressed by using the closed reaction system with an additional source of oligomer as described above and shown in Fig. 4.2 (b). By the application of sealed stainless steel container, the total cross-linking time decreased into ~1/3 compared to using conventional glass tube process, which is longer than five days after ten impregnation/pyrolysis cycles.

Fig. 4.3 gives the relative density of FRC using the two different equipments for cross-linking. Usually, the efficiency of impregnation/pyrolysis decreases with increasing number of process cycles, which is a consequence of the formation of closed pores [95Nak]. The

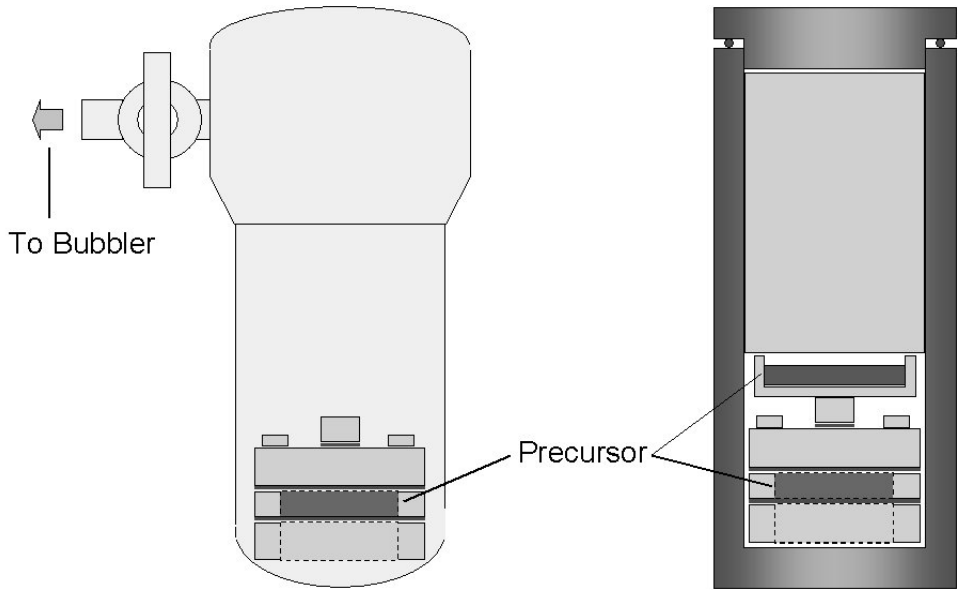

Fig. 4.2: Equipments used for cross-linking (a) open glass tube (b) sealed stainless steel container

relative density of the FRC which was cross-linked in the glass tube increased slowly with the number of impregnation/pyrolysis cycle because evaporated oligomers could escape freely through the bubbler. According to Kroke *et al.* [00Kro], the most important prerequisite to raise ceramic yields during pyrolysis is to prevent evolution of volatile Si-containing species.

Using the metal container, in contrast, resulted in an increased densification per PIP cycle even the density was already increased in earlier cycles using glass tube (Fig. 4.3). Similar aspects were stated by Zou *et al.* [99Zou1, 99Zou2] who reported that the relative density of FRC were improved by increasing the pressure during cross-linking and pyrolysis from 0.1 MPa to 5.0 MPa. Some condensed liquid precursor, however, was still found at the container wall after the cross-linking.

Another important item during cross-linking of the polymer is the formation of bubbles. They represent severe defects which can not be removed during pyrolysis. In order to prevent the formation of bubbles, slow heating (15h 40min) has to be applied for cross-linking when using glass tube. In contrast, increased vapor pressure of the precursor inside the sealed metal container suppressed its evaporation and thus bubble formation was not observed in the cross-linked precursor in spite of the fast heating rate. Consequently, the benefit using the metal container technique should also cause improvements of the mechanical properties of FRC (see section 4.2.3.).

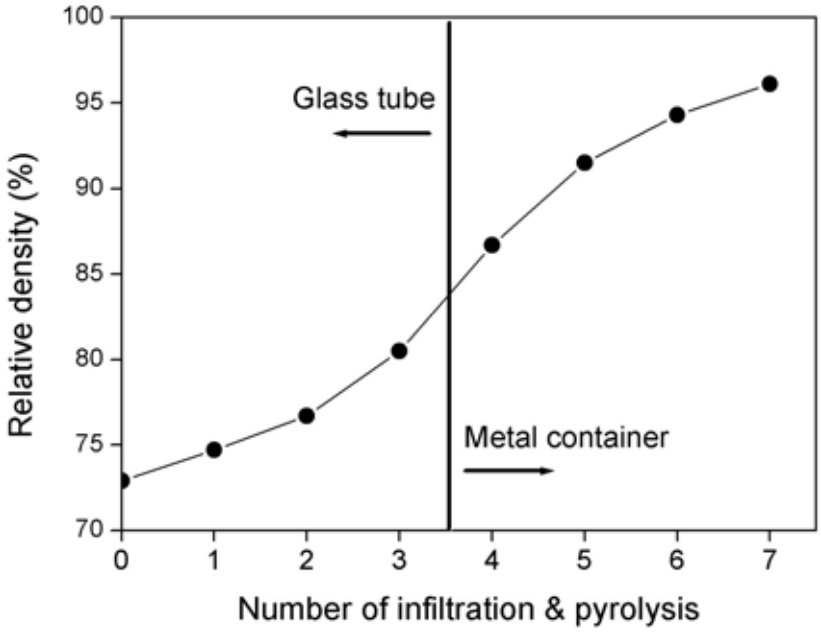

Fig. 4.3: Relative density of the FRC for different cross-linking equipments using fast heating rate. Relative density was estimated from the dimensions of sample and weight gains after each cycle (see chapter 1). Swelling of FRC after the first pyrolysis is not considered. Different from the general behavior (decrease of the efficiency with processing cycles), the efficiency of impregnation/pyrolysis cycle was enhanced even after the fourth cycle by changing the cross-linking conditions.

4.2.2. Densification

Fig. 4.4 shows the estimated relative densities of FRC after each processing step. Almost full density was acquired after the impregnation of liquid precursor irrespective of the presence of a filler material. Intensive weight loss was observed after cross-linking, especially without using fillers. The reason for the higher weight loss of FRC without filler can unequivocally be attributed to the higher amount of precursor which is introduced into the free space between the fibers. The difference in relative density of the samples with and without filler was ~15% after the second process cycle. The figure gives an idea about how the improvement of process can decrease the processing time of PIP technique.

Fig. 4.5 shows the relative density of FRC with increasing number of impregnation/pyrolysis cycles. The relative density of the green C_{fiber}/SiC_{filler} compact is already very high (>70%). However, it decreased by the swelling of FRC during the first pyrolysis cycle. The reason for this is that the cross-linked precursor softened above 175°C, which was confirmed by the increased amplitude of vibration in TMA testing (Fig. 4.6) [96Sei]. Obviously, the softened precursor could not prevent swelling of the green body, which presumably was a consequence of the gas formation during pyrolysis. Swelling, in contrast, was not observed after the second and further process cycles due to the formation of a rigid Si-C-N ceramic network.

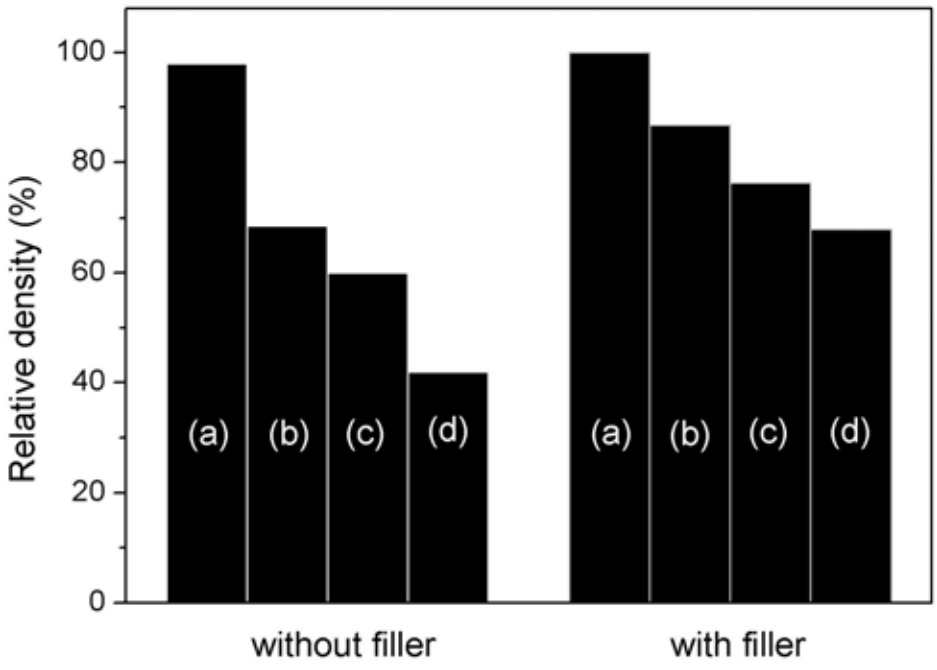

Fig. 4.4: The relative density of the FRC after two cycles of precursor impregnation, cross-linking and pyrolysis with and without SiC filler (The swelling of the FRC after the first pyrolysis is not considered): (a) after precursor impregnation (b) after cross-linking (370°C, in glass tube) (c) after pyrolysis (5°C/min, 1400°C, 2h) and (d) stacked woven carbon fiber fabric with or without filler.

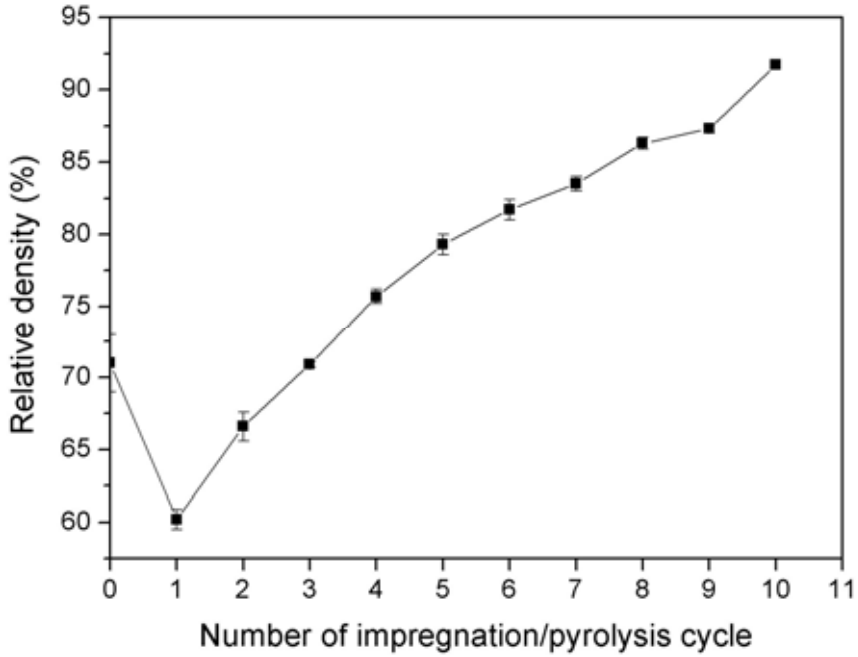

Fig. 4.5: Relative density of FRC vs. number of impregnation/pyrolysis cycles using stainless steel container for cross-linking. The strong decrease in relative density after the first process cycle is a consequence of a swelling due to the softening of the cross-linked precursor and the evaporation of gaseous pyrolysis products.

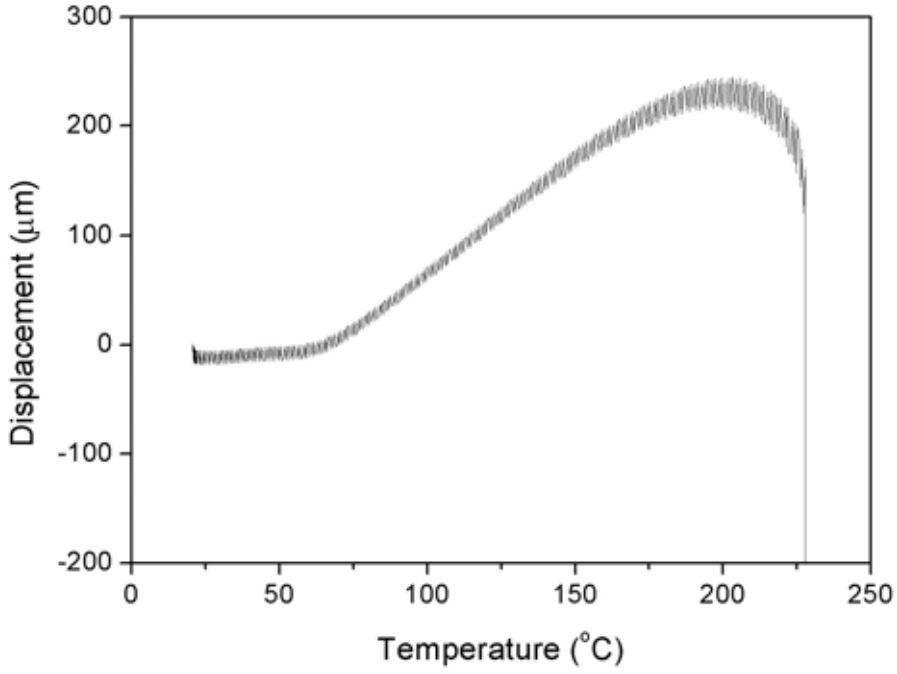

Fig. 4.6: TMA data of cross-linked precursor (Ar, 5°C/min). The amplitude of vibrations increased above 175°C due to the softening of precursor. The precursor compact was broken at 230°C.

The relative density of FRC increased further even during the 10th cycle. The final density of the FRC described here was 2.14 g/cm^3 (relative density: ~92 %). There have been some reports which show a similar density increase with repeated impregnation/pyrolysis cycles [98Zhe, 00Nec].

4.2.3. Microstructure and mechanical behavior

Fig 4.7 shows large cracks formed in FRC during processing. They form a somewhat regular array and still exist after repeated impregnation and pyrolysis cycles (Fig. 4.7 (a)). Ziegler *et al.* [99Zie] reported a similar behavior of C_{fiber}/Si-C-N_{matrix} FRC obtained by PIP.

In addition, fine microcracks are observed in areas which are located between the individual woven fabrics (Fig. 4.7 (b)). Reasons for the formation of such cracks might be shrinkage of the infiltrated SiC slurry during drying and/or gas evolution and resultant swelling of FRC during precursor pyrolysis. The fine cracks could not be removed completely even after 10 process cycles, the formation of which can be possibly suppressed by increasing the solid loading of SiC slurry and by suppressing the swelling of FRC during pyrolysis.

The average diameter of fiber and filler particles used in the present investigation was 8.5μm and 0.5μm, respectively. The ratio of both values (0.06) is slightly higher than the ideal value (< 0.05) for the homogeneous infiltration of fillers as proposed by Lange *et al.* [95Lan]. Nevertheless, a homogeneous microstructure was observed after the final process cycle (Fig. 4.7 (c)).

Fig. 4.8 (a) and (b) show the morphology of carbon fibers at the fracture surface before and after 10 impregnation/pyrolysis cycles, respectively. Although even small amounts of oxygen and/or moisture in the pyrolysis atmosphere can oxidize the carbon fibers during repeated pyrolysis and deteriorate the mechanical properties of FRC [95Nak], in the present experiment, oxidation of carbon fiber was prevented by strictly controlling the pyrolysis atmosphere as described in chapter 1. Most of the very thin (~500 nm) pyrocarbon coating was well preserved after FRC processing (Fig. 4.8 (b)). Only some damage of the coatings (Fig. 4.7 (c), Fig. 4.9 (a)) occurred presumably not by oxidation but by mechanical deterioration due to the pressurization during molding (see chapter 3, Fig. 3.1 (d)).

In spite of the rather large amount of extended cracks formed in matrix phase in FRC (Fig. 4.7 (a)), the average bending strength of FRC which was determined by 4-point bending test was fairly high (286 MPa). The strength of C_{fiber}/Si-C-N_{matrix} FRC made by PIP technique has been generally reported to be lower than 200 MPa (185 MPa [95Nak], 150-200 MPa [99Rot]), although Zheng *et al.* reported a fairly high value of 700 MPa by using PAN-based carbon fibers [98Zhe]. Ziegler *et al.* [99Zie] compared the bending strength of

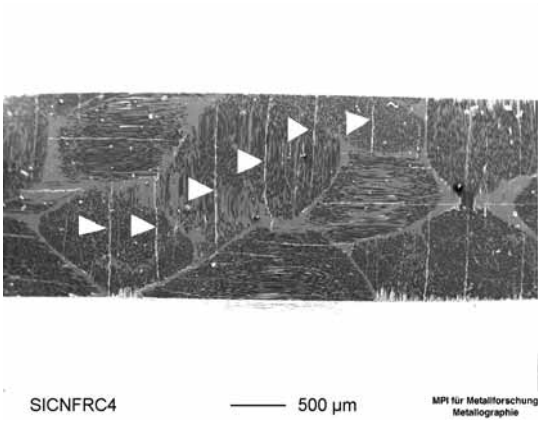

(a)

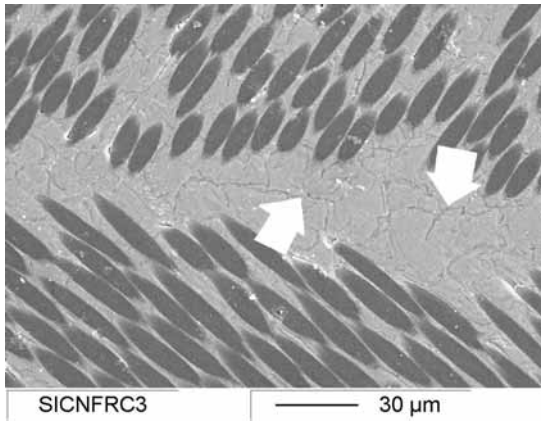

(b)

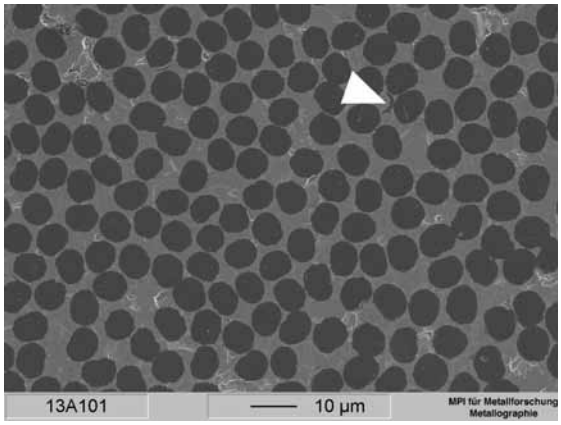

(c)

Fig. 4.7: Crack formation in FRC after the densification (a) regular crack formation observed at the polished surface (▷) by the difference of CTE between fiber and matrix, (b) microcracks in the matrix, located between individual fiber bundles (⇨) and (c) microstructure of FRC ((▷: detached pyrocarbon coating)

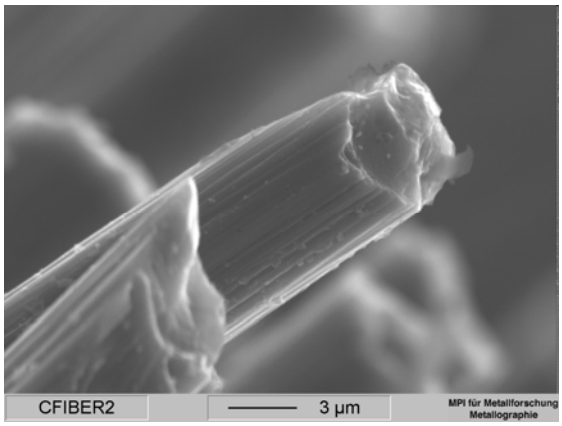

(a)

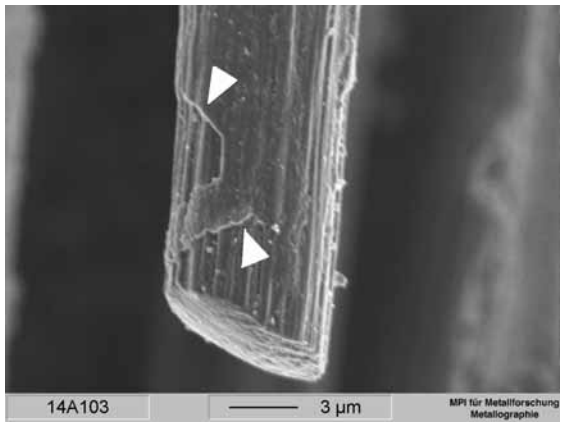

(b)

Fig. 4.8: Morphology of carbon fiber (a) as-received and (b) after 10 times of pyrolysis (▷: pyrocarbon coating)

C_{fiber}/Si-C-N_{matrix} FRC and SiC_{fiber}/Si-C-N_{matrix} FRC made by PIP technique, and reported that the former one had a much lower strength (125 MPa vs. 950 MPa) due to regular crack formation. They also reported that C_{fiber}/Si-C-N_{matrix} FRC showed brittle fracture behavior.

Presumably, the strength of the FRC in the present investigation was enhanced by the matrix phase composed of SiC filler and Si-C-N matrix. The improvement of cross-linking and pyrolysis process, together with the application of appropriate filler material and modified infiltration process investigated in the earlier chapters, may result in a SiC_{filler}/Si-C-N matrix having high strength and toughness (see Table 2.3).

Since the pyrocarbon coating on the carbon fiber provided a weak bonding between fiber and matrix [95Hel], cracks propagated predominantly along this coating (Fig. 4.9 (a)), and

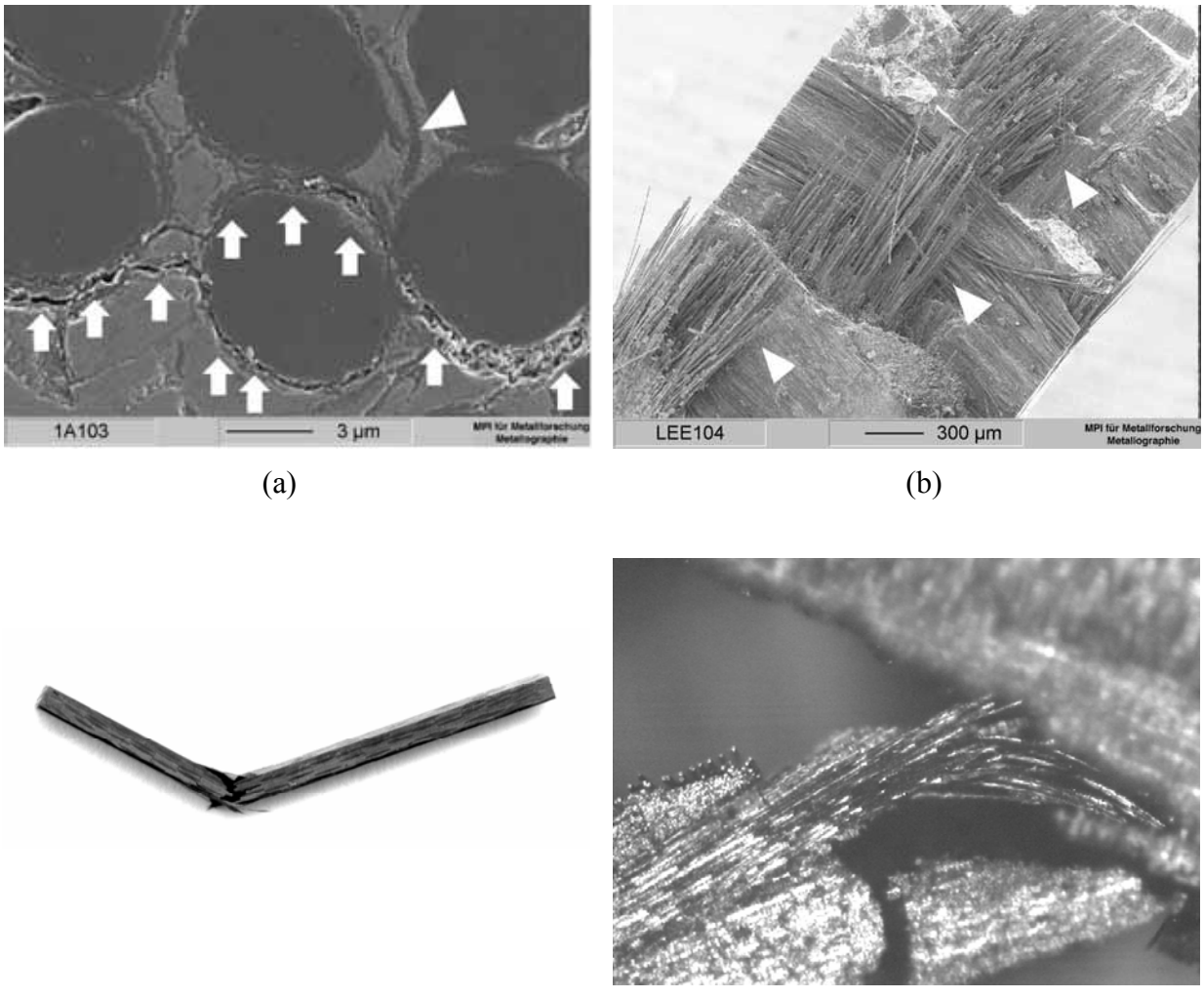

(a) (b)

(c) (d)

Fig. 4.9: Microstructure and morphology of FRC after bending test (a) cracks propagate through the pyrocarbon coatings (⇨: crack propagation, ▷: detached coating)
(b) fiber pull-out (▷: pulled-out fibers at different layers)
(c) bar sample after the bending test (d) fiber bending and bridging

fiber pull-out (> 200 μm) was observed at the fracture surface indicating an appropriate bonding strength between fiber and matrix (Fig. 4.9 (b)) [94Eva]. The entire bar samples were bent. Some samples had bending angles of > 40^{o} (Fig. 4.9 (c)), but were not fractured, because some fibers bridged the samples (Fig. 4.9 (d)).

The high strength of the FRC in spite of the regular cracks in the present experiment is partly attributed to the improved damage tolerance offered by the fiber-reinforcement based on a fiber pull out effect due to a weak bonding strength between fiber and matrix.

4.3. Summary and conclusions

Processing, microstructure and mechanical behavior of FRC prepared by the deform-casting process were investigated for $C_{fiber}/SiC_{filler}/Si\text{-}C\text{-}N_{matrix}$ system. The cross-linking time for the production of FRC was reduced into ~1/3 and flaw formation was suppressed by the application of sealed metal container for cross-linking. Swelling of the FRC occurred during the first pyrolysis due to the softening of the cross-linked precursor and gas formation. The density of the FRC was 2.14g/cm^3 after 10 process cycles. Crack formation occurred in the FRC due to the difference of CTE between fiber and matrix. Nevertheless, a fairly high room temperature bending strength of 286MPa was achieved. Cracks propagated through pyrocarbon coatings, and substantial toughening was observed by a well-developed fiber pull out. Thus, the FRC showed enhanced mechanical properties in spite of the crack formation induced by the carbon fiber.

5. Effect of oxide surface layer of SiC particles for the processing, mechanical and thermal properties of particulate-filled and fiber-reinforced precursor-derived Si-C-N composites

This chapter deals with the high temperature properties of the FRC described in the last chapter, and analyzes the reasons of deterioration of the FRC after heat treatment.

Carbon is one of the most stable materials at extremely high temperature [89Fit], and carbon /carbon composites retain their strength even after the heat treatment at 2500^{o}C [96Kow]. Although crack formation in carbon fiber-reinforced FRC due to the difference of CTE may limit its possible application temperature, it is applicable in the temperature range where commercial SiC fibers lose their strength due to the crystallization and coarsening of SiC (>1350-1400^{o}C) [00Shi].

It has been reported that room and high temperature strength of SiC or Si_3N_4 particulate-reinforced FRC are often inferior to those of FRC without filler [95Nak, 98Tan]. There have been some results, however, suggesting a beneficial effect of fillers at high temperature. Interrante *et al.* [97Int] reported that the strength of FRC using β-SiC as filler was higher (~60 MPa) after heating at 1600^{o}C than that of as-pyrolyzed samples. The reason of these contradicting results is not clear yet. It may be due to oxide layer at the surface of the filler materials.

The surface of SiC and Si_3N_4 powders is commonly covered with SiO_2 originated from the reaction of SiC or Si_3N_4 units with moisture and oxygen in the atmosphere. Lee *et al.* [90Lee] measured the oxygen content of air-exposed surface of sputter deposited SiC film with auger electron spectroscopy (AES). He reported that the thickness of the SiO_2 layer of SiC formed by the exposure was several nanometer. During the heating at temperature above 1300^{o}C in an inert atmosphere, SiO_2 and SiC react and form SiO and CO gas [00Nag]. The decomposition of SiO_2 surface layer of SiC filler may deteriorate the material and thus may affect the mechanical and thermal properties of composites. Si_3N_4 also has an oxide layer at the surface with thicknesses of several tens nanometer [89Jen] which may result in a similar behavior.

In this chapter, the strength of $C_{fiber}/SiC_{filler}/Si\text{-}C\text{-}N_{matrix}$ FRC was measured after the heat treatment at 1350^{o}C for 24h in Ar, and the possible mechanisms of the deterioration of SiC_{filler}/Si-C-N matrix were investigated. For that purpose, $SiC_{filler}/Si\text{-}C\text{-}N_{matrix}$ PRC (termed SiC-PRC) having different amount of surface oxide were prepared, and their high temperature properties were investigated.

5.1. Experimental procedure

Details on the preparation of $C_{fiber}/SiC_{filler}/Si\text{-}C\text{-}N_{matrix}$ FRC are described in chapter 4. Four-point bending strength testing samples were prepared and heated at 1350°C for 24h in purified Ar using alumina tube furnace. Heat treatment temperature (1350°C) was selected based on the TGA data of SiC-PRC (see Fig. 1.2) above which the deterioration of SiC_{filler}/Si-C-N matrix occurs. After the heat treatment, four-point bending strength was measured using the same conditions as described in chapter 4. Following, microstructure and phase evaluation of the heat treated FRC were investigated by scanning electron microscopy (SEM, Stereoscan 200, Oxford) and X-ray powder diffraction using CuK_α radiation (XRD, D 5000, Siemens).

After the bending test, it was informed that the bending strength of heat-treated FRC was lower than that of as-fabricated ones. The intrinsic deterioration of fiber at high temperature can not be the reason due to its excellent high temperature properties [89Fit]. Accordingly, SiC-PRC, which is a matrix material of particulate-filled FRC, were examined to understand the reason of matrix deterioration.

Details on the preparation of the SiC pellets are provided in chapter 1. After the shaping of the pellets, SiO_2 impurities of the filler was removed by a heat treatment in Ar at 1300°C, 1400°C and 1650°C (see page 19, reaction (1.2)), and the oxygen content of resultant SiC pellets was measured using carrier gas hot extraction method (TC436DR, Leco) [93Sun].

Based on the analysis of oxide content of heat treated SiC, heat treatment of the SiC pellets was performed as follows in order to clarify the effect of SiO_2 surface layer of SiC filler on the deterioration of SiC-PRC after heat treatment:

1. The pellets were dried in a vacuum at 350°C for 6h according to the procedure described in chapter 4 in order to simulate the matrix of FRC (termed 350-PRC). In chapter 4, SiC filler in the FRC was not heat treated at 1750°C but dried at 350°C for the continuous processing (see Fig. 4.1), and thus contains surface SiO_2 layer.
2. SiC pellets were heated in an Ar atmosphere at 1750°C for 2h to remove surface SiO_2 (termed 1750-PRC).

The heat-treated SiC pellets were impregnated with liquid precursor, and the polymer was cross-linked and pyrolyzed subsequently using the conditions reported in chapter 1. Two different heating rates (1°C/min, 5°C/min) were applied during pyrolysis. The relative density of both PRC was measured with increasing the number of impregnation/pyrolysis cycles as described in chapter 1. Following, microstructure and phase evaluation of the PRC were investigated by SEM and XRD.

After six times of impregnation and pyrolysis, the PRC samples were cut into disks (diameter: 10 mm, thickness: ~ 300 μm). The strength, Poisson's ratio, hardness and fracture surface of the samples were measured using the methods described in chapter 1 before and after the heat treatment in purified Ar at 1400°C for 2h. A Netzsch STA 501 was used for the high-temperature TGA of the PRC after the first impregnating/pyrolysis cycle in an argon atmosphere over a temperature range of 25-1780°C using BN crucible (heating rate: T<1400°C - 5°C/min, T>1400°C - 2°C/min). To measure the creep behavior (Amsler DSM 6101), the samples were machined into $2\times2\times8mm^3$, and a compressive load of 100 MPa was applied at 1350°C for 60h in air.

5.2. Results and discussion

5.2.1 Microstructure and mechanical properties of FRC after heat treatment

After the heat treatment at 1350°C in purified Ar for 24h, some white coating were formed on the surface of FRC. Fig. 5.1 shows the XRD patterns of FRC before and after the heat treatment. Heating increased the intensity of SiC reflections, due to the crystallization of the Si-C-N matrix and/or the formation of SiC whiskers on the surface of the sample. Cristobalite (SiO_2) reflections were not observed in as-pyrolyzed materials, but were detected after the heat treatment. The main peak of which can be seen clearly, while less intensive peaks are mostly overlapped by those of SiC. Si_3N_4 reflections, which are often observed during the crystallization of Si-C-N ceramics, were not detected after heat treatment. The XRD analysis informs that this coating layer contains SiO_2 and SiC.

Fig. 5.2 shows the surface morphology and microstructure of FRC before and after the heat treatment. The white coating, which was formed during the heat treatment, can be seen in

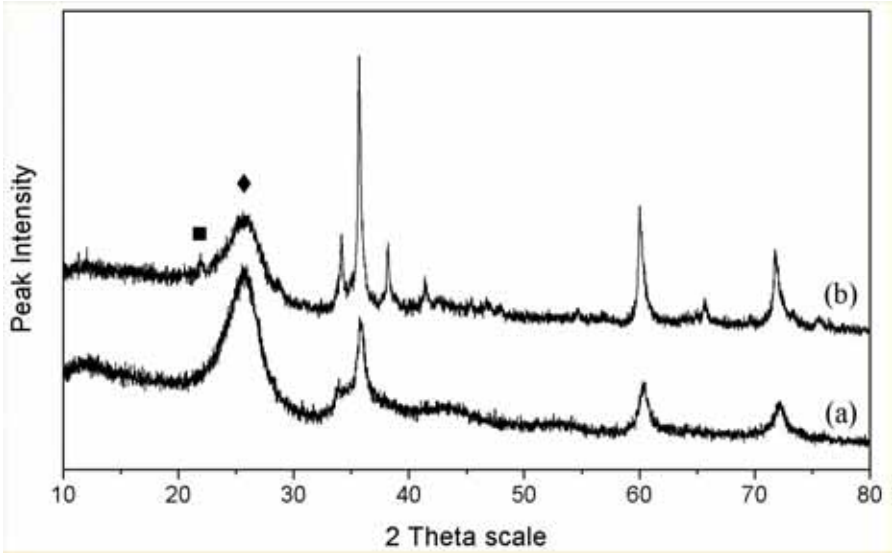

Fig. 5.1: XRD data of FRC (a) before and (b) after heat treatment at 1350°C for 24h in purified Ar and (■: cristobalite, ◆: graphite, others: SiC).

Fig. 5.2 (a) and (b).The burn-out of carbon fibers located just beneath the coating layer was not clearly visible (Fig. 5.2 (b)), which means that the SiO_2 was not formed by oxidation; otherwise the carbon fiber should be damaged. Before heat treatment, the carbon fibers were bonded homogeneously to the dense and crack-free matrix (Fig. 5.2 (c)). After the heat treatment, fibers in surface near areas (< 20 μm) of FRC were only slightly burned out. However, deterioration of matrix, with a pronounced crack formation, occurred strongly even inside the sample (Fig. 5.2 (d)).

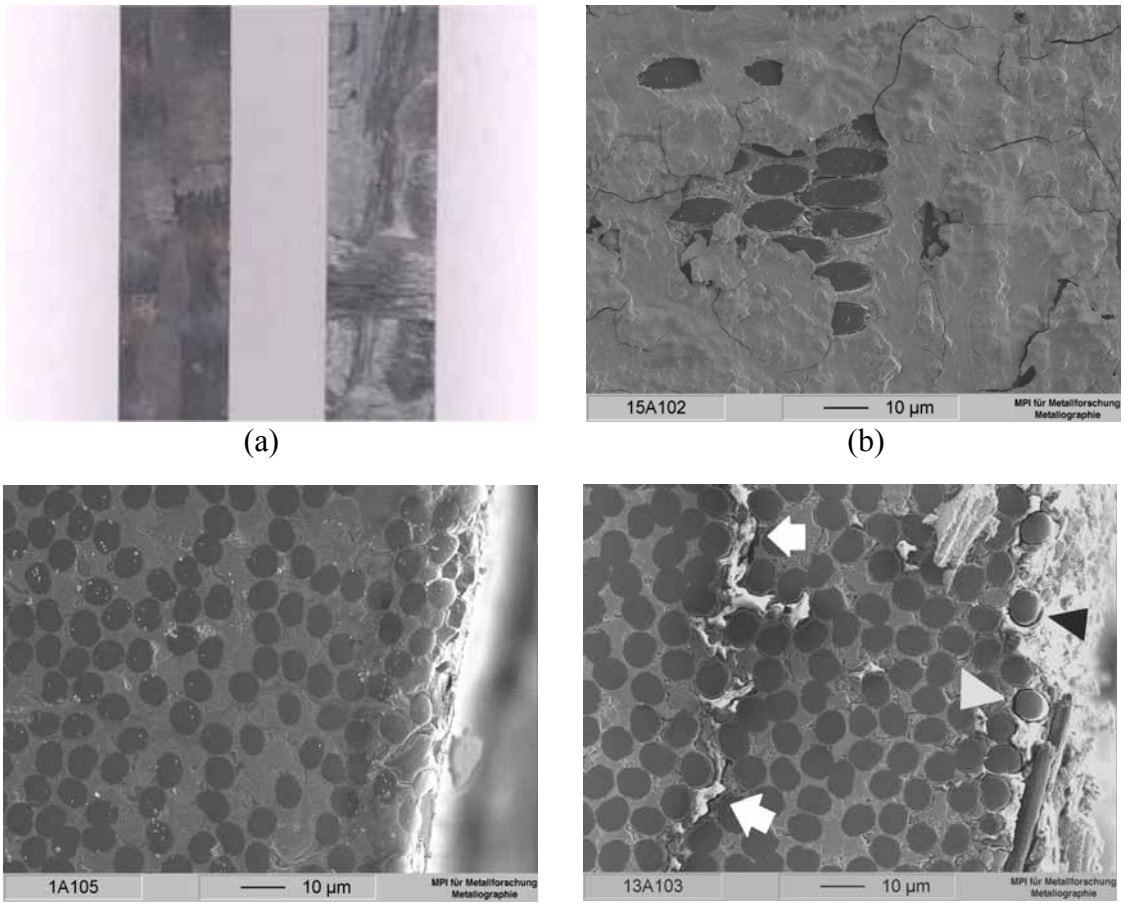

(a) (b)

(c) (d)

Fig. 5.2: Morphology and microstructure of FRC (a) formation of white coating at the surface of FRC (left: before heat treatment. right: after heat treatment). (b) magnified view of (a) after heat treatment. Coating is clearly seen at the surface of FRC. The carbon fibers beneath the coating were not burned-out. (c) cross-sectional morphology of surface-near area before heat treatment. Deterioration of fibers or matrix is not observed. (d) cross-sectional morphology of surface near area after heat treatment (▷: fiber-matrix debonding by the slight burn-out of fiber, ⇨: crack)

Table 5.1 shows the strength retention and weight loss of $C_{fiber}/SiC_{filler}/Si\text{-}C\text{-}N_{matrix}$ FRC after the heat treatment. The strength decreased by 27% after the treatment.

There are mainly four reasons to explain this weakening :

1. Burn-out of the carbon fibers
2. Crystallization and/or decomposition of the Si-C-N matrix
3. Changing of the bonding between fiber and matrix.
4. Decomposition of surface SiO_2 of SiC filler

The burn-out of carbon fibers did occur slightly at the very surface of FRC even if the reaction was suppressed by the application of purified Ar (Fig. 5.2 (d)) during the prolonged heat treatment (24h) at 1350°C. However, the strength of FRC may not be affected so critically as with monolithic ceramics by the minute surface damage when considering the high intrinsic flaw density and high damage tolerance of FRC [90Kot]. Besides, the massive weight loss of FRC (2.4%) during the heat treatment can not be explained solely by the slight burn-out of carbon fiber.

Decomposition and crystallization of precursor-derived ceramics during heat treatment may be considered as a possible mechanism of the deterioration. Sato *et al.* [02Sat] reported that the crystallization of Si-C-N matrix decreased the strength of FRC made by PIP technique. Ichikawa *et al.* [98Ich] and Shimoo *et al.* [01Shi] also reported that the crystallization of SiC-based Hi-Nicalon fibers which are derived from precursor decreased their tensile strength. Crystallization and/or decomposition of Si-C-N matrix may decrease the strength of FRC in the present experiment, too. However, Si_3N_4 reflections, which have been often observed by the crystallization of Si-C-N ceramics (Fig. 1.12, [00Kro] [01Iwa]), were not detected after the heat treatment (Fig. 5.1). Also, after heating SiC-PRC at 1400°C, which is a matrix of the FRC investigated, deterioration by the crystallization and/or decomposition of Si-C-N matrix was not observed, which will be reported in the following paragraphs.

Table 5.1. Properties of FRC before and after the heat treatment in purified Ar atmosphere at 1350°C for 24h

As-fabricated strength (MPa)	Weight loss after heat treatment (%)	Strength after heat treatment (MPa)
286	2.4	209

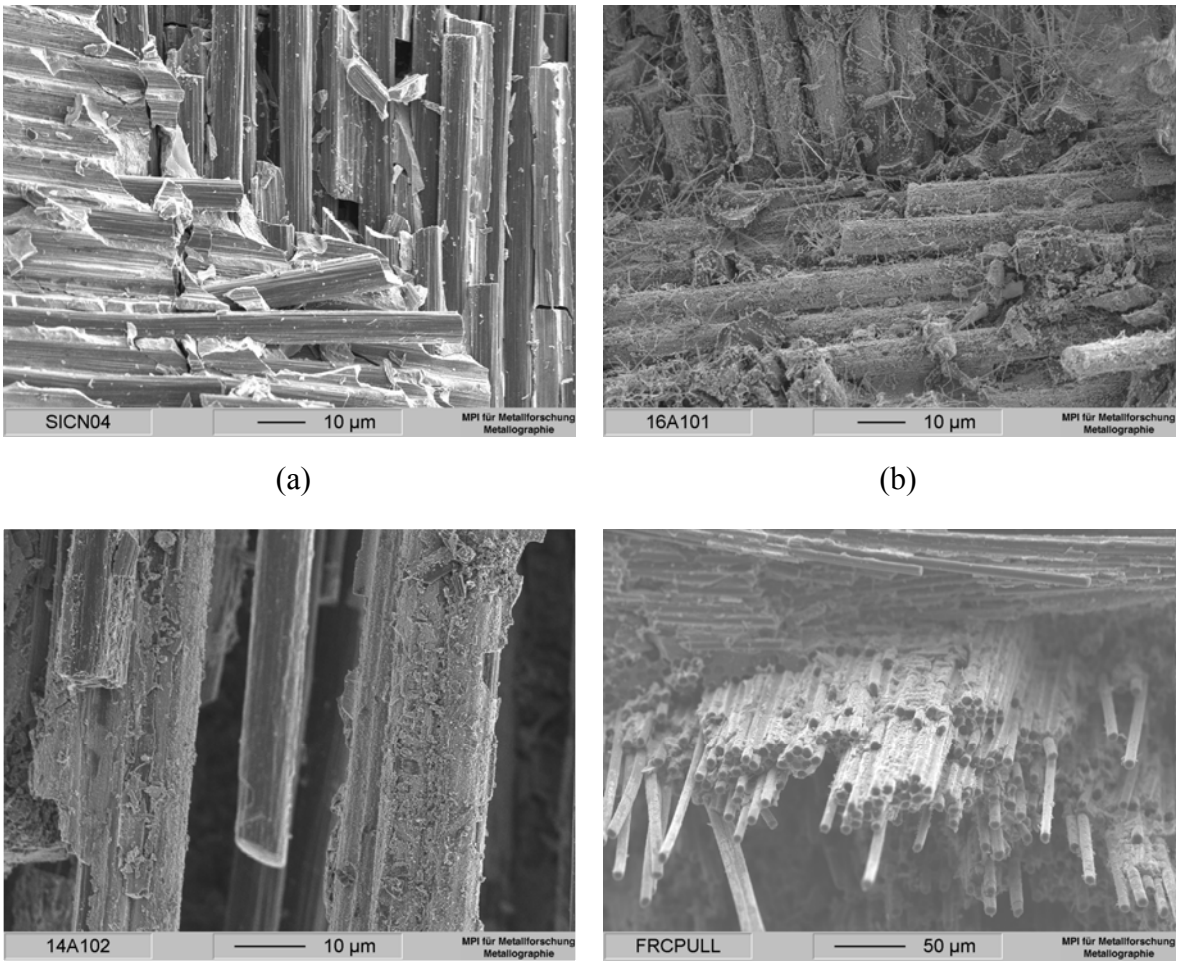

Fig. 5.3: Microstructure of fracture surface before and after heat treatment under purified Ar atmosphere (a) fracture surface of as-fabricated FRC, (b) fracture surface after heat treatment in purified Ar, (c) magnified view of pulled-out fibers after heat treatment and (d) fiber pull out after the heat treatment

Fig. 5.3 (a) and (b) show fracture surfaces of FRC before and after heat treatment, respectively. From Fig. 5.3 (a), it can be concluded that there is weak bonding between matrix and carbon fiber. The rough surface of carbon fiber can be clearly observed due to the easy detachment between fiber and matrix. In contrast, it is evident from Fig. 5.3 (b) and (c) that matrix material is attached to pulled-out fibers after heat treatment. Accordingly, this attachment of matrix to fibers must have appeared during the post-thermolysis heat treatment, which presumably affected the strength of FRC. Fiber pull-out was still observed at the fracture surface after the heat treatment (Fig. 5.3 (d)), which means that the strong bonding between fiber and matrix did not occur during the heat treatment regardless of the attachment of matrix to fibers.

The last possible reason for the deterioration is the reaction of the SiO_2 surface layer of SiC with the filler itself and with Si-C-N matrix by reaction (1.1) and/or (1.2) (see page 19). The mechanical strength of matrix and the adherence of the matrix to the filler are expected to decrease by such reactions.

Beside the loss of bending strength, delamination was observed in heat treated FRC during bending, and whisker formation was observed at the delaminated surface (Fig. 5.3 (b)) as well as the surface of the sample. This reason can also explains the formation of SiO_2 and SiC whiskers at the sample surface during the heat treatment of FRC (Fig. 5.1, Fig. 5.2). It was reported that SiC whisker formation frequently occurs in gas phase reactions of SiO and CO due to the reaction [92Wan]

$$SiO_{(g)} + 3CO_{(g)} \rightarrow SiC_{(s)} + 2CO_{2(g)}. \quad (5.1)$$

Besides, the following reactions may also induce the formation of SiO_2 and SiC.

$$3SiO_{(g)} + CO_{(g)} \rightarrow 2SiO_{2(s)} + SiC_{(s)}, \quad (5.2)$$

$$2SiO_{(g)} + O_{2(g)} \rightarrow 2SiO_{2(s)}. \quad (5.3)$$

The O_2 gas in reaction (5.3) might be supplied from the leak and/or alumina tube by diffusion during pyrolysis at 1350°C [99Heu].

Choi *et al.* [98Cho] analyzed the amount of SiC whiskers formed by reaction (5.1), and reported that only 10-30% of SiO gas reacted with CO to form SiC whiskers, and the residual SiO gas formed SiO_2 phase. This is in agreement with findings of Sorarù *et al.* [99Sol] who observed SiO_2 coating formation on the surface of amorphous Si-O-C during a post-thermolysis heat treatment and reported that this was due to the decomposition of Si-O-C into SiO and CO gas.

5.2.2. Decomposition of surface SiO_2 layer of SiC filler

In order to analyze the effect of surface SiO_2 of SiC filler on the deterioration described above in more detail, SiC-PRC, which is a matrix material of particulate-filled FRC, were fabricated.

Table 5.2 shows the oxygen content of the SiC powder used as filler before and after heat treatment in Ar atmosphere at different temperatures. The amount of oxygen decreases from 0.9wt% to 0.7wt% after its annealing at 1300°C for 2h. During heating at 1400°C and 1650°C for the same time, the amount of oxygen decreases further to 0.4wt% and 0.1wt%, respectively. This result confirms the decomposition of the oxide surface layer of SiC due to reaction (1.2).

Table 5.2. Oxygen content of SiC filler after heat treatment at different temperatures (Ar atmosphere, 2h, heating rate: 5°C/min).

	Raw powder	1300°C	1400°C	1650°C
Oxygen content (wt%)	0.9	0.7	0.4	0.1

Fig. 5.4 shows the effect of surface SiO_2 layer of SiC filler on the morphology of PRC. After the first impregnation/pyrolysis cycle of PRC made with dried SiC powder (350-PRC), the formation of SiO_2 (white coating, Fig. 5.4 (a)) and SiC whisker (Fig. 5.4 (c)) was observed on the sample surface. In contrast, the formation of neither SiO_2 nor SiC whisker could be observed when using the filler that was heat treated at 1750°C (1750-PRC, oxygen content: <0.1%, Fig. 5.4 (b)). These results clearly points to the fact that surface oxide layer of SiC filler particles was responsible for the formation of both SiO_2 coating and SiC whiskers during extended heat treatment of PRC and subsequently of particulate-filled FRC.

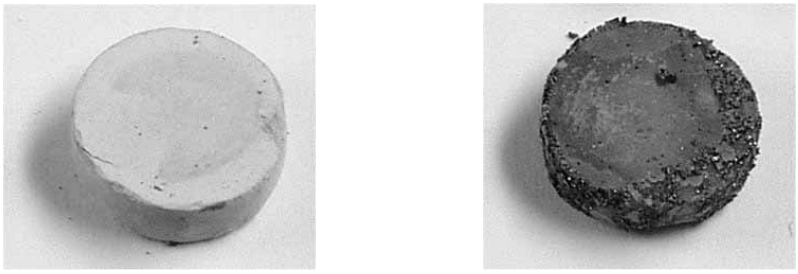

(a) (b)

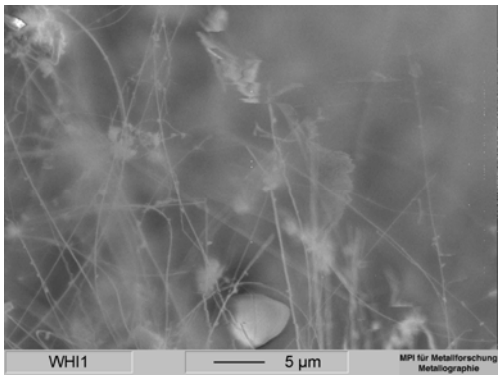

(c)

Fig. 5.4: SiO_2 coating formation on PRC after the first impregnation/pyrolysis cycle (1400°C, 2 h, heating rate: 5°C/min) with different pre-treatment of SiC pellets. (a) 350-PRC (b) 1750-PRC. Formation of SiO_2 coating was completely suppressed if surface oxide of SiC filler is removed by heat treatment and (c) whisker formation at the surface of 350-PRC

Fig. 5.5 shows thermogravimetric analysis of 1750- and 350-PRC after the first impregnation/pyrolysis. A continuous weight loss occurs between 1350°C and 1780°C in both samples. Since 1750-PRC does not contain major amount of oxygen as shown above, decomposition must be due to a carbothermal reaction of Si-N units in the matrix as it is also the case with 350-PRC. Accordingly the weight loss behavior of both samples was similar. Additionally, 350-PRC had mass loss due to the oxygen contamination from the filler which results in the formation of SiO and CO formed by reaction (1.1) and (1.2), and accordingly had higher weight loss than 1750-PRC.

5.2.3 Effect of surface SiO_2 of SiC filler on densification

Fig. 5.6 shows the increase of the relative density of PRC with the number of precursor impregnation/pyrolysis cycles applied. The relative density of 1750-PRC increased from ~60% in the SiC compact to ca. 91% when applying a heating rate of 5°C/min and to 86% when heating with 1°C/min to 1350°C. In contrast, the density of 350-PRC did not increase substantially after the fourth cycle. Presumably, precipitated SiO_2 coating closed the open pore of 350-PRC in such a way that the penetration of liquid precursor was strongly hindered after four process cycles. As a result, the final relative density of 350-PRC was lower (~83%, 1°C/min) than those of the 1750-PRC.

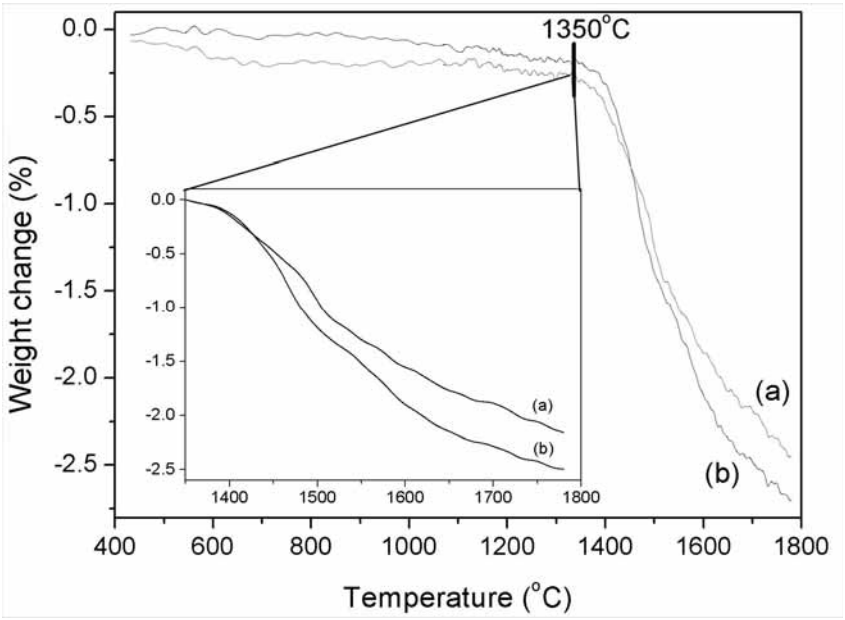

Fig. 5.5: TGA of (a) 1750-PRC and (b) 350-PRC in Ar atmosphere after the first impregnation/pyrolysis cycle. Weight loss is almost identical until 1350°C. The data in a box represent the weight loss above 1350°C.

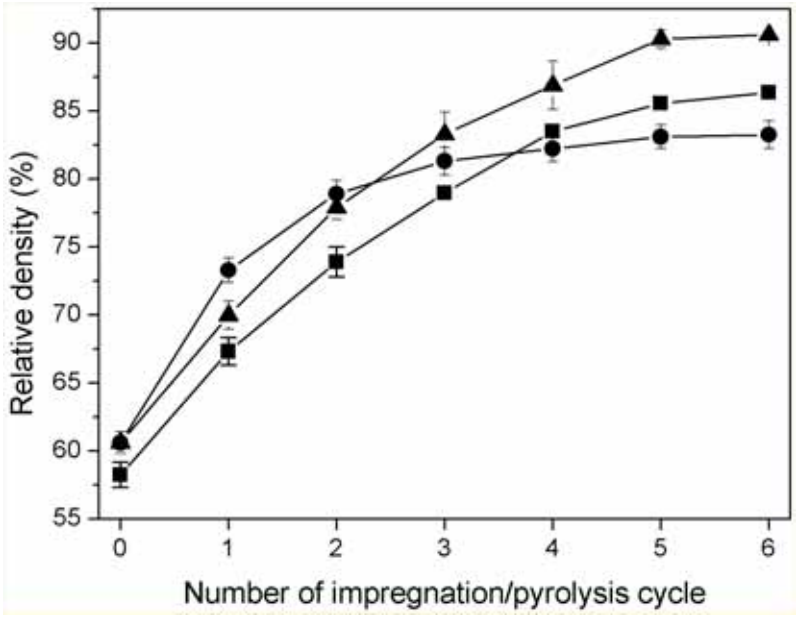

Fig. 5.6: Relative density of the PRC with different pre-heat treatment of SiC pellet vs. number of impregnation/pyrolysis cycles in Ar at 1350°C for 2h (cycle number 0: relative density of SiC compact). (▲: 1750-PRC, 5°C/min, ■: 1750-PRC, 1°C/min, ●: 350-PRC, 1°C/min)

5.2.4 Effect of surface SiO_2 of SiC filler on room- and high temperature properties

Table 5.3 gives the values of the relative density, weight loss, hardness and strength of samples before and after the heat treatment at 1400°C for 2h. The different final density of the PRC presumably affected the room temperature mechanical properties according to formula (2.3), and consequently 1750-PRC had higher room temperature strength and hardness than 350-PRC.

The weight loss of 350-PRC was higher than that of 1750-PRC due to the decomposition of SiO_2. During the heat treatment at 1400°C, SiO_2 in 350-PRC disappeared by decomposition reactions, and accordingly deterioration of strength and hardness occurred (Table 5.3). Since 350-PRC comprised the matrix phase of particulate-filled FRC described in chapter 4, the results clearly informs that the decrease of bending strength of the FRC after heat treatment is partly due to the decrease of strength of SiC_{filler}/Si-C-N matrix in between the fiber at high temperature.

On the other hand, the strength and hardness of 1750-PRC increased in spite of the weight loss caused by the decomposition of Si-C-N matrix. The result shows that the deterioration of FRC was not originated from the decomposition of Si-C-N matrix (see page 65). The strength of 1750-PRC became rather high during the heat treatment and therefore could not be measured

Table 5.3. Processing and mechanical properties of PRC before and after heat treatment (Ar/1400°C/2h, heating rate: 5°C/min).

	1750-PRC	350-PRC
Relative density (%)	90.6	83.2
Weight loss after heat treatment (%)	2.2	5.7
Hardness before heat treatment (Hv)	775	722
Hardness after heat treatment (Hv)	1068	542
Strength before heat treatment (MPa)	576	497
Strength after heat treatment (MPa)	> 639	329

accurately, because the applied force to break the samples exceeded the capacity of the load cell in use (20N).

Importantly, the strength and hardness of 1750-PRC was almost two times higher than that of 350-PRC after the heat treatment at 1400°C. The results strongly imply that the high temperature properties of particulate-filled FRC can be also improved by removing surface SiO_2 layer from SiC filler before the impregnation of liquid precursor.

The fracture surface of both PRC before and after heat treatment is shown in Fig. 5.7. The presence of a thin SiO_2 layer on the surface of SiC affected the fracture behavior of PRC even at room temperature. 350-PRC revealed both inter- and transgranular fracture (Fig. 5.7 (a)), while a dominant transgranular fracture behavior occurred in 1750-PRC (Fig. 5.7 (b)), even if the grain size of SiC filler in both PRC was basically the same. Rice [00Ric] reported that for a broad range of stress conditions the fracture is mainly intergranular for finer grains, and it transits into transgranular as grain size increases, which is in accordance with the fracture behavior of 350-PRC. In contrast, filler and matrix could not be differentiated in the fracture surface of 1750-PRC, and the composite microstructure was unveiled only after the plasma etching (Fig. 5.7 (e) (f)).

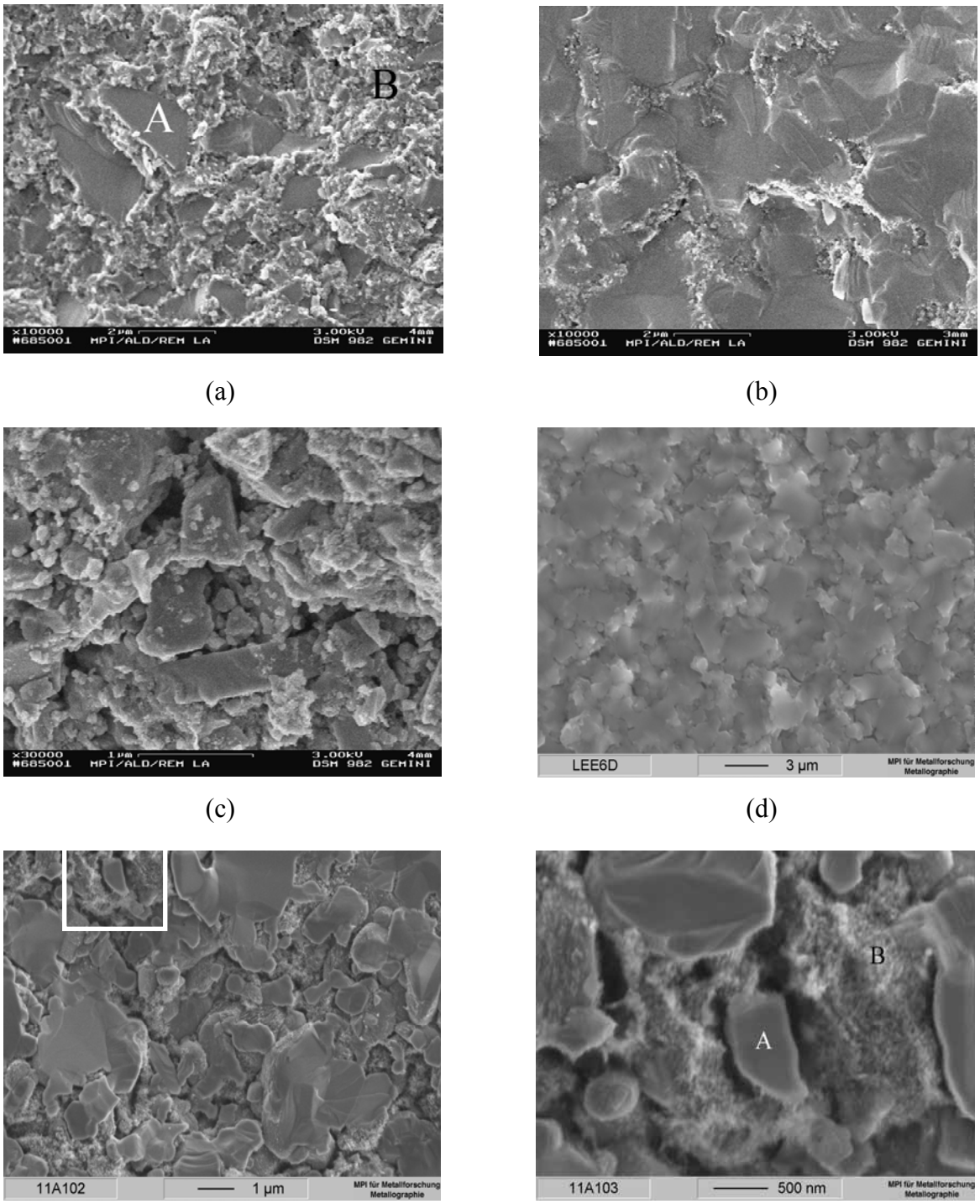

Fig.5.7: Microstructure of fractured surface (a) 350-PRC, room temperature (A: filler , B: matrix), (b) 1750-PRC, room temperature, (c) 350-PRC, after heat treatment at 1400^{o}C, (d) 1750-PRC, after heat treatment at 1400^{o}C, (e) after plasma etching of 1750-PRC, room temperature and (f) magnified view of (e) (A: filler, B: matrix)

In 350-PRC, SiC grains were pulled out during fracture due to the weak bonding between filler and matrix after the heat treatment (Fig. 5.7 (c)). In contrast, the fracture behavior of 1750-PRC was not much affected by the heat treatment (Fig. 5.7 (d)). These figures also show that the decrease of strength of the FRC after heat treatment was partly due to the deterioration of the matrix.

The creep behavior of PRC is also affected by surface SiO_2 of the SiC filler (Fig. 5.8). The creep strain of 1750-PRC did not increase much after 5h and was 0.21% after 60h. In contrast, a continuous creep strain was observed in 350-PRC up to 60h, although the strain rate tended to decrease with time. The creep strain of 350-PRC was 0.37% after 60h. Grathwohl *et al.* [78Gra] measured the creep of reaction-bonded silicon nitride (RBSN) in air, and reported that the partial conversion of the nitride to oxide phase during the test by oxidation changed the chemical composition and microstructure of RBSN, which increased the creep rate. They insisted that this behavior should be the result of the increase of the amount of oxide. The weight gain of 350- and 1750-PRC after the creep test by oxidation was similar (ca. 1 mass %), but the initial oxygen content of fillers was ~0.9% and ~0.1%, respectively.

The results clearly show that the surface SiO_2 of SiC filler must be removed prior to the impregnation of liquid precursor to increase relative density, mechanical properties such as hardness, strength, creep resistance, and high temperature stability of PRC and particulate-filled FRC made by PIP technique.

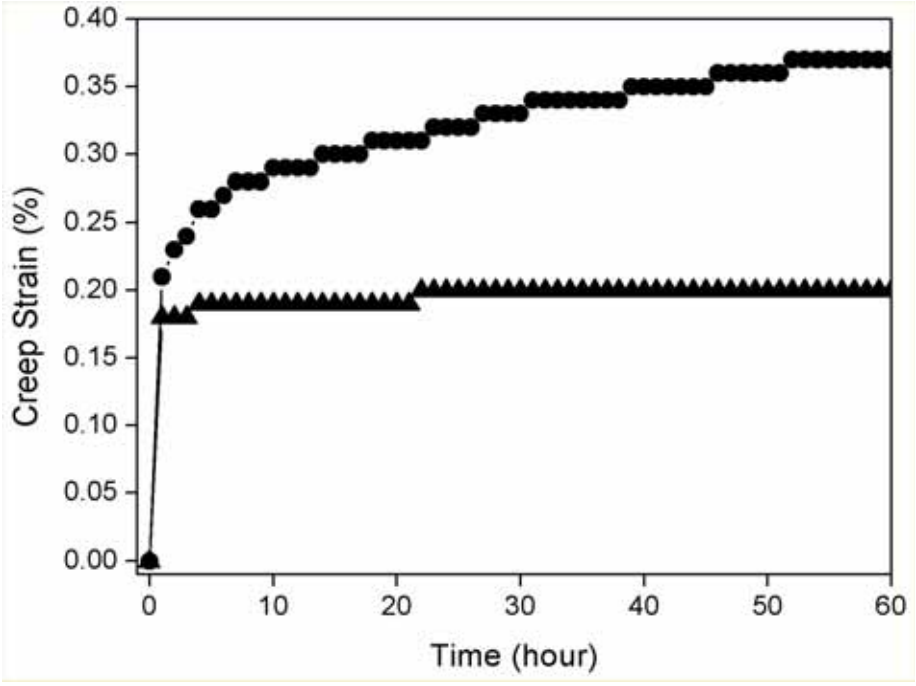

Fig. 5.8: Creep behavior of PRC. (●: 350-PRC, ▲:1750-PRC)

5.3. Summary and Conclusions

The $C_{fiber}/SiC_{filler}/Si\text{-}C\text{-}N_{matrix}$ FRC retained 73% of the strength after the heat treatment at 1350°C for 24h in Ar. The XRD and microstructure analysis informed about the deterioration of SiC_{filler}/Si-C-N matrix after the heat treatment. Surface SiO_2 layer of the filler material induced the formation of SiO_2 coating and SiC whisker on the surface of PRC and particulate-filled FRC after the heat treatment. Relative density, mechanical properties such as room temperature strength and hardness, high temperature stability and creep resistance of the SiC-PRC were clearly worsened by the surface SiO_2 layer of SiC filler. The strength and hardness of SiO_2-free PRC was almost two times higher than those of SiO_2-containing PRC after a heat treatment at 1400°C. The results explain that the deterioration of $C_{fiber}/SiC_{filler}/Si\text{-}C\text{-}N_{matrix}$ FRC after heat treatment was partly due to the weakening of the particulate-reinforced matrix by the decomposition of SiO_2. Removing surface SiO_2 layer of SiC filler is therefore considered as an important pre-requisite before the impregnation of liquid precursor for the fabrication of PRC and particulate-filled FRC using the PIP method.

References

[Ency] Encyclopaedia of materials : science and technology, Vol. 4, edited by K. H. J. Buschow, R. W. Chan, M. C. Flemings, B. Ilschner, E. J. Kramer, S. Mahajan, Elsevier, Oxford, 2001, pp3210-3211

[Kion] Technical bulletin from the producer. http://www.kioncorp.com/bulletins/general.html

[Toray] Technical reference from the producer. http://www.torayca.com/techref/index.html

[64Clo] P. J. Clough, Ultra fine powders – their production and characteriatic, in Metallurgical society conferences Vol. 23, edited by H. H. Hausner, Gordon and breach science publishers, London, 1964, pp 9-19

[69Gun] R. D. Gunn, C. Judson King, AIChE J., **15**, 507 - 514 (1969)

[75Gau] L. J. Gauckler, H. L. Lucas, G. Petzow, Contribution to phase-diagram Si_3N_4-AlN-Al_2O_3-SiO_2, J. Am. Ceram. Soc., **58**, 346-347 (1075)

[75Yaj] S. Yajima, J. Hayashi, M. Omori, Continuous silicon-carbide fiber of high-tensile strength, Chem. Lett., **9**, 931-936 (1975)

[76Wil] R. R. Wills, S. Holmquist, J. M. Wimmer, J. A. Cunningham, Phase relationships in the system Si_3N_4-Y_2O_3-SiO_2, J. Mater. Sci., **11**, 1305-1309 (1976)

[77Ric] R. W. Rice, Microstructural dependence of mechanical behavior of ceramics, in Material Science and Technology , Vol. 11, edited by R. W. Cahn, P. Haasen, E. J. Kramer, Academic press, New York, 1977, pp 191-381

[78Gra] G. Grathwohl, F. Thuemmler, Creep of reaction-bonded silicon nitride, J. Mater. Sci., **13**, 1177-1186 (1978)

[78Nai] I. K. Naik, L. J. Gauckler, T. Y. Tien, Solid-liquid equilibria in the system Si_3N_4-AlN-SiO_2-Al_2O_3, J. Am. Ceram. Soc., **61**, 332-335 (1978)

[80Gau] L. J. Gauckler, H. Hohnke, T. Y. Tien, The system Si_3N_4-SiO_2-Y_2O_3, J. Am. Ceram. Soc., **63**, 35-37 (1980)

[81Ans] G. R. Anstis, P. Chantikul, B. R. Lawn, D. B. Marshall, A critical evaluation of indentation techniques for measuring fracture toughness: 1, direct crack measurements, J. Am. Ceram. Soc., **64**, 533-538 (1981)

[86Ric] R. Rice, Perspective on fractography, in Advances in ceramics, Vol. 22,

Fractography of glasses and ceramics, The American Ceramic Society, Inc., Ohio, 1986, pp 27-28

[88Nik] K. G. Nickel, M. Hoffmann, P. Greil, G. Petzow, Thermodynamic calculations for the formation of SiC-whisker-reinforced Si_3N_4 ceramics, Adv. Ceram. Mater., **3**, 557-562 (1988)

[88Sin] R. N. Singh, and A. R. Gaddipati, Fiber-containing composite, U. S. patent., No. 5,407,734

[88Wie] S. M. Wiederhorn, D. E. Roberts, T. J. Chuang, Damage-enhanced creep in a siliconized silicon carbide: phenomenology, J. Am. Ceram. Soc., **71**, 602-608 (1988)

[89Car] D. F. Carroll, R. E. Tressler, Effect of creep damage on the tensile creep behavior of a siliconized silicon carbide, J. Am. Ceram. Soc., **72**, 49-53 (1989)

[89Fit] E. Fitzer, PAN-based carbon-fibers present state and trend of the technology from the view point of possiblilities and limits to influence and to control the fiber properties by the process parameters, Carbon, **27**, 621-645 (1989)

[89Jen] H. Jenett, H. Bubert, E. Grallath, Comparative surface and bulk analysis of oxygen in Si_3N_4 powders, Fresenius Z. Anal. Chem., **333**, 502-506 (1989)

[90Kot] T. Kotil, J. W. Holmes, M. Comninou, Origin of hysterisis observed during fatigue of ceramic-matrix composites, J. Am. Ceram. Soc., **73**, 1879-1883 (1990)

[90Lee] R. C. Lee, C. R. Aita, N. C. Tran, The air-exposed surface of sputter deposited silicon carbide studied by x-ray photoelectron spectroscopy, J. Vac. Sci. Techol. A, **9**, 1351-1354 (1991)

[90Sir] F. Sirieix, P. Goursat, A. Lecomte, A. Dauger, Pyrolysis of polysilazanes-relationship between precursor architecture and ceramic microstructure, Compos. Sci. Technol., **37**, 7-19 (1990)

[91Bao] Y. Bao, J. R. G. Evans, Kinetics of capillary extraction of organic vehicle from ceramic bodies. Part 1: flow in porous media. J. Eur. Ceram. Soc., **8**, 81-84 (1991)

[91Bib] G. S. Bibbo, P. M. Benson, C. G. Pantano, Effect of carbon monoxide partial pressure on the high-temperature decomposition of Nicalon fiber, J. Mater. Sci., **26**, 5075-5080 (1991)

[92Bah] D. Bahloul, M. Pereira, P. Goursat, Silicon carbonitride derived from an organometallic precursor: Influence of the microstructure on the oxidation

behavior, Ceram. Inter., **18**, 1-9 (1992)

[92Cho] N. S. Choong Kwet Yive, R. J. P. Corriu, D. Leclercq, P. H. Mutin, A. Vioux., Silicon carbonitride from polymeric precursors : thermal cross-linking and pyrolysis of oligosilazane model compounds, Chem. Mater., **4**, 141-146 (1992)

[92Hoc] B. J. Hockey, S. M. Wiederhorn, Effect of microstructure on the creep of siliconized silicon carbide, J. Am. Ceram. Soc., **75**, 1822-1830 (1992)

[92Kre] W. Krenkel, P. Schanz, Fiber ceramic structures based on liquid impregnation technique, Acta Astronautica, **28**, 159-169 (1992)

[92Nai] S. V. Nair, P. Z. Q. Cai, J. E. Ritter, A. Lightfoot, J. S. Haggerty, Mechanical behavior of silicon carbide particulate reinforced reaction bonded silicon nitride matrix composites, in Ceramic engineering & science proceedings, edited by M. Mendelson, The American ceramic society, Westerville, 1992, pp 81-89

[92Rie] R. Riedel, G. Passing, H. Schönfelder, R. J. Brook, Synthesis of dense silicon-based ceramics at low-temperatures, Nature, **355**, 714-717 (1992)

[92Wan] L. Wang, H. Wada, L. F. Allard, Synthesis and characterization of SiC whiskers, J. Mater. Res., **7**, 148-163 (1992)

[93Bah] D. Bahloul, M. Pereira, P. Goursat, N. S. Choong, Kwet Yive, R. J. P. Corriu, Preparation of silicon carbonitrides from an organosilicon polymer : 1, Thermal decomposition of the cross-linked polysilazane, J. Am. Ceram. Soc., **76**, 1156-1162 (1993)

[93Nat] S. Natansohn, A. E. Pasto, W. J. Rourke, Effect of powder surface modification on the properties of silicon nitride ceramics, J. Am. Ceram. Soc., **76**, 2273-2284 (1993).

[93Sun] J. D. Sunderkötter, E. Grallath, H. Jenett, Combined bulk and surface analysis of oxygen species in Si_3N_4 powders by means of carrier-gas heat-extraction methods and auger electron spectrometry, Fresenius J. Anal. Chem., **346**, 237-240 (1993)

[94Che] H.-K. Chen, C.-I. Lin, C. Lee, Kinetics of the reduction of carbon/alumina powder mixture in a flowing nitrogen stream, J. Am. Ceram. Soc., **77**, 1753-1756 (1994)

[94Eva] A. G. Evans, F. W. Zok, Review-The physics and mechanics of fibre-reinforced brittle matrix composites, J. mater. Sci., 29 3857-3896 (1994)

[94Kag] Y. Kagawa, Effect of thermally induced stress on fracture toughness of SiC fiber-glass matrix composites, Mater. Trans. JIM, **35**, 363-369 (1994)

[94Shi] D.-W. Shin, H. Tanaka, Low-temperature processing of ceramic woven fabric/ceramic matrix composites, J. Am. Ceram. Soc., **77**, 97-104 (1994)

[95Bla] H. Blaha, K. L. Komarek, The reduction of yttria and thoria-yttria with graphite, High Temp. Mater. Sci., **34**, 29-38 (1995)

[95Eck] A. J. Eckel, J. D. Cawley, T. A. Parthasarathy, Oxidation kinetics of a continuous carbon phase in a nonreactive matrix, J. Am. Ceram. Soc., **78**, 972-980 (1995)

[95Gre] P. Greil, Active-filler-controlled pyrolysis of preceramic polymers, J. Am. Ceram. Soc., **78**, 835-848 (1995)

[95Hel] T. Helmer, H. Peterlik, K. Kromp, Coating of carbon fibers-the strength of the fibers, J. Am. Ceram. Soc., **78**, 133-136 (1995)

[95Lan] F. F. Lange, W. C. Tu, A. G. Evans, Processing of damage-tolerant. Oxidation-resistant ceramic-matrix composites by a precursor infiltration and pyrolysis method, Mat. Sci. Eng. A-Sturucture, **195**, 145-150 (1995)

[95Lee] J. S. Leed, Principles of ceramics processing, 2nd. Ed.;. John Wiley & Sons, Inc., New York, 1995, pp 295-297

[95Nak] K. Nakano, A. Kamiya, Y. Nishino, T. Imura, T.-W. Chou, Fabrication and characterization of three-dimensional carbon fiber reinforced silicon carbide and silicon nitride composites, J. Am. Ceram. Soc., **78**, 2811-2814 (1995)

[95Rie] R. Riedel, H.-J. Kleebe, H. Schönfelder, F. Aldinger, A covalent micro/nano-composite resistant to high-temperature oxidation, Nature, **374**, 526-528 (1995)

[95Tan] T. Tanaka, N. Tamari, I. Kondoh, M. Iwasa, Fabrication and evaluation of 3-dimensional tyranno fiber reinforced SiC composites by repeated infiltration of polycarbosilane, J. Ceram. Soc. Jpn., **103**, 1-5 (1995)

[95Tu1] W.-C. Tu, F. F. Lange, Liquid precursor infiltration processing of powder compact : 1, kinetic studies and microstructure development, J. Am. Ceram. Soc., **78**, 3277-3282 (1995)

[95Tu2] W.-C. Tu, F. F. Lange, Liquid precursor infiltration processing of powder compact : 2, fracture toughness and strength, J. Am. Ceram. Soc., **78**, 3283-3289 (1995)

[95Wie] S. M. Wiederhorn, E. R. Fuller, Jr., Creep deformation of particulate-reinforced ceramic matrix composites, in High temperature mechanical behavior of ceramic composites, edited by S. V. Nair, K. Jakus, Butterworth-Heinemann, Newton,

1995, pp 155-191

[96Bis] R. Biswas, J. L. Henshall, R. J. Wakeman, Modelling stress distributions in brittle particulate-brittle matrix composites, in Fracture mechanics of ceramics, Vol. 12, edited by R. C. Bradt, D. P. H. Hasselman, D. Munz, M. Sakai, V. Ya. Shevchenko, Plenum press, New York, 1996, pp399-412

[96Don] A. Donato, C. A. Nannetti, A. Alberto, E. Borsella, S. Botti, S. Casadio, G. D′Alessandro, A. A. Licciulli, S. Mattelli, A. Masci, Process for producing ceramic matrix composites by liquid infiltration of ceramic polymeric precursors, U. S. patent No. 5,853,653

[96Kow] W. Kowbel, V. Chellapa, J. C. Withers, Properties of C/C composites produced in one low cost manufacturing step, Carbon, **34**, 819-821 (1996)

[96Rie] R. Riedel, Advanced ceramics from inorganic polymers, in Materials science and technology, Vol. 17B, Processing of ceramics part 2, edited by R. J. Brook, VCH verlagsgesellschaft mbH, Weinheim, 1996, pp2-47

[96Sei] J. Seitz, J. Bill, Production of compact polysilazane-derived Si/C/N-ceramics by plastic forming, J. Mater. Sci. Lett., **15**, 391-393 (1996)

[97Int] L. V. Interrante, J. M. Jacobs, W. Sherwood, C. W. Whitmarsh, Fabrication and properties of fiber- and particulate-reinforced SiC matrix composites obtained with (A)HPCS as the matrix source, in Key Engineering Materials, Vols. 127-131, edited by M. Fuentes, J. M. Martínez-Esnaola, A. M. Daniel, Trans Tech Publication, Zuerich, 1997, pp 271-278

[97Ken] T. Kennedy, M. Poorteman, F. Cambier, and S. Hampshire, Silicon nitride-silicon carbide nanocomposites prepared by water processing of commercially available powders, J. Europ. Ceram. Soc., **17**, 1917-23 (1997)

[97Ohz] Y. Ohzawa, M. Takahashi, K. Sugiyama, Pressure-pulsed chemical vapour infiltration of SiC into two-dimensional-Tyranno/SiC particulate preforms from $SiCl_4$-CH_4-H_2, J. Mater. Sci., **32**, 4289-4294 (1997).

[97Sut] D. Suttor, T. Erny, P. Greil, Fiber-reinforced ceramic-matrix composites with a polysiloxane/boron-derived matrix, J. Am. Ceram. Soc., **80**, 1831-1840 (1997)

[98Cho] H. J. Choi, J. G. Lee, Synthesis of silicon carbide whiskers (1) : reaction mechanism and rate-controlling reaction, J. Kor. Ceram. Soc., **35**, 1329-1336 (1998)

[98Ich] H. Ichikawa, M. Takeda, T. Noda, High performance SiC fibers for ceramic matrix composites, in Ceramic transactions, vol. 99, edited by Nobuo Takeda, American Ceramic Society, Westerville, 1998, pp 109-118

[98Kle] H.-J. Kleebe, D. Suttor, H. Mueller, G. Ziegler, Decomposition-crystallization of polymer-derived Si-C-N ceramics, J. Am. Ceram. Soc., **81**, 2971-2977 (1998)

[98Lau] S. Lau, S. J. Calandra, R. W. Ohnsorg, Process for making silicon carbide reinforced silicon carbide composite, US parent No. 5,840,221 (1998)

[98Ric] R. W. Rice, Porosity of ceramics, Marcel Dekker Inc., New York, 1998, pp73 – 74

[98Tak] T. Takagi, M. Hatori, S. Aoki, and H. Matsubara, Synthesis and evaluation of three-dimensional fiber reinforced ceramics, in Ceramic Transaction, Vol. 99, edited by. N. Takeda, L. M. Sheppard, and J. Kon, The American ceramic society, Westerville, OH, 1998, pp. 335-346

[98Tan] T. Tanaka, N. Tamari, I. Kondo, M. Iwasa, Fabrication of three-dimensional tyranno fibre reinforced SiC composite by the polymer precursor method, Ceram. Int., **24**, 365-370 (1998)

[98Wil] D. S. Wilkinson, Creep mechanism in multiphase ceramic materials, J. Am. Ceram. Soc., **81**, 275-279 (1998)

[98Zhe] G. Zheng, H. Sano, Y. Uchiyama, K. Kobayashi, K. Suzuki, H. Cheng, Preparation and fracture behavior of carbon fiber/SiC composites by multiple impregnation and pyrolysis of polycarbosilane, J. Ceram. Soc. Jpn., **106**, 1155-1161 (1998)

[99Bal] P. Baldus, M. Jansen, D. Sporn, Ceramic fibers for matrix composites in high-temperature engine application, Science, **285**, 699-703 (1999)

[99Che] K. W. Chew, A. Sellinger, R. M. Laine, Processing aluminium nitride-silicon carbide composites via polymer infiltration and pyrolysis of polymethyl silane, a precursor to stoichiometric silicon carbide, J. Am. Ceram. Soc., **82**, 857-866 (1999)

[99Col] P. Colombo, M. Modesti, Silicon oxicarbide foams from a silicon preceramic polymer and polyurethane, J. Sol-Gel Sci. Tech., **14**, 103-111 (1999)

[99Gon] M. F. Gonon, S. Hampshire, Comparison of two processes for manufacturing ceramic matrix composites from organometallic precursors, J. Europ. Ceram. Soc., **19**, 285-291 (1999)

[99Hau] R. Haug, M. Weinmann, J. Bill, F. Aldinger, Plastic forming of preceramic polymers, J. Europ. Ceram. Soc., **19**, 1-6 (1999)

[99Heu] A. H. Heuer, K. P. D. Lagerlöf, Oxygen self-diffusion in corundum (α-Al_2O_3): a conundrum, Phil. Mag. Lett., **79**, 619-627 (1999)

[99Imu] M. Imuta, J. Gotoh, Development of high temperature materials including CMCs for space application, in Key Engineering Materials, Vols. 164-165, edited by K. Niihara, Trans Tech Publication, Zuerich, 1999, pp 439-444

[99Lee] S. H. Lee, S. C. Choi, New method for the testing of porous ceramic materials, in British ceramic proceedings, No. 60, Vol. 2, University press Cambridge, London, 1999, pp 135-136

[99Mas] S. Masaki, T. Yamamura, High performance tyranno (Si-C-M-O) fibers for composites, in Key Engineering Materials, Vols. 164-165, edited by K. Niihara, Trans Tech Publication, Zuerich, 1999, pp 67-72

[99Müh] A. Mühlratzer, Production, properties and application of ceramic matrix composites, Ceram. Forum Int., **76**, 30-35 (1999)

[99Muk] Mukundhan, P., Wu, J. & Du, H. H., Oxidation behavior of NBD 200 silicon nitride ceramics, J. Am. Ceram. Soc., **82**, 2260-2262 (1999)

[99Rot] B. Rothe, D. Suttor, G. Ziegler, Processing and mechanical properties of C-fiber reinforced SiCN-CMCs, in Key Engineering Materials, Vols. 164-165, edited by K. Niihara, Trans Tech Publication, Zuerich, 1999, pp 103-104

[99Sei] H. J. Seifert, Reaction path simulations in multicomponent materials, Z. Metallkd., **90**, 1016-1024 (1999)

[99Sor] G. D. Sorarù, D. Suttor, High temperature stability of sol-gel derived SiOC glass, J. Sol-Gel Sci. Tech., **14**, 69-74 (1999)

[99Sug] M. Sugimoto, Y. Morita, T. Seguchi, K. Okamura, Development of SiC fiber-reinforced SiC composites by radiation-cured preceramic polymer, in Key Engineering Materials, Vols. 164-165, edited by K. Niihara, Trans Tech Publication, Zuerich, 1999, pp 11-14

[99Tak] N. Takamura, K. Taguchi, T. Gunji, Y. Abe, Preparation of silicon oxicarbide ceramic films by pyrolysis of polymethyl- and polyvinylsilsequioxanes, J. Sol-Gel Sci. Tech., **16**, 227-234 (1999)

[99Thu] G. Thurn, J. Canel, J. Bill, F. Aldinger, Compression creep behavior of precursor-derived Si-C-N ceramics, J. Europ. Ceram. Soc., **19**, 2317-2323 (1999)

[99Wei] M. Weinmann, T. W. Kamphowe, P. Fischer, F. Aldinger, Tris(hydridosilylethyl)boranes: highly reactive synthons for polymeric compounds, J. Organometal. Chem., **592**, 115-127 (1999)

[99Zie] G. Ziegler, I. Richter, D. Suttor, Fiber-reinforced composites with polymer-derived matrix : processing, matrix formation and properties, Composites : part A, **30**, 411-417 (1999)

[99Zou1] W. Zou, T. Wan, J. Su, L. Yan, J. Lu, An effective process for silicon carbide matrix composites : Dual-composition solution impregnation and pyrolysis under medium pressure, in Key Engineering Materials, Vols. 164-165, edited by K. Niihara, Trans Tech Publications, 1999, pp77-80

[99Zou2] W. Zou, M. Song, T. Wan, L. Yan, K. Wan, Triaxially braided C/SiC composites : research and development by the combined process of CVI+PIP, in Key Engineering Materials, Vols. 164-165, edited by K. Niihara, Trans Tech Publications, 1999, pp213-216

[00Bha] R. T. Bhatt, Tensile properties and microstructural characterization of Hi-Nicalon SiC/RBSN composites, Ceram. Inter., **26**, 535-539 (2000)

[00But] E. Butchereit, K. G. Nickel, Oxidation behavior of precursor-derived ceramics in the system Si-(B)-CN, in key Engineering. Materials, Vols. 175-176, edited by P. Šajgalík, Z. Lenčéš, Trans Tech Publications, Zuerich, 2000, pp 69-78

[00Gre] P. Greil, Polymer derived engineering ceramics, Advanced Engineering Mater., 2 [6], 339-348 (2000)

[00Hal] C. Haluschka, H.-J. Kleebe, R. Franke, R. Riedel, Silicon carbonitride ceramics derived from polysilazane, part1. Investigation of compositional and structural properties, J. Eur. Ceram. Soc., **20**, 1355-1364 (2000)

[00Jon] R. E. Jones, D. Petrak, J. Rabe, A. Szweda, SYLAMICTM SIC fibers for CMC reinforcement, J. Nucl. Mater., **283-287**, 556-559 (2000)

[00Koh] A. Kohyama, M. Kotani, Y. Katoh, T. Nakayasu, M. Sato, T. Yamamura, K. Okamura, High-performance SiC/SiC composites by improved PIP processing with new precursor polymers, J. Nucl. Mater., **283-287**, 565-569 (2000)

[00Kro] E. Kroke, Y. –Li Li, C. Konetschny, E. Lecomte, C. Fasel, R. Riedel, Silazane derived ceramics and related materials, Mater. Sci. Eng., **26**, 97-199 (2000)

[00Nec] M. A. Nechanicky, K. W. Chew, A. Sellinger, R. M. Laine, α-silicon carbide/β-silicon carbide particulate composites via polymer infiltration and pyrolysis (PIP) processing using polymethylsilane, J. Europ. Ceram. Soc., **20**, 441-451 (2000)

[00Ric] R. W. Rice, Mechanical properties of ceramic and composites, Marcel Dekker, New York, 2000, pp54-55

[00Shi] T. Shimoo, F. Toyoda, K. Okamura, Thermal stability of low-oxygen silicon carbide fiber (Hi-Nocalon) subjected to selected oxidation treatment, J. Am. Ceram. Soc., **83**, 1450-1456 (2000)

[00Tak1] M. Takeda, A. Saeki, J.-I. Sakamoto, Y. Imai, H. Ichikawa, Effect of hydrogen atmosphere on pyrolysis of cured polycarbosilane fibers, J. Am. Ceram. Soc., **83**, 1063-1069 (2000)

[00Tak2] M. Takeda, Y. Imai, Y. Kagawa, S.-Q. Guo, High-temperature thermal stability of Hi-Nicalon^{TM} SiC fiber/SiC matrix composites under long term heating, Mater. Sci. Eng., A286, 312-323 (2000)

[00Wan] J. Wan, M. J. Gasch, A. K. Mukherjee, Silicon carbonitride ceramics produced by pyrolysis of polymer ceramic precursor, J. Mater. Res., **15**, 1657-1660 (2000)

[00Wei] M. Weinmann, T. W. Kamphowe, J. Schuhmacher, K. Müller, F. Aldinger, Design of polymeric Si-B-C-N ceramic precursors for application in fiber-reinforced composite materials, Chem. Mater., **12**, 2112-2122 (2000)

[01Bau] A. Bauer, M. Christ, A. Zimmermann, F. Aldinger, Fracture toughness of amorphous precursor-derived ceramics in the silicon-carbon-nitrogen system, J. Am. Ceram. Soc., **84**, 2203-2207 (2001)

[01Chr] F. Christin, Design, fabrication and application of C/C, C/ Si, and SiC/ SiC composites, in High temperature ceramic matrix composites, edited by W. Krenkel, R. Naslain, H. Schneider, Wiley-VCH, Weinheim, 2001, pp732-743

[01Elh] H. A. El-Hija, W. Krenkel, Cost analysis for the manufacture of C/C-SiC structural parts, in High temperature ceramic matrix composites, edited by W. Krenkel, R. Naslain, H. Schneider, Wiley-VCH, Weinheim, 2001, pp846-853

[01Fle] H. A. Flegel, New technologies in the light of materials, in Ceramic materials and components for engines, edited by J. G. Heinrich, F. Aldinger, Weley-VCH, Weinheim, 2001, pp3-6

[01Gad] R. Gadow, M. Speicher, Multilayer C/SiC composites for automotive brake systems, in Ceramic materials and components for engines, edited by J. G. Heinrich, F. Aldinger, Wiley-VCH, Weinheim, 2001, pp 565-570

[01Gal] D. Galusek, F. L. Riley, R. Riedel, Nanoindentation of a polymer-derived amorphous silicon carbonitride ceramic, J. Am. Ceram. Soc., **84**, 1164-1166

(2001)

[01Iwa] Y. Iwamoto, W. Voelger, E. Kroke, R. Riedel, Crystallization behavior of amorphous silicon carbide ceramics derived from organometallic precursors, J. Am. Ceram. Soc., **84**, 2170-2178 (2001)

[01Li1] R. Li, Temperature-induced direct casting of SiC, Ph. D. Thesis, Stuttgart University, 2001

[01Li2] Y.-L. Li, E. Kroke, R. Riedel, C. Fasel, C. Gervais, F. Babonneau, Thermal cross-linking and pyrolytic conversion of poly (ureamethylvinyl)silazanes to silicon-based ceramics, App. Organometal. Chem., **15**, 820-832 (2001)

[01Lie] L.A. Liew, W.G. Zhang, V. M. Bright, L. N. An, M. L. Dunn. R. Raj, Fabrication of SiCN ceramic MEMS using injectable polymer-precursor technique, Sensors & Actuators A-Physical, **89**, 64-70

[01Lut] K. L. Luthra, G. S. Corman, Melt infiltrated (MI) SiC/SiC composites for gas turbine application, in High temperature ceramic matrix composites, edited by W. Krenkel, R. Naslain, H. Schneider, Wiley-VCH, Weinheim, 2001, pp744-753

[01Pai] U. Paik, J. P. Kim, Y. S. Jung, Y. G. Jung, T. Katoh, J. G. Park, and V. A. Hackley, The effect of Si dissolution on the stability of silica particles and its influence on chemical mechanical polishing for interlayer dielectrics, J. Kor. Phys. Soc., **39**, S201-S204 (2001)

[01Raj] R. Raj, L. An, S. Shah, R. Riedel, C. Fasel, H.-J. Kleebe, Oxidation kinetics of an amorphous silicon carbonitride ceramic, J. Am. Ceram. Soc., **84**, 1803-1810 (2001)

[01Rak] Z. Rak, A process for C_f/SiC composites using liquid polymer infiltration, J. Am. Ceram. Soc., **84**, 2235-2239 (2001)

[01Sei] H. J. Seifert, J. Peng, J. Golczewski, F. Aldinger, Phase equilibria of precursor-delived Si-(B)-C-N ceramics, App. Organometallic Chem., **15**, 794-808 (2001)

[01Shi] T. Shimoo, M. Ito, K. Okamura, M. Takeda, Effect of vacuum heat treatment on electron-beam-irradiation-cured polycarbosilane fibers, J. Am. Ceram. Soc., **84**, 111-116 (2001)

[02Bor] A. Borger, P. Supancic, R. Danzer, The ball on three balls test for strength testing of brittle discs: stress distribution in the disc, J. Europ. Ceram. Soc., **22**, 1425-1436 (2002)

[02Dan] R. Danzer, Mechanical failure of advanced ceramics : The value of fractography,

in Key Engineering Materials, Vol. 223, edited by J. Dusza, Trans Tech Publication, Zuerich, 2002, pp 1-18

[02Pen] J. Peng, "Thermochemisrty and constitution of precursor-derived Si-(B-)C-N ceramics", Ph. D. Thesis, University of Stuttgart, 2002, pp 103-109

[02Sat] K. Sato, H. Morozumi, O. Funayama, T. Isoda, Influence of crystallinity of matrix on mechanical properties of fiber-reinforced composites prepared by polysilazanes as matrix precursor, J. Ceram. Soc. Jpn., **110,** 775-779 (2002)

[02Sch] M. Schiavon, G. Soraru, I. Yoshida, Synthesis of a polycyclic silazane network and its evolution to silicon carbonitride glass, J. Non-Crystalline Solids, **304**, 76-83 (2002)

[02Wag] S. Wagner, H. J. Seifert, F. Aldinger, High-temperature reactions of C/C-SiC composites with precursor-derived ceramic coatings, Mater. Manuf. Process., **17**, 619-635 (2002)

[02Wan] J. Wan, M. J. Gasch, A. K. Mukherjee, Silicon nitride-silicon carbide nanocomposites fabricated by electric-field-assisted sintering, J. Am. Ceram. Soc., **86**, 526-528 (2002)

[02Zim] A. Zimmermann, A. Bauer, M. Christ, Y. Cai, F. Aldinger, High-temperature deformation of amorphous Si-C-N and Si-B-C-N ceramics from polymers, Acta Mater., 50, 1187-1196 (2002)

Zusammenfassung

Die Arbeit widmet sich Faktoren, die bei der Herstellung von keramischen Faser-Matrix-Verbundwerkstoffen (FRC, fiber-reinforced composites) deren mechanische und thermische Eigenschaften beeinflussen. Insbesondere wurden der Einfluss von Füllstoffen und die Optimierung des PIP-Verfahrens (Precursor Impregnation and Pyrolysis) zur Herstellung kohlenstofffaserverstärkter Si-C-N-Precursorkeramiken untersucht. Dabei wurden fünf Bereiche betrachtet, die jeweils in einem Kapitel dargelegt wurden.

Im Kapitel 1 wurden die Herstellungsbedingungen für partikelverstärkte Keramiken (PRC, particulate-reinforced ceramics) und vor allem der Einfluss der Atmosphäre während der Pyrolyse eines kommerziell erhältlichen Precursors (VL20, Fa. Kion) untersucht und optimiert. Derartige PRC bilden die Matrix für die hier interessierenden Faser-Verbund-werkstoffe. Die Pyrolysezeit konnte im Vergleich zu den aus der Literatur bekannten Verfahren auf ungefähr ein Drittel reduziert werden, ohne dass eine Verschlechterung der mechanischen Eigenschaften festgestellt wurde. Während der Pyrolyse von mit SiC-Füll-stoffen versetzten Polymeren trat eine Oberflächenoxidation auf, die so an reinen Si-C-N-Precursorkeramiken nicht beobachtet wird. Die Oxidation wurde höchstwahrscheinlich durch die größere spezifische Oberfläche (8,5 m^2/g) im Vergleich zu reinen Si-C-N-Keramiken (0,27 m^2/g) verursacht. Die Oberflächenoxidation beeinflusst die mechanischen Eigenschaften und die Temperaturstabilität der Verbundwerkstoffe, so dass bei der Darstellung von PRC oder teilchenverstärkten FRC der strikte Ausschluss von Sauerstoff in der Pyrolyseatmo-sphäre eine äußerst wichtige Vorraussetzung ist.

Im zweiten Kapitel wurde die Anwendung von Füllstoffen für die Matrixphase mit dem Ziel untersucht, die Herstellungszeit zu verringern und das übermäßige Schrumpfen der faserverstärkten Grünkörper während der Pyrolyse zu unterbinden. Zu diesem Zweck wurden vier unterschiedliche Füllstoffe (Al_2O_3, Y_2O_3, SiC und Si_3N_4) getestet. Die oxidischen Füll-stoffe reagieren während der Pyrolyse mit der Si-C-N-Matrix, es tritt Volumenschrumpfung in Verbindung mit Zweitphasenbildung (Si_5AlON_7, $Y_8Si_4N_4O_{14}$) auf. Oxidische Füllstoffe zeigen auch eine sechs- bis achtfach geringere Schneiderate nach der ersten Pyrolyse als nichtoxidische Füllstoffe, und es wurden Schädigungen durch Rissbildung nach wiederholten Pyrolysezyklen beobachtet. Die unterschiedlichen Wärmeausdehnungskoeffizienten von Füllstoff und Matrix (Al_2O_3: $8x10^{-6}$ K^{-1}, Si-C-N: $3x10^{-6}$ K^{-1}) und die Zweitphasenbildung dürften der Grund für die Rissbildung während der Thermolyse von oxidischen PRC sein. Die Verstärkung mit SiC-Teilchen erbrachte die höchsten Werte von relativer Dichte (~91%),

Festigkeit (525 MPa), Elastizitätsmodul (240 GPa), Härte (1622 Hv) und Bruchzähigkeit (4,0 MPa $m^{1/2}$) aller untersuchten PRC. SiC-PRC wies außerdem den geringsten Gewichtsverlust und die höchste Hochtemperatur-Kriechbeständigkeit aller untersuchten PRC auf.

In Kapitel 3 wurde ein neues Verfahren zur Infiltration von SiC-Schlickern in Fasergelege entwickelt und optimiert. Im Gegensatz zu den konventionell eingesetzten starren Matrizen verfügt die hier verwendete Form über eine verformbare Folie. Dies ermöglicht eine hohe Feststoffbeladung des SiC-Schlickers (bis 43%) sowie eine homogene Injektion eines Schlickers in die gestapelten Fasergelege. Auf diese Weise konnten sehr dichte C_{fiber}/SiC_{filler}-Formkörper (relative Dichte ~72%) erhalten werden.

Auf der Grundlage dieser Ergebnisse wird in Kapitel 4 die Herstellung von faserverstärkten Verbundwerkstoffen auf der Basis von Kohlenstoff-Fasern, SiC-Füller und einer Matrix aus polymerabgeleiteter Keramik ($C_{fiber}/SiC_{filler}/Si\text{-}C\text{-}N_{matrix}$) beschrieben. Die Herstellungszeit konnte durch die Steigerung der Gründichte und die Optimierung der Vernetzungs- und Pyrolysebedingungen reduziert werden. Für die Untersuchung des Vernetzungsverhaltens der polymeren Precursoren wurde ein versiegeltes Metallgefäß verwendet, um ein Verdampfen des zu infiltrierenden Oligomers während dessen Vernetzung zu vermeiden. Auf diese Weise konnte auch die Bildung von Blasen im vernetzten Polymer wirksam unterdrückt werden. Die Dichte der FRC nach zehn Prozesszyklen beträgt 2.14 g/cm^3. Ein den Prozess begleitendes Risswachstum erfolgte bevorzugt entlang der Pyrokohlenstoffbeschichtung auf der Ober-fläche der Fasern. Daher war ein ausgeprägter Faser-Pull-Out war nach dem Biegetest auf den Bruchflächen zu beobachten. Nach dem Test waren zwar alle Proben gebogen, jedoch nicht gebrochen; einzelne intakte Kohlenstofffasern überbrückten nach wie vor die Bruchstelle. Die mittlere Biegefestigkeit der $C_{fiber}/SiC_{filler}/Si\text{-}C\text{-}N_{matrix}$-FRC betrug 286 MPa.

Im letzten Kapitel wurde die Hochtemperaturfestigkeit der FRC untersucht. Nach einer Wärmebehandlung bei 1350°C für 24h in Ar blieben 73% der Festigkeit erhalten. Eine Schädigung der SiC_{filler}/Si-C-N-Matrix, die Bildung von SiO_2-Schichten an der Oberfläche der Probe und die Bildung von SiC-Whiskern im Inneren der Probe konnten durch Gefüge-analyse und Röntgendiffraktometrie nachgewiesen werden. Um den Mechanismus der Matrixschädigung aufzuklären, wurden SiC-PRC aus unterschiedlich wärmebehandelten SiC-Pellets hergestellt. Mit einer Wärmebehandlung bei 1750°C in Ar konnte das SiO_2 auf der Oberfläche des Füllstoffes entfernt werden, das die Ursache für die Entstehung der SiO_2-Oberflächenschichten und der SiC-Whisker von PRC und partikelverstärkten FRC nach der Auslagerung ist. Es konnte gezeigt werden, dass die relative Dichte, die mechanischen Eigen-schaften wie Festigkeit und Härte, die Hochtemperaturstabilität und die Kriechbeständigkeit durch das SiO_2 an den Oberflächen der Füllerteilchen ungünstig beeinflusst werden. Die Werte für Festigkeit und Härte von SiO_2-freien PRC (>639 MPa, 1068 Hv) waren doppelt so hoch wie diejenigen der SiO_2 enthaltenden PRC (329 MPa, 542 Hv) nach 2h bei 1400°C.

Die Ergebnisse zeigen, dass die Verschlechterung der mechanischen Eigenschaften von $C_{fiber}/SiC_{filler}/Si\text{-}C\text{-}N_{matrix}$-FRC bei hohen Temperaturen teilweise auf die Schwächung der partikelverstärkten Matrix durch die Zersetzung von SiO_2 zurückzuführen ist. Die Entfernung

dieser Oxidschichten durch eine Wärmevorbehandlung der Füllstoffe ist daher eine sehr wichtige Voraussetzung zur Herstellung von FRC für Hochtemperaturanwendungen nach der PIP-Methode.

Lebenslauf

Personalien	Name	Sea-Hoon LEE
	Geburtsdatum	27. 12. 1969
	Geburtsort	Seoul, Republik Korea
Schulbildung	03. 1976-02. 1982	Grundschule
	03. 1982-02. 1985	Mittelschule
	03. 1985-02. 1988	Oberschule
Studium	03. 1990-02. 1994	Keramikingenieurwissenschaften an der „Hanyang University“
	03. 1996-02. 1998	Diplomarbeit mit dem Thema „Fabrication of 3Y-TZP/SUS 316 functionally graded materials using alumina mold casting method“
Promotion	seit 01. 07. 2000	Wissenschaftliche Tätigkeit am Max-Planck-Institut für Metallforschung und an der Universität Stuttgart, Abteilung Prof. Aldinger mit dem Ziel der Promotion
Berufstätigkeiten	03. 1998-02. 1999	Gastwissenschaftler an der „Hanyang University“, Abteilung Prof. Dr. Sung-Churl Choi
	07. 1999-06. 2000	Gastwissenschaftler am Max-Planck-Institut für Metallforschung, Abteilung Prof. Aldinger, PML
	seit 01. 07. 2000	Wissenschaftlicher Angestellter am Max-Planck-Institut für Metallforschung und an der Universität Stuttgart, Abteilung Prof. Aldinger